VOL. XIV - Nº 4 1992 ISSN 0100-7386

REVISTA BRASILEIRA DE CIÊNCIAS MECÂNICAS

JOURNAL OF THE BRAZILIAN SOCIETY OF MECHANICAL SCIENCES

PUBLICAÇÃO DA ABCM
ASSOCIAÇÃO BRASILEIRA DE CIÊNCIAS MECÂNICAS

REVISTA BRASILEIRA DE CIÊNCIAS MECÂNICAS
JOURNAL OF THE BRAZILIAN SOCIETY OF MECHANICAL SCIENCES

Publicado pela / Published by

ASSOCIAÇÃO BRASILEIRA DE CIÊNCIAS MECÂNICAS, ABCM /
BRAZILIAN SOCIETY OF MECHANICAL SCIENCES

Secretário da ABCM: Sr. Antonio Paulo da Costa Maruques
Av. Rio Branco, 124-18º andar - Rio de Janeiro - Brasil
Tel. / Fax (021) 222-7128

Presidente: Arthur Palmeira Ripper
Secret. Geral: Agamenon R. E. Oliveira
Diretor de Patrimônio: Luiz Fernando Salgado Candiota

Vice-Presidente: Sidney Stuckenbruck
Secretário: Carlos Alberto de Almeida

Programa de Apoio a Publicações Científicas
MCT CNPq FINEP

RBCM – J. of the Braz.Soc.Mech.Sc. ISSN 0100-7386
Vol.XIV – nº 4 – 1992 Impresso no Brasil

Editorial

A Associação Brasileira de Ciências Mecânicas pode, com orgulho, falar em tradição e continuidade da REVISTA BRASILEIRA DE CIÊNCIAS MECÂNICAS. Ao longo de 14 anos, esta publicação vem espelhando a produção científica de nossa comunidade de pesquisadores. Chamada à vida sem setembro de 1979 pelo seu primeiro editor, o Prof. Luiz Bevilacqua, permaneceu em suas mãos até dezembro de 1983; sua continuidade foi garantida pelo Prof. Rubem Sampaio até julho de 1988, quando o atual corpo de editores a assumiu. Passamos por um período de imensas dificuldades econômicas. Embora irregular, os órgãos governamentais tem mantido o apoio à publicação desta Revista. Assim, entregamo-la em dia ao nosso sucessor Prof. Leonardo Goldstein incorporando uma série de pequenas modificações que profissionalizaram o trabalho: maior homogeneidade temática, maior uniformidade editorial, lombada e várias outras. Embora nunca tenha sido mencionada a palavra mandato, os três períodos acima são de 4,5 anos, caracterizando pelo menos uma curiosa coincidência. Ao encerrar esta fase, apresentamos algumas estatísticas que permitirão uma avaliação crítica da evolução da Revista.

Nos seus primeiros 09 anos de existência, a Revista publicou 140 artigos, em 29 números (4,8 artigos/número) de 152 autores diferentes, pertencentes a 33 Instituições Nacionais e 22 Estrangeiras. Destes, 28,5% foram escritos em inglês e 3,5% em espanhol. Eles, em média, apresentam 13,3 páginas. As Instituições mais presentes foram a PUC-Rio, cujo nome consta como afiliação de pelo menos um dos autores em 31,5% dos artigos, a UFRJ e o LNCC/CNPq com 11,5% cada, CTA/ITA (9,3%), UFSC (8%), UNICAMP (4,3%), INPE (3,5%), UFU (3%) e outras.

A atualização destes números para o período atual (4,5 anos) permite contabilizar 84 artigos (4,9 artigos/número), de 138 autores pertencentes a 25 Instituições Nacionais e 24 Estrangeiras. Destes autores apenas 30 fazem parte do rol dos autores antigos. A análise destes números mostra uma diversificação maior de seu público autor. A porcentagem da presença do nome das Instituições pelos artigos mostra a PUC-Rio com 19%, a UFRJ (10,7%), UFSC (9,5%), CTA/ITA (8,3%), LNCC/CNPq (7,1%), UFU (7,1%), UFMG (4,8%), UNICAMP (4,8%). Houve também no período um aumento de número de artigos em inglês (49,4%), mantendo-se os em espanhol (3,4%).

São submetidos em média 25 artigos por ano e publicados 20, com uma média de 19 páginas por artigo. O número reduzido de artigos submetidos caracteriza um problema congênito à comunidade científica brasileira: tendo em vista as particularidades das publicações em anais de congressos, rápidas e de revisão mais simples, quando um autor prepara um artigo para uma revista, prefere

fazê-lo em uma revista editada no exterior. Por isso encaramos como um sucesso a Revista atualmente ter a metade dos textos em inglês.

Outra análise realizada procura levantar a distribuição por áreas dos artigos publicados, visando avaliar a criação nesta gestão, das editorias associadas. O resultado obtido entre 1988 e 1991 indica 54% dos artigos em Ciências Térmicas, 24% em Mecânica dos Sólidos, 12% em Dinâmica, 7,5% em Fabricação e Materiais e 2,5% em Métodos Numéricos. Se isto representa a demanda real da comunidade, o nível de atuação do respectivo editor ou uma mistura de ambos fatores, que deixamos como interrogação na cabeça do leitor. Todavia, seu reflexo já se dará na composição do novo corpo de editores.

Cabe mencionar ainda que os editores associados atuaram com uma autonomia a altura de suas idiossincrasias, mantendo-se o controle de recebimento e de publicação com o editor chefe. A descentralização funcionou bem, mas de acordo com o que cada um definiu de objetivos para si. A publicação final viabilizou-se em grande parte pela atuação do Presidente da ABCM na obtenção dos recursos tendo os trabalhos de digitação, de correção e de gráfica permanecido no Rio de Janeiro.

É sempre bom saber que chegamos a um porto com a consciência da missão cumprida. Agradecemos aos autores e leitores e, em especial, aos revisores que nos ajudaram a manter o padrão da Revista.

Os Editores

The main effort in editing a scientific journal in Brazil is to guarantee its continuity. After three periods of 4.5 years, each under the responsibility of a different editor but always oriented by the goals of the Brazilian Society of Mechanical Sciences, our journal is still a mirror of the brazilian related scientific production. The main achievements in this last period are certainly the more homogeneous numbers concerning the research areas, the increase to about 50% on the number of english published papers and the spread of authors over a large number of institutions, representing a more diversified group of authors. In spite of a non-regular scheduling of publication we did not lose continuity as we kept publishing 4 numbers every year: and for that we thank very much to authors and readers of the english language.

We still would like to have many more papers submitted – and we need it to justify the existence of the journal to our financing agencies. All the difficulties to get this proposal are discussed over and over by ABCM members but we have reached to a point when some concret actions are needed, so that the authors are aware of the advantages of publishing in our country. Continuity and tradition are certainly ones; the scientific level and the international distribution are other requisites. There are still several others that the next editor of RBCM, Prof. Leonardo Goldstein, may try. We wish him a good luck in this endeavor.

The Editors

RBCM – J. of the Braz.Soc.Mech.Sc. ISSN 0100-7386
Vol.XIV – nº 4 – pp. 299 – 326 – 1992 Impresso no Brasil

ANALYSIS OF COMPOSITE LAMINATES USING VARIABLE KINEMATIC FINITE ELEMENTS

ANÁLISE DE LAMINADOS COMPOSTOS UTILIZANDO ELEMENTOS FINITOS COM CINEMÁTICA VARIÁVEL

J.N. Reddy
D.H. Robbins, Jr.
Department of Mechanical Engineering
Texas A& M University
College Station, Texas 77843-3123
USA

ABSTRACT

Traditionally, composite laminates are treated as equivalent-single layers (ESL) by integrating through the laminate thickness. However, they are inadequate in correctly modeling the response characteristics of thick composites and localized phenomena such as free-edge effects, delaminations, and three-dimensional effects. Layerwise theories are proposed to account for these effects. Various equivalent single-layer thoeries and layerwise theories are reviewed, and an efficient and robust computational procedure based on variable kinematic finite elements and mesh superposition technique is proposed. The computational procedure developed by the authors permit a convenient, accurate and economic determiantion of ply level stresses within localized regions of interest in practical laminated structures.

Keywords: Composite Laminates ▪ Free-Edge Effects ▪ Delamination ▪ Three-Dimensional Effects ▪ Variable Kinematic Finite Elements ▪ Mesh Superposition Technique

RESUMO

Tradicionalmente laminados de materiais compostos são tratados como sendo equivalentes a uma única camada, integrando através da espessura do laminado. Entretanto, são inadequadas para modelar corretamente as características de materiais compostos espessos, os aspectos dinâmicos de materiais compostos finos e espessos e em localizar fenômenos tais como o efeito da borda livre, delaminação e efeitos tridimensionais. Teorias lâmina a lâmina são propostas para explicar os últimos. Neste trabalho, tanto teorias de uma única camada equivalente, como teorias lâmina a lâmina são revisadas, e uma unificação destas teorias e um procedimento computacional eficiente e robusto, baseado em elementos finitos com cinemática variável e na técnica de superposição de malhas são propostos. O modelo teórico e o procedimento computacional desenvolvidos pelos autores permite uma determinação conveniente, precisa e econômica das tensões a nível de cada lâmina dentro de regiões localizadas de interesse em estruturas laminadas de interesse prático.

Palavras-chave: Laminados Compostos ▪ Efeito de Borda Livre ▪ Delaminação ▪ Efeitos Tridimensionais ▪ Elementos Finitos com Cinemática Variável ▪ Técnica da Superposição de malhas

---

Invited Lecture Presented at 7th SIBRAT, Florianópolis, Brazil

INTRODUCTION

Composite materials consist of two or more different materials that are combined together to achieve desirable structural properties (e.g., stiffness, strength, low density, impact strength, so on) that the constituent materials, acting alone, do not exhibit. Composites are used in space and underwater structures, medical prosthetic equipment, sports equipment, automobiles, and electronic circuitry. Because of the increased use of composite materials, polymer chemists, material scientists and mechanics community are working to develop better material systems, structural models, and analysis methods to assess the strength and reliability.

Composite materials are made in different forms. Often they are made in the form of layers, known as laminae. A typical layer may consist of fibers, long or short, reinforced in a matrix material. The layers are then used to form a composite laminate of desired shape and thickness. Because of the different material properties of differente layers, the resulting laminate is in general anisotropic, and its global deformation is characterized by complex coupling between extension, bending and shearing modes. In addition, composite laminates exhibit many unique localized phenomena such as free edge effects, delamination, matrix cracking, fiber breakage, and complex load redistribution as the laminate undergoes continuous damage (i.e., microscopic failures).

Current laminate theories can be divided into two broad classes based on the assumed variation of the displacement field through the laminate thickness (see [1–3]): the "equivalent single-layer" theories, and the layerwise theories. The equivalent single-layer theories (or ESL theories) are characterized by displacement components that are assumed to be C^1–continuous (i.e., displacements as well as strains are continuous) through the laminate thickness. The assumed variation of the displacement components through the laminate thickness allows the virtual work statement to be pre-integrated with respect to the thickness coordinate, thus reducing the 3–D elasticity problem to a 2–D problem (i.e., the primary variables are functions of the in-plane coordinates only). For laminated composite plates and shells, this amounts to replacing the heterogeneous laminate with a statically equivalent (in the integral sense), single, homogeneous layer. For many applications, the ESL models provide a

sufficiently accurate description of the global laminate response (e.g., transverse deflection, fundamental vibration frequency, critical buckling load, force and moment resultants); however, the ESL models are often inadequate for determining the 3–D stress field at the ply level. The main advantages of the ESL models are their inherent simplicity and their low computational cost due to the relatively small number of dependent variables that must be solved for. The major deficiency of the ESL models in modeling composite laminates is that the transverse strain components are continuous across interfaces between dissimilar materials; thus, the transverse stress components are discontinuous at the layer interfaces. This deficiency is most evident in relatively thick laminates, in localized regions of complex loading or near a geometric discontinuity.

Most engineering structures where composites are used are complex. They contain geometric as well as material singularities and regions of 3–D stress states. In the analysis of composite laminates with imbedded delaminations, free edges, or regions of 3–D stress fields, one must use a theory based on 3–D kinematics and develop a computational model that is more efficient than the conventional 3–D finite element model. These requirements motivated several researchers to develop layerwise laminated plate theories. Unlike the ESL theories, the layerwise theories assume separate displacement field expansions within each material layer, thus providing a much more kinematically correct representation of the strain field in discrete layer laminates, and allowing accurate ply level stresses to be determined.

In layerwise theories, the displacement field is expanded independently within each layer. Mau [4] used the first-order shear deformation kinematics through each layer. He used the interlayer shear stresses as Lagrange multipliers to satisfty the displacement continuity at the layer intefaces, and the governing equations were derived by minimizing a modified total potential energy functional (in the spirit of hybrid formulations of Pian and his associates). Rehfield and Murthy [5] and Rehfield and Valisetty [6] assumed layerwise distribution of the six stress components, and the layer stress-strain and strain-displacement relations are used to compute the displacements by integration. The constants of integration are determined such that the displacements are continuous at layer interfaces. Murakami [7] and Toledano and Murakami [8] used independent expansions of the displacements and stresses through each layer, and Reissner's mixed variational principle was used to obtain

the governing equations. Hinrichsen and Palazotto [9] used cubic splines to express the displacements through each layer. Cubic splines, by definition, give continuity of the displacements and their derivatives at the layer interfaces. The continuity of the transverse strains at layer interfaces is exactly what one wants to avoid while achieving the continuity of the stresses. These and other layerwise models (see Srinivas [10], Epstein and Glockner [11], Epstein and Huttelmaier [12] and Di Sciuva [13,14]) are developed for various reasons other than to model three-dimensional effects such as delaminations or free-edge stress fields. Further, these models are algebraically complex and computationally very expensive, comparable to that of 3–D models, while not having any advantages over the 3–D models.

In some layerwise theories, displacement continuity across layer interfaces is enforced by constraint equations that allow some of the dependent variables to be eliminated during the model development. Alternately, some layerwise models are developed by organizing stacks of 3–D finite elements. However, in the layerwise theory of Reddy [15,16] the transverse variation of the displacement field is defined in terms of a 1–D, Lagrangian, finite element representation, that automatically enforces C^0 continuity of the displacement components, thus resulting in trasverse strains that are piecewise continuous through the laminate thickness. The transverse variation of the displacements can be represented to any desired level of accuracy by simply increasing the number of 1–D finite elements (i.e., numerical layers) or increasing the order of the transverse interpolation polynomials. Thus the *layerwise theory of Reddy* provides a generalization of the layerwise displacement field concept. The basic idea and accuracy of the layerwise theory of Reddy [15,16] will be discussed in Section 3. The extension of the layerwise laminated plate theories to laminated shells was carried out by the senior author [17]. The most significant aspect of the layerwise theory of Reddy is that it has a data structure that saves computational time when compared to the conventional 3–D displacement finite element model, while giving exactly the same results for comparable meshes.

While layerwise finite elements allows accurate determination of 3–D stress fields, they are computationally expensive to use due to the large number of degrees of freedom per element, comparable to stacks of 3–D finite elements. Thus it is often impractical to discretize an entire laminate with layerwise finite elements. Further, for many laminate applications, the indiscriminant use of

layerwise elements is a waste of computational resources since significant 3–D stress states are usually present only in localized regions of complex loading or geometric discontinuities. A logical idea is to subdivide the laminate into regions that can be adequately described by ESL models and other regions that require some type of layerwise model (i.e., a simultaneous *global/local* strategy). In this way, the most appropriate model is chosen for each region, thereby increasing solution economy without compromizing solution accuracy. Such global/local schemes can be developed using established finite element technology (see [18] for a review); however, currently available methods make implementation extremely cumbersome. The primary source of difficulty is the enforcement of displacement continuity across boundaries that separate incompatible subdomains. Currently established methods of acheiving displacement continuity between incompatible regions include: (1) multi-point constraint equations via Lagrange multipliers, (2) penalty function methods, and (3) special transition elements. Each of these methods are too cumbersome for extensive use under a wide veriety of operating conditions. Thus, there is a need for the development of a global/local analysis procedure that provides greater robustness, simpler computer implementation, and wider applicability to practical composite structures.

For a global/local model to be successful and see extensive use, it must be robust, simple to develop, convenient to use, and applicable to a wide range of practical problems. To this end, the overall objective of this study is to develop a methodology that will allow these qualities to be realized in a finite element code. By developing methods that significantly increase the adaptability and convenience of the *global/local* finite element code, the operating envelope is extended, since more types of problems become tractable in terms of model development, much in the same way that automatic mesh generators allow the creation of models that would be intractable to create manually.

In the present paper an overview of the equivalent single-layer theories is presented, the layerwise theory of Reddy is reviewed, and a discussion of a hierarchical, displacement-based, global-local computational procedure is presented. To permit the accurate, efficient, and convenient analysis of localized 3–D effects in laminated composite plates and shells, a hierarchical (and, perhaps an iterative), global/local finite model is proposed using a multiple assumed displacement field. The multiple assumed displacement field concept

is used on two different levels. First, a hierarchical, variable kinematic (and constitutive), master finite element is developed by superimposing several assumed displacement fields of differing levels of kinematic complexity in the same finite element domain. Second, the resulting variable kinematic elements are used in a mesh superposition technique that allows a local mesh of variable kinematic elements to be superimposed on an existing global mesh of ESL elements. The resulting model allows the coupling of subdomains that are incomplatible with respect to both the in-plane and transverse discretizations. In addition, the method allows different sections of the computational domain to be described by different mathematical models. Thus localized, three-dimensional subregions can be discretized with a high order, layerwise mesh to extract accurate 3–D stress fields, while the surrounding regions are discretized with an ESL mesh.

EQUIVALENT SINGLE-LAYER LAMINATE THEORIES

In the classical laminated plate theory, it is assumed that (the *Kirchhoff hypothesis*),

1. straight lines normal to midsurface do not undergo deformation along their lengths (i.e., inextensible),

2. straight lines perpendicular to the midsurface before deformation remain straight after deformation, and

3. the straight lines rotate such that they remain perpendicular to the midsurface after deformation.

The first two assumptions imply that the transverse displacement is independent of the thickness coordinate and the transverse normal strain is zero. The third assumption results in zero transverse shear strains. Thus, in the classical laminae theory all transverse stresses are neglected.

Shear deformation theories are those in which the transverse shear stresses are accounted for. These theories are based either on assumed displacement field or assumed stress field. In the displacement-based theories the three components of the displacement vector are represented as polynomials in the thickness coordinate. The coefficients of the polynomial are functions of the in-plane

coordinates. The governing equations are then derived using the principle of virtual displacements. An equivalent single-layer theory is called the *n-th order plate theory* if the in-plane displacements are expanded up to and including the n-th power in the thickness coordinate.

The first-order shear deformation theory is based on the following displacement field:

$$u_1(x,y,z) = u + z\phi_1,\ u_2 = (x,y,z) = v + z\phi_2,\ u_3(x,y,z) = w \qquad (1)$$

Here $u = u(x,y)$, $v = v(x,y)$, and $w = w(x,y)$, denote the displacement components in the x, y, and z directions and $\phi_1 = \phi_1(x,y)$ and $\phi_2 = \phi_2(x,y)$ are the rotations of a transverse normal about the $y-$ and $x-$axes, respectively. Note that the transverse inextensibility is assumed by assuming that the transverse deflection is constant through the thickness, which can be removed if one wishes. In the first-order theory we account for layer-wise constant states of transverse shear stresses [i.e. assumption (iii) of the classical plate theory is removed]. However, the actual distribution of the transverse shear stresses is quadratic or higher. The discrepancy is corrected in computing the shear force resultants by the introduction of *shear correction coefficients*. The first-order shear deformation theory for isotropic plates is often referred in the literature as the *Mindlin* or *Reissner-Mindlin* plate theory. Since the kinematics of the first-order theory was due to several others before Reissner and Mindlin (see [19–22]), it is most appropriate not to name the theory after these authors.

Second- and third-order theories have also beer proposed in the literature (see [23–29]). In the third-order theory we account for layer-wise quadratic approximation of transverse shear stresses [i.e. assumptions (ii) and (iii) are removed]. The third-order theory does not require shear correction factors because it accounts for quadratic distribution of transverse shear stresses. There are a number of third-order theories proposed in the literature [24–29]. Many of these theories can be obtained as special cases of the general third-order theory presented by Reddy [29]. The generalized third-order theory of Reddy is based on the displacement field:

$$\begin{aligned} u_1(x,y,z) &= u + \alpha z\,\frac{\partial w}{\partial x} + \beta z\phi_1 + \lambda z^2\psi_1 + \gamma z^3\theta_1 \\ u_2(x,y,z) &= u + \alpha z\,\frac{\partial w}{\partial y} + \beta z\phi_2 + \lambda z^2\psi_2 + \gamma z^3\theta_2 \\ u_3(x,y,z) &= w + \mu z\psi_3 + \eta z^2\theta_3 \end{aligned} \qquad (2)$$

Here (u, v, w), denote the displacement components in the x, y, and z directions, ϕ_1 and ϕ_2 are the rotations of a transverse normal about the $y-$ and $x-$axes, respectively, and ψ_i and θ_i are undetermined functions. All of the generalized displacements are functions of x and y. The displacements fields of various theories can be obtained from Eq.(5) by giveing proper values to the constants, called *tracers*: α, β, λ, γ , μ, and η. For example, we have,

$$\begin{aligned}
\text{Classical theory: } & \alpha = -1,\ \beta = \lambda = \gamma = \mu = \eta = 0; \\
\text{First-order theory: } & \alpha = 0,\ \beta = 1,\ \lambda = \gamma = \mu = \eta = 0; \\
\text{Second-order theory: } & \alpha = 0,\ \beta = 1,\ \lambda = 1,\ \gamma = 0; \\
\text{Third-order theory of Reddy [27,28]: } & \alpha = 0,\ \beta = 1,\ \lambda = 0,\ \gamma = 1,\ \mu = \eta = 0; \\
& \theta_1 = -\frac{4}{3h^2}\left(\phi_1 + \frac{\partial w}{\partial x}\right) \\
& \theta_2 = -\frac{4}{3h^2}\left(\phi_2 + \frac{\partial w}{\partial y}\right) \\
& \theta_3 = 0\ . \qquad (3)
\end{aligned}$$

The displacement fields of many other single-layer third-order theories can be deduced from the present theory. Table 1 of Reference 29 shows the relationship between the displacements used in various third-order theories.

In most plate problems transverse normals do not experience significant extensions in their lengths, and therefore one can assume, without loss of accuracy, that u_3 is independent of the thickness coordinate (i.e., $\mu = \eta = 0$). However, such an assumtion is not necessary in developing higher-order theories. In order to have the same order terms in thickness coordinate from each of the displacement components to the strains of a third-order theory, Reddy [29] used the displacement field (2) and developed a strain-consistent third-order theory.

THE LAYERWISE LAMINATE PLATE THEORY OF REDDY

Displacement Field

Recall that all equivalent single-layer laminate theories are based on one displacement expansion throughout the thickness of the laminate. Consequently,

the transverse strains are continuous through the laminate thickness. Such theories cannot accurately model laminates made of dissimilar material layers. Noting this restriction of the traditional plate theories, Reddy [15] proposed a layerwise displacement plate theory. The main ideas underlying the theory are presented here for a laminated circular cylindrical shell.

The layerwise theory of Reddy is based on the following displacement expansion through the laminated shell thickness. The i-th displacement component is expressed as,

$$u_i(x,y,z) = \sum_{J=1}^{N} U_i^J(x,y)\ \Phi^J(z) = U_i^J(x,y)\ \Phi^J(z) \tag{4}$$

where $i = 1,2,3, N$ is the number of subdivisions (e.g., finite-element discretization) through the thickness of the laminate, and Φ^J are known functions of the thickness coordinate, z. Summation on repeated indices is implied in Eq.(4). While the same interpolation functions are used in Eq.(4) for all three displacements for simplicity, independent interpolation of the displacements (especially u_3) can be used. The functions Φ^J are piecewise continuous functions, defined only on two adjacent layers, and can be viewed as the global Lagrange interpolation functions associated with the J-th interface of the layers through the laminate thickness, and (U_J, V_J, W_J) denote the nodal values of (u,v,w) at the nodes through the thickness. Because of this local nature of Φ^J the displacements are continuous through the thickness but their derivatives with respect to z are not required to be continuous. This implies that the transverse strains can be discontinuous at discrete layer interfaces, leaving the possibility that the interlaminar transverse stresses computed from the layer constitutive equations can be continuous. The inplane strains $(\varepsilon_x, \varepsilon_y, \varepsilon_{xy})$ will be continuous but the inplane stresses $(\sigma_x, \sigma_y, \sigma_{xy})$ will be discontinuous at layer interfaces because of the difference in material properties of adjacent layers. The resulting theory will have $3N$ variables and as many differential equations in two dimensions. An advantage of the layerwise theory is that it requires only 2–D finite elements.

The value of N in Eq.(4) can be appropriately selected. When N is chosen such that at least one element per layer is used, the interlaminar stress distributions can be determined accurately. The sublaminate concept can be used to model

several indentical layers as one equivalent layer, in which case N is less than the number of layers in the laminate. The layerwise theory also yields single-layer theories as special cases, as shown by Reddy [15].

Strains in the Shell

Here we consider a laminated composite circular cylindrical shell with radius R, lenght L, and total thickness h. We use the strain-displacement relations of Donnell's theory, but also include the transverse strains and the von Kármán nonlinear strains. We have (see Reddy [18])

$$\varepsilon_1 = \frac{\partial u}{\partial x} + \frac{1}{2}\left(\frac{\partial w}{\partial x}\right)^2 = \frac{\partial u_I}{\partial x}\,\Phi^I + \frac{1}{2}\left(\frac{\partial w_I}{\partial x}\,\Phi^I\right)\cdot\left(\frac{\partial w_J}{\partial x}\,\Phi^J\right),$$

$$\varepsilon_2 = \frac{\partial v}{\partial y} + \frac{1}{2}\left(\frac{\partial w}{\partial y}\right)^2 + \frac{w}{R} + \frac{\partial v_I}{\partial y}\,\Phi^I + \frac{1}{2}\left(\frac{\partial w_I}{\partial y}\,\Phi^I\right)\cdot\left(\frac{\partial w_J}{\partial y}\,\Phi^J\right) + \frac{w_I}{R}\,\Phi^I,$$

$$\varepsilon_3 = \frac{\partial w}{\partial z} = w_I\,\frac{d\Phi^I}{dz},$$

$$\varepsilon_4 = \frac{\partial v}{\partial z} + \frac{\partial w}{\partial y} - \frac{v}{R} = v_I\,\frac{d\Phi^I}{dz} + \frac{\partial w_I}{\partial y}\,\Phi^I - \frac{v_I}{R}\,\Phi^I,$$

$$\varepsilon_5 = \frac{\partial u}{\partial z} + \frac{\partial w}{\partial x} = u_I\,\frac{d\Phi^I}{dz} + \frac{\partial w_I}{\partial x}\,\Phi^I,$$

$$\varepsilon_6 = \frac{\partial u}{\partial y} + \frac{\partial v}{\partial x} + \frac{\partial w}{\partial x}\,\frac{\partial w}{\partial y} = \left(\frac{\partial u_I}{\partial y} + \frac{\partial v_I}{\partial x}\right)\Phi^I + \left(\frac{\partial w_I}{\partial x}\,\Phi^I\right)\cdot\left(\frac{\partial w_J}{\partial y}\,\Phi^J\right). \quad (5)$$

Governing Equations

The governing equations for the nodal variables (U_J, V_J, W_J) can be derived using the principle of virtual displacements. The equations of equilibrium of the layer-wise theory are:

$$\frac{\partial M_1^I}{\partial x} + \frac{\partial M_6^I}{\partial y} - Q_1^I = 0, \qquad \frac{\partial M_6^I}{\partial x} + \frac{\partial M_2^I}{\partial y} - Q_2^I + \frac{K_2^I}{R} = 0,$$

$$\frac{\partial K_1^I}{\partial x} + \frac{\partial K_2^I}{\partial y} - \left(\frac{M_2^I}{R} + Q_3^I\right) + \frac{\partial}{\partial x}\left(S_1^{IJ}\,\frac{\partial w_J}{\partial x} + S_6^{IJ}\,\frac{\partial w_J}{\partial v}\right) + \\ + \frac{\partial}{\partial y}\left(S_6^{IJ}\,\frac{\partial w_J}{\partial x} + S_2^{IJ}\,\frac{\partial w_J}{\partial y}\right) \quad (6)$$

for $I = 1, 2, \ldots, N$, where the resultants are defined by

$$M_i^I = \int_{-h/2}^{h/2} \sigma_i \Phi^I(z)\, dz, \quad S_i^{IJ} = \int_{-h/2}^{h/2} \sigma_i \Phi^I(z)\, \Phi^J(x)\, dz, \ (i = 1, 2, 6)$$

$$Q_1^I = \int_{-h/2}^{h/2} \sigma_5 \frac{d\Phi^I}{dz}\, dz, \quad Q_2^I = \int_{-h/2}^{h/2} \sigma_4 \frac{d\Phi^I}{dz}\, dz, \quad Q_3^I = \int_{-h/2}^{h/2} \sigma_3 \frac{d\Phi^I}{dz}\, dz,$$

$$K_1^I = \int_{-h/2}^{h/2} \sigma_5 \Phi^I dz, \quad K_2^I = \int_{-h/2}^{h/2} \sigma_4 \Phi^I dz\ . \tag{7}$$

Thee are $3N$ differential equations in $3N$ variables (U_I, V_I, W_I).

Numerical Results

Numerical results are presented here to illustrate the accuracy of the layerwise theory. The numerical results were obtained using a displacement finite element model of the layerwise theory described above. The reader is referred to the report by Robbins and Reddy [30] for a description of the finite element model and additional numerical results.

Consider a cross-ply laminate (0/90/0) subjected to sinusoidal transverse load at the top surface of the plate. This problem has the 3-D elasticity (see Pagano [31]) solution. The plies are of equal thickness ($h/3$), and the material properties of each ply are:

$$E_1 = 25\ msi, \quad E_2 = 1\ msi, \quad E_3 = E_2, \quad G_{12} = 0.5\ msi\ ,$$

$$G_{13} = G_{23} = 0.2\ msi, \quad \nu_{12} = \nu_{13} = \nu_{23} = 0.25\ . \tag{8}$$

The intensity of the sinusoidally distributed load is denoted q_0. Two different finite element meshes are used. The two meshes differ form each other only in the mesh refinements through the thickness. A 2 by 2 mesh of eight-node quadratic elements is used in a quadrant of the laminate. The mesh used through the thickness are as follows:

Mesh 1: Three quadratic elements through the laminate thickness (441 degrees of freedom).

Mesh 2: Six quadratic elements throught the laminate thickness (969 degrees of freedom).

Figures 1–4 contain plots of nondimensional stresses $(\sigma_1, \sigma_3, \sigma_4, \sigma_5)$ through the thickness of the square laminate $(b/h = 4)$. The stresses are nondimensionalized as follows:

$$\bar{\sigma}_1 = \sigma_1(a_c, a_c, z)\ h^2/(b^2 q_0), \quad \bar{\sigma}_3 = \sigma_3(a_c, a_c, z)/q_0,$$
$$\bar{\sigma}_4 = \sigma_4(a_c, b_c, z)\ h/(bq_0), \quad \bar{\sigma}_5 = \sigma_5(b_c, a_c, z)\ h/(bq_0), \tag{9}$$

where $a_c = 0.105662(b/2)$, $b_c = 0.894338(b/2)$ are the (reduced order) gauss points closest to the points of maximum stresses. The coordinate system is taken in the midplane of the laminate, with the origin of the coordinate system being at the center of the laminate. In Figures 1–4, the solid line represents the exact 3–D elasticity solution of Pagano [31], the solid circles represent the finite element stresses at the gauss points for Mesh 1, the open circles represent the finite element solution at the gauss points for Mesh 2 (refined), and bronken lines correspond to the classical and first-order theories. Excellent agreement is found between the 3–D elasticity results and the finite element results based on the layerwise laminate theory. The deflection $w(x, y)$ coincides with the exact 3–D elasticity solution and is not shown here.

All stresses in the layerwise theory were computed in the post-computation using the displacement field, linear strain-displacement relations, and linear constitutive relations. The inplane normal stress (σ_1) in the classical (CLT) and the first-order (FSDT) theories were post-computed at the gauss points using the constitutive equations. The transverse shear stresses (σ_4, σ_5) in the CLT was post-computed from the first two equilibrium equations of the 3–D elasticity, whereas they are post-computed in the FSDT both from constitutive and 3–D elasticity equations.

From the plot of the inplane normal stress σ_1, it is seen that both CLT and FSDT predict wrong sign of the stress at the layer interfaces. This is due to the fact that the stress is approximated in the classical and first-order theories by a linear expansion. In trying to best approximate the nonlinear stress distribution by a linear variation, both CLT and FSDT yield wrong interface stress values. This can lead to inaccurate prediction of failure load and failure

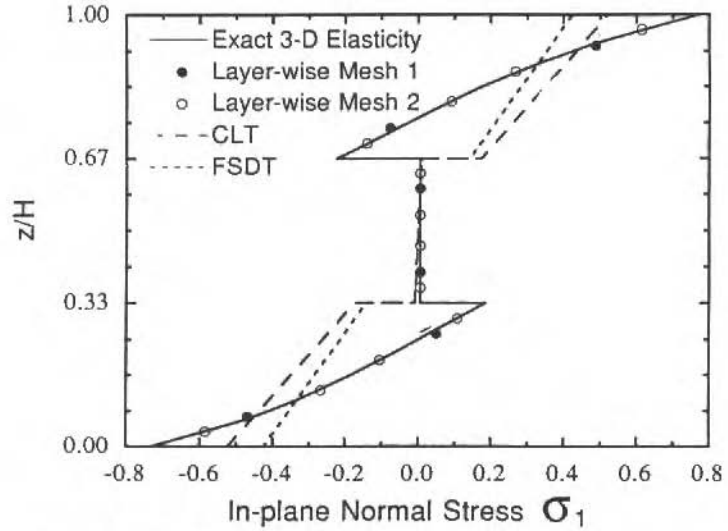

Figure 1. Distribution of in-plane normal stress ($\bar{\sigma}_1$) through the thickness of a simply supported, square (0/90/0) laminate under sinusoidal transverse loading, $L/H = 4$.

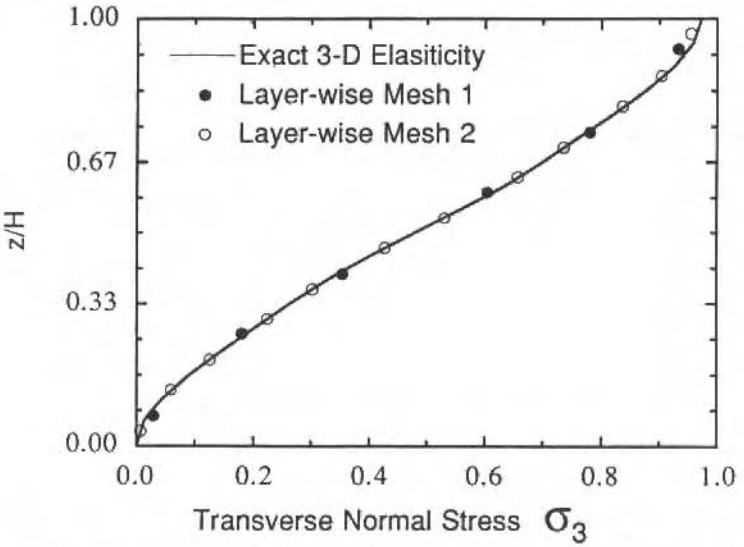

Figure 2. Distribution of transverse normal stress ($\bar{\sigma}_3$) through the thickness of a simply supported, square (0/90/0) laminate under sinusoidal transverse loading, $L/H = 4$.

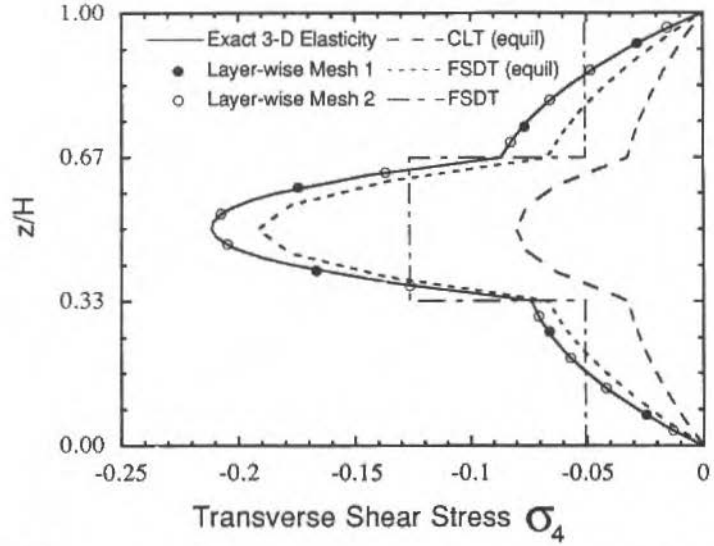

Figure 3. Distribution of transverse shear stress ($\bar{\sigma}_4$) through the thickness of a simply supported, square (0/90/0) laminate under sinusoidal transverse loading, $L/H = 4$.

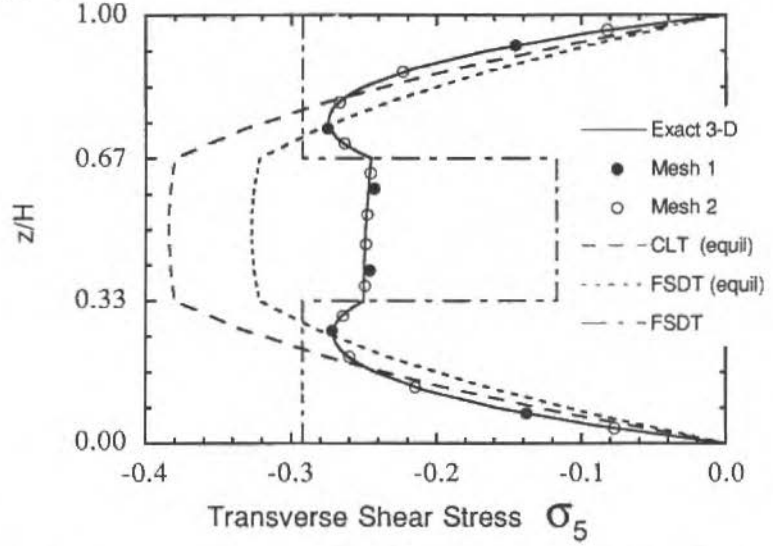

Figure 4. Distribution of transverse shear stress ($\bar{\sigma}_5$) through the thickness of a simply supported, square (0/90/0) laminate under sinusoidal transverse loading, $L/H = 4$.

mode. The equilibrium-based stresses (σ_4, σ_5) from the single-layer theories are in considerable error compared to the 3–D elasticity solutions; in fact, they predict maximum value of σ_5 in the middle layer while the 3–D elasticity gives in the outer layers. Note that the error introduced in the computation of the inplane stresses ($\sigma_1, \sigma_2, \sigma_6$) through constitutive equations will influence the accuracy of the transverse stresses computed using the equilibrium equations. The transverse shear stress computed in the FSDT by constitutive equations is in qualitative agreement with the 3–D elasticity results. For all stresses, the layerwise theory yields accurate results.

Discussion

The numerical results discussed for a simply-supported square laminate (0/90/0) under sinusoidally distributed transverse load indicate that the single-layer theories do not yield accurate interlaminar stresses, while the layerwise theory of Reddy yields values that are in excellent agreement whith the 3–D elascticity solutions. The inaccuracy of the single-layer theories in the prediction of interlaminar and free-edge (not discussed here but can be found in Robbins and Reddy [30,32]) stress distributions will be amplified in laminates with higher degree of anisotropy and geometric and material discontinuities. Although different refined single-layer theories have been developed to improve stress distributions, it remains that none of the single-layer theories can give accurate interlaminar stresses because they are not based on 3–D kinematics. The layerwise theory of Reddy is a 3–D kinematic theory with a 2–D type data structure that saves computational time compared to the 3–D displacement finite element model.

While the finite element model based on the layerwise theory of Reddy allows an accurate determination of 3–D stress fields, it is computationally expensive compared to the single-layer theories. Therefore, the use of the layer-wise elements in the modeling of a practical laminated structure is precluded, even with the present day supercomputers. On the other hand, it is not necessary to model entire structure with such refined elements. Use of the 3–D or layerwise elements can be restricted to local regions of a structure where 3–D stress fields exist, and the single-layer elements can be used in the remaining part of the structure. Such an approach is called a *global/local approach* (see Reddy

[18]). A hierarquical global/local computational procedure based on *variable kinematic finite elements* is discussed in the next section.

VARIABLE KINEMATIC FINITE ELEMENTS

The variable kinematic, finite element is developed by superimposing several types of assumed displacement fields within the finite element domain. In general, the multiple assumed displacement field can be expressed as,

$$u_\alpha(\xi,\eta,\zeta) = u_\alpha^{ESL}(\xi,\eta,\zeta) + u_\alpha^{LW}(\xi,\eta,\zeta) + u_\alpha^{D}(\xi,\eta,\zeta) \quad (\alpha = 1,2,3) \qquad (10)$$

where u_1 and u_2 are the local in-plane displacement components, and u_3 is the local transverse displacement component. The coordinates ξ and η represent the local curvilinear in-plane coordinates and ζ is the local transverse coordinate. The underlying foundation of the displacement field is provided by $u_\alpha^{ESL}(\xi,\eta,\zeta)$ which represents the assumed displacement field for any desired "equivalent single-layer" theory (e.g., the first order shear deformation theory). The second term $u_\alpha^{LW}(\xi,\eta,\zeta)$ represents the assumed displacement field for any desired layerwise theory (e.g., the layerwise theory of Reddy). The layerwise displacement field is included as an incremental enhancement to the basic ESL displacement field, so that the element can have full 3-D modeling capability when needed. Depending on the desired level of accuracy, the element can use all, part, or none of the layerwise field to create a series of different elements having a wide range of kinematic complexity. For example, discrete layer transverse shear effects can be added to the element by including $u_1^{LW}(\xi,\eta,\zeta)$ and $u_2^{LW}(\xi,\eta,\zeta)$, resulting in a type I layerwise element (or LW1 element). Further, discrete layer transverse normal effects can be added to the element by also including $u_3^{LW}(\xi,\eta,\zeta)$, resulting in a type II layerwise element (or LW2 element). Finally, $u_\alpha^{D}(\xi,\eta,\zeta)$ represents a simple displacement field that is piecewise constant with respect to the thickness coordinate and is used to model the kinematics of multiple delaminations [32,33]. Displacement continuity is maintained between these different types of elements by simply enforcing certain homogeneous essential boundary conditions, thus eliminating the need for multi-point constraints, penalty function methods, or special transition elements. Such variable kinematic plate elements have been developed by Robbins and Reddy [34] and show much potential for a wide variety of global/local composite plate problems; however, the concept needs to be extended to general composite shells.

To demonstrate the accuracy and efficiency of the variable kinematic finite elements, a global/local analysis is performed to determine the nature of the free edge stress field of the free edge effect in a thick, symmetric angle-ply laminate under imposed axial extension. Consider a thick, symmetric, angle-ply laminate $(45/-45)_s$ subjected to axial displacements on the ends. The laminate has a length of $2L$, width $2W$, and thickness $4h$, with $L = 10\ W$ and $W = 8h$ (see Figures 5 and 6). Each of the four material layers is of equal thickness h, and is idealized as a homogeneous, orthotropic material with the following properties expressed in the material coordinate system:

$$E_L = 20 \times 10^6 psi, \quad E_T = E_Z = 2.1 \times 10^6 psi\ ,$$

$$G_{LT} = G_{LZ} = 0.85 \times 10^6 psi, \quad \mu_{LT} = \mu_{LZ} = \mu_{TZ} = 0.21$$

where subscript L denotes the direction parallel to the fibers, subscript T denotes the in-plane direction perpendicular to the fibers, and subscript z denotes the out-of-plane direction. The origin of the global coordinate system coincides with the centeroid of the 3–D composite laminate. The x-coordinate is taken along the length of the laminate; the y-coordinate is taken along the width of laminate; and the z-coordiante is taken through the thickness of the laminate. Since the laminate is symmetric about the xy-plane, only the upper half of the laminate is modeled. Thus the computational domain is defined by $(-L \le x \le L, -W \le y \le W, 0 \le z \le 2h)$. The displacement boundary conditions for this problem are:

$$u_1(L, y, z) = u_0, \quad u_1(-L, y, z) = 0\ ,$$

$$u_2(-L, 0, 0) = 0, \quad u_2(L, 0, 0) = 0\ ,$$

$$u_3(x, y, 0) = 0$$

The variable kinematic finite elements are used in a global/local analysis to determine interlaminar free edge stresses near the middle of one of the two free edges (see Figures 5 and 6). The global region is modeled using first order shear deformable elements; the local region is modeled with $LW2$ elements in order to capture the 3–D stress state near the free edge. Five different finite element meshes are used. The in-plane discretization for all five meshes is exactly the same, consisting of a 5×11 mesh of eight-node quadratic 2–D finite elements.

All elements have the same length ($2L/5$). However, the width of the elements decreases as the free edge at (x, W, z) is approached. The widths of the eleven rows of elements, as one moves away from the refined free edge are: $h/16$, $h/16$, $h/8$, $h/4$, $h/2$, h, h, $2h$, $3h$, $3h$, $5h$, where h is the ply thickness. The five meshes differ only in the size of the local region that is discretized with $LW2$ elements. The $LW2$ elements used in the local region employ eight quadratic layers through the laminate thickness (four per material layer). The thickness of the numerical layers decreases as the $(+45/-45)$ interface is approached. From bottom to top, the layer thicknesses are $0.533h$, $0.267h$, $0.133h$, $0.083h$, $0.083h$, $0.133h$, $0.267h$, $0.533h$ (see Figure 6).

The five meshes used in this problem are summarized below.

Mesh 1: 3×4 local mesh of $LW2$ elements, centered about the point $(0, W, 0)$. The $LW2$ elements extend a distance of $h/2$ away from the free edge (2354 active global degrees of freedom).

Mesh 2: 3×5 local mesh of $LW2$ elements, centered about the point $(0, W, 0)$. The $LW2$ elements extend a distance of h away from the free edge (2740 active global degrees of freedom).

Mesh 3: 3×6 local mesh of $LW2$ elements, centered about the point $(0, W, 0)$. The $LW2$ elements extend a distance of $2h$ away from the free edge (3226 active global degrees of freedom).

Mesh 4: 3×7 local mesh of $LW2$ elements, centered about the point $(0, W, 0)$. The $LW2$ elements extend a distance of $3h$ away from the free edge (3512 active global degrees of freedom).

Mesh 5: 5×11 mesh of $LW2$ elements in the entire domain. This mesh is used as a control mesh for comparison. (9116 active global degrees of freedom).

Figures 7 and 8 show the distribution of the interlaminar stress σ_{xz} and σ_{zz}, respectively, through the laminate thickness. All stresses are nondimensionalized by multiplying them by the factor $(20\varepsilon_0/E_L$, where ε_0 is the nominal applied axial strain of $u_0/2L$). The stresses are computed at the reduced Gauss points nearest the middle of the refined free edge, i.e., along the line $(-0.115L,\ 0.998W, z)$. In Figure 7, all four global/local meshes compare very

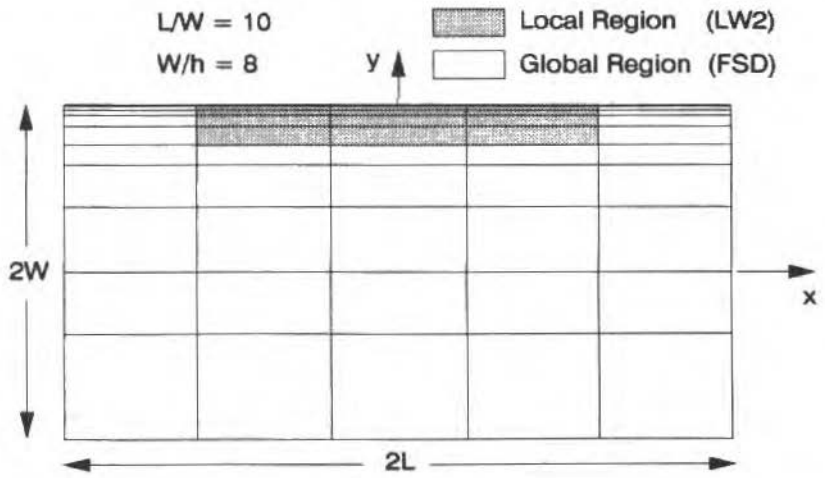

Figure 5. In-plane discretization of a $(45/-45)_s$ laminate under axial extension ($LW2$ = Layerwise elements; FSD = single-layer, first-order shear deformable elements).

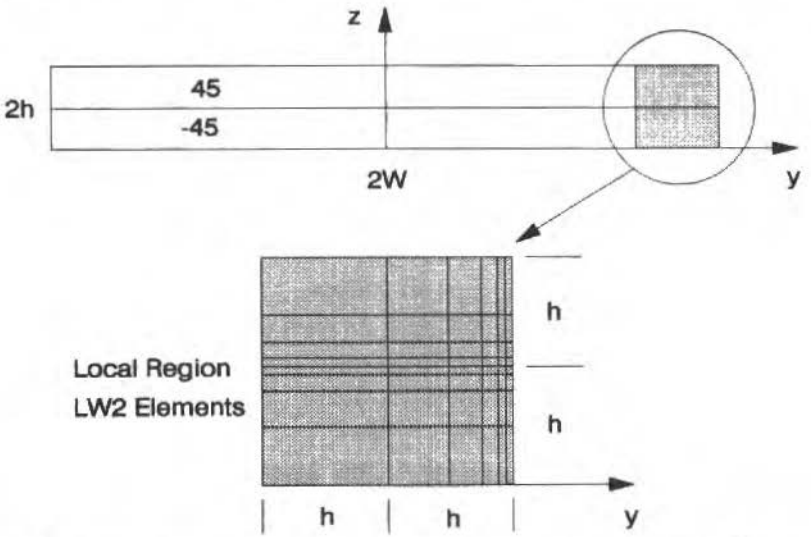

Figure 6. Laminate cross section showing layerwise discretization of the local region.

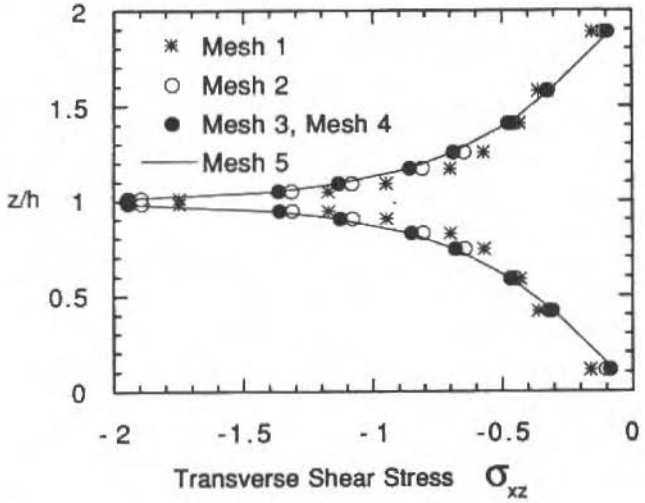

Figure 7. Interlaminar shear stress distribution near the free edge of a $(+45/-45)_s$ laminate under axial extension.

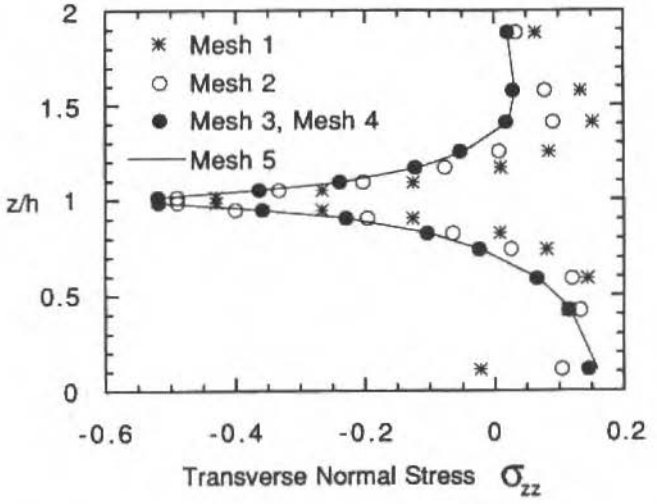

Figure 8. Interlaminar shear stress distribution near the free edge of a $(+45/-45)_s$ laminate under axial extension.

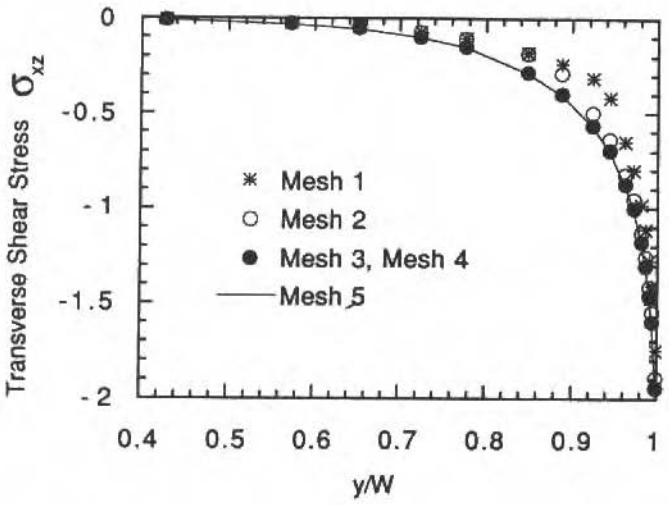

Figure 9. Interlaminar shear stress distribution across the width of a $(+45/-45)_s$ laminate under axial extension.

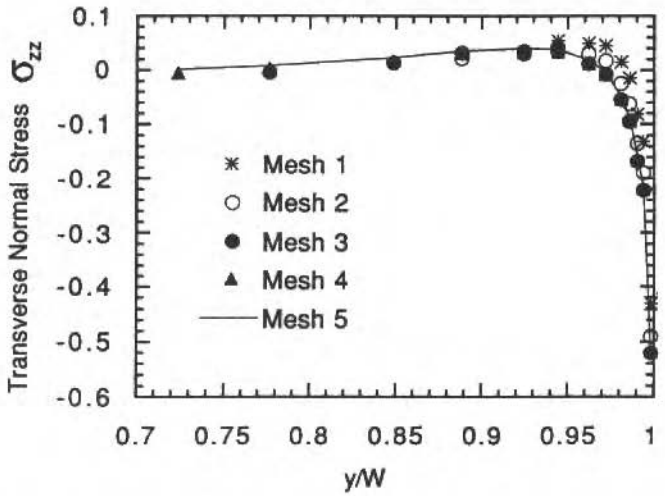

Figure 10. Interlaminar shear stress distribution across the width of a $(+45/-45)_s$ laminate under axial extension.

well with the control mesh. In Figure 8, meshes 1 and 2 show some error; however, the distributions are qualitatively similar to the control mesh. Meshes 3 and 4 are practically indistinguishable from the control mesh.

Figures 9 and 10 show the distribution of the interlaminar stresses σ_{xz} and σ_{zz}, respectively, across the width of the laminate near the $(+45/-45)$ interface. The stresses are computed at the reduced Gauss points closest to the line $(0, y, h)$, i.e., along the line $(-0.115L, y, 1.014h)$. In both Figures 9 and 10, the interlaminar stresses computed with meshes 3 and 4 are very close to the stresses obtained with the control mesh. Once again, the stresses computed with meshes 1 and 2 show a slight error; however, the distributions are qualitatively similar to the other meshes.

CONCLUSIONS

The results of the above example problem suggest that highly accurate free edge stress fields can be economically obtained using the variable kinematic elements. As long as the local region completely encompasses the boundary layer region where the interlaminar stresses are significant (i.e., meshes 3 and 4), the global/local solution is indistinguishable from the control solution. Even if the region does not extend the entire width of the boundary layer region (i.e., meshes 1 and 2), the global/local solution was qualitatively similar to the control solution, and the quantitative error was relatively small.

While the use of variable kinematic elements allow regions with different transverse discretizations to be joined together, they still require that the in-plane discretizations be compatible. Thus the localized regions of layerwise elements require the two-dimensional global mesh to contain transition zones to connect the coarse global mesh to the highly refined local mesh. These transition zones are troublesome for several reasons:

1. The mesh of transition zones is more difficult to generate than the more regularly discretized regions, thus complicating the mesh generation process.

2. Transition zones often result in highly distorted elements, possibly causing numerical difficulties.

3. Transition regions often result in excessive discretization for noncritical regions, thus wasting computational resources.

4. Transition regions greatly reduce the adaptability of the model since the entire finite element mesh has to be reformed each time the localized region of interest is changed.

To circumvent the difficulties associated with transition zones, the recently developed mesh superposition method (see [35]) will be used to allow two-dimensional subregions with different in-plane discretizations to be joined together. This method allows an independent, refined local mesh to be superimposed on an existing global mesh.. The displacement field within the region of superposition is the sum of the displacement fields from both meshes. The displacements in the local mesh serve as incremental enhancements to the underlying global displacement field. In recently reported applications of the mesh superposition method [36,37], both the global mesh and the superimposed local mesh use finite elements based on the same mathematical models. In contrast, the present proposed application of the mesh superposition method involves overlaying a global mesh of ESL elements with an independent, local mesh of variable kinematic elements. The resulting finite element model would allow abrupt changes in mesh discretization and abrupt changes in mathematical model type. The local overlay mesh can include ESL elements and/or layerwise elements. The transition regions are no longer necessary. Displacement continuity between the global and local regions is maintained by simply enforcing homogeneous essential boundary conditions on the global/local boundary. That is, the added incremental displacements are zeroed on the global/local boundary. This process can easily be automated and removed from further concern. Thus the inconvenience of using multi-point constraints, penalty function methods, or special transition elements is circumvented.

One of the primary advantages of the mesh superposition method is that local meshes can easily be created and superimposed anywhere within the original global mesh. Thus, several different potential "hot spots" can be investigated (simultaneously or sequentially) without having to reformulate the global mesh.

Within the context of the proposed computational procedure, several topics require special investigation (see [34,38]):

1. Investigate the effect of maintaining transverse displacement continuity across boundaries separating regions that explicitly model transverse normal strain and other regions that implicity model transverse normal strain.

2. Investigate the size and mesh density of layerwise mesh overlays necessary for accurate local stress field determination.

3. Investigate efficient solution techniques that capitalize on the hierarchical nature of the model, e.g., an independent global solution might serve as a starting vector for an iterative solution technique. This would be particularly advantageous for geometrically nonlinear problems in which local refinement is unlikely to drastically change the global behavior.

4. Develop error estimators to determine when local stresses can be extracted using post-processing instead of incorporating additional degrees of freedom in the structural model.

5. Develop strategies for modeling mechanisms of progressive failure.

6. Develop appropiate preconditioners to assure good convergence of iterative solvers, particularly for highly nonlinear problems.

ACKNOWLEDGEMENTS

The research reported herein was carried out on research projects from the NASA Langley Research Center Grant NAG-1030 and the National Science Foundation Grant INT-8908307.

REFERENCES

[1] REDDY, J.N. On Refined Computational Models of Composite Laminates", International Journal for Numerical Methods in Engineering, Vol. 27, pp. 361–382, 1989.

[2] REDDY, J.N. A Review of Refined Theories of Laminated Composite Plates", Shock & Vibration Digest, Vol. 22, No. 7, pp. 3–17, 1990.

[3] REDDY, J.N. On Refined Theories of Composite Laminates, Meccanica, Vol. 25, No. 4, pp. 230–238, 1990.

[4] MAU, S.T. A Refined Laminated Plate Theory, Journal of Applied Mechanics, Vol. 40, No. 2, pp. 606–607, 1973.

[5] REHFIELD, L.W. and MURTHY, P.L.N. Toward a New Engineering Theory of Bending: Fundamentals, AIAA Journal, Vol. 20, No, 5, pp. 693-699, 1982.

[6] REHFIELD, L.W. and VALISETTY, R.R. A Comprehensive Theory for Planar Bending of Composite Laminates, Computers & Structures, Vol. 15, pp. 441–447, 1983.

[7] MURAKAMI, H. Laminated Composite Plate Theory with Improved In-Plane Responses, Journal of Applied Mechanics, Vol. 53, No. 3, pp. 661–666, 1986.

[8] TOLEDANO, A. and MURAKAMI, H. A Higher-Order Laminated Composite Plate Theory with Improved In-Plane Responses, International Journal of Solids and Structures, Vol. 23, No. 1, pp. 111–131, 1987.

[9] HINRICHSEN, R.L. and PALAZOTTO, A.N. Nonlinear Finite Element Analysis of Thick Composite Plates Using Cubic Spline Functions, AIAA Journal, Vol. 24, No. 11, pp. 1836–1842, 1986.

[10] SREENIVAS, S. A Refined Analysis of Composite Laminates, Journal of Sound & Vibration, Vol. 30, No. 4, pp. 495–507, 1973.

[11] EPSTEIN, M. and GLOCKNER, P.G. Nonlinear Analysis of Multilayered Shells, International Journal of Solids & Structures, Vol. 13, pp. 1081–1089, 1977.

[12] EPSTEIN, M. and HUTTELMAIER, H.P. A Finite Element Formulation for Multilayered and Thick Plates, International Journal of Solids & Structures, Vol. 16(5), pp. 645–650, 1983.

[13] DI SCIUVA, M. Bending Vibration and Buckling of Simply Supported Thick Multilayered Orthotropic Plates: An Evaluation of a New Displacement Model, Journal of Sound & Vibration, Vol. 105, No. 3, pp. 425–442, 1986.

[14] DI SICIUVA, M. An Improved Shear Deformation Theory for Moderately Thick Multilayered Anisotropic Shells and Plates, Journal of Applied Mechanics, Vol. 54, No. 3, pp. 589–596, 1987.

[15] REDDY, J.N. A Generalization of Two-Dimensional Theories of Laminated Composite Plates, Communications in Applied Numerical Methods, Vol. 3, pp. 173–180, 1987.

[16] REDDY, J.N. On the Generalization of Displacement-Based Laminate Thoeries, Applied Mechanics Reviews, Vol. 42, No. 11, Part 2, S213–S222 (1989).

[17] REDDY, J.N. A Layerwise Shell Theory with Applications to Buckling and Vibration of Cross-Ply Laminated Stiffened Circular Cylindrical SHells, Research Report CCMS-92-01, Virginia Polytechnic Institute and State University, Blacksburg, VA.

[18] REDDY, J.N., On Computational Schemes for Global-Local Stress Analysis, Workshop on Computational Methods for Structural Mechanics and Dynamics, NASA Langley Research Center, Hampton, VA, 29–31 June 1985.

[19] BASSET, A.B. On the Extension and Flexure of Cylindrical and Spherical Thin Elastic Shells, Philosophical Transactions of the Royal Society (London), Vol.181, series A, No. 6, pp. 433–480, 1890.

[20] HENCKY, H. Uber due Berucksichtigung der Schbvedrzerrung in Ebenen Platten, Ingenier Archieve, Vol.16, pp. 72–76, 1947.

[21] HILDEBRAND, F.B., REISSNER, E. and THOMAS, G.B. Notes on the Foundation of the Theory of Small Displacements of Orthotropic Shells, NACA TN-1833, Washington, D.C., 1949.

[22] MINDLIN, R.D. Influence of Rotatory Inertia and Shear on Flexural Motions of Isotropic, Elastic Plates, Journal of Applied Mechanics, Vol.18, pp. 31–38, 1951.

[23] LO, K.H., CHRISTENSEN, R.M. and WU, E.M. A High-Order Theory of Plate Deformation: Part 1: Homogeneous Plates, Part 2: Laminated Plates, Journal of Applied Mechanics, Vol.44, No.4, pp. 663-676, 1977.

[24] VALSOV, B.F., Ob Uravnieniakh Izgiba Plastinok (On the Equations of the Bending of Plates), Dokla. Aka. Nauk Azerbeijanskoi SSR, Vol.3, pp. 955–959, 1957.

[25] JEMIELITA, G. Techniczna Teori Plyt Sredniej Grubbosci (Technical Theory of Plates with Moderate Thickness), Rozprawy Inzynierskie, Polska Akademia Nauk, Vol.23, No.3, pp. 483–499, 1975.

[26] KRISHNA MURTY, A.V. Higher-Order Theory for Vibration of Thick Plates, AIAA Journal, Vol.15, No.12, pp. 1823–1824, 1977.

[27] REDDY, J.N. A Simple Higher-Order Theory for Laminated Composite Plates, Journal of Applied Mechanics, Vol.51, pp. 745–752, 1984.

[28] REDDY, J.N. A Refined Nonlinear Theory of Plates with Transverse Shear Deformation, International Journal of Solids & Structures, Vol.20, Nos.9/10, pp. 881–896, 1985.

[29] REDDY, J.N. A General Non-Linear Third-Order Theory of Plates with Moderate Thickness, Journal of Non-Linear Mechanics, Vol.25, No.6, pp. 677–686, 1990.

[30] ROBBINS, D.H., Jr. and REDDY, J.N. Modeling of Thick Composites Using a Layerwise Laminate Theory, International Journal of Numerical Mehtods in Engineering, in press.

[31] PAGANO, N.J. Exact Solutions for Rectangular Bidirectional Composites and Sandwich Plates, Journal of Composite Materials, Vol.4, pp. 20–34, 1970.

[32] ROBBINS, D.H., Jr. and REDDY, J.N. On the Modeling of Free-Edge Stress Fields and Delaminations in Thick Composite Laminates, in Composite Structures for Aerospace Applications, Eds. J.N. Reddy and A.V. Krishna Murty, Narosa Publishing House, New Delhi, India, 1992.

[33] ROBBINS, D.H. Jr. and REDDY, J.N. The Effect of Kinematic Assumptions on the Computed Strain Energy Release Rates for Delaminated Composite Plates, Journal of Modeling and Scientific Computing, in press.

[34] ROBBINS, DH., JR. and REDDY, J.N. Global/Local Analysis of Laminated Composite Plates Using Variable Kinematic Finite Elements. AIAA/ASME/ASCE/AHS/ASC 33rd Structures, Structural Dynamics, and Materials (SDM) Conference, Dallas, Texas, 13–15 April 1992.

[35] FISH, J. The *s*-Version of the Finite Element Method, Computers and Structures, Vol.43, No.3, pp. 539–547, 1992.

[36] FISH, J. and MARKOLEFAS, S. The *s*-Version of the Finite Element Method for Multilayer Laminates, in International Journal of Numerical Methods in Engineering, Vol.33, No.5, pp. 1081–1105, April 1992.

[37] KIM, Y.H. LEVIT, I. and STANELY, G. A Finite Element Adaptive Mesh Refinement Technique that Avoids Multipoint Constraints and Transition Zones, ASME Winter Annual Meeting, December 2–6, 1991, Atlanta, Georgia.

[38] WHITCOMB, J.D. and WOO, K. Global/Local Finite Element Analysis of Geometrically Nonlinear Structures, Research Report 02/92-A-27-100, Offshore Technology Research Center, Texas A&M University, College Station, TX, 77843, February 1992.

RBCM – J. of the Braz.Soc.Mech.Sc. ISSN 0100-7386
Vol.XIV – nº 4 – pp. 327 – 345 – 1992 Impresso no Brasil

UNIFIED LAGRANGIAN DISPLACEMENT FORMULATION OF THE NON-LINEAR THEORY OF THIN SHELLS

FORMULAÇÃO LAGRANGIANA UNIFICADA BASEADA EM DESLOCAMENTOS DA TEORIA NÃO-LINEAR DE CASCAS FINAS

W. Pietraszkiewicz
Institute of Fluid-Flow Machinery
Polish Academy of Sciences
UL. Fiszera 14, 80-952 Gdańsk
Poland

ABSTRACT

Deformation of a thin shell is described entirely by three displacements of its reference surface. No restrictions are imposed on magnitudes of the displacements, rotations, strains and/or changes of curvatures of the surface. Explicit form of Lagrangian incremental shell equations is derived for arbitrary configuration-dependent external static surface and boundary loads as well as for arbitrary work-conjugate static and geometric boundary conditions. The most general form of the Lagrangian buckling equations for thin shells is presented.

Keywords: Shells ▪ Non-Linear Theory ▪ Incremental Formulations ▪ Buckling Equations

RESUMO

Neste trabalho o campo de deformações de uma casca fina é inteiramente descrito por três deslocamentos definidos em sua superfície de referência. Não há restrições impostas sobre as magnitudes dos deslocamentos, rotações, deformações e/ou variações de curvatura da superfície. Uma forma explicita das equações incrementais lagrangianas de cascas é obtida para carregamentos externos estáticos arbitrários, de superfície e de fronteira, dependentes da configuração, bem como para condições de contorno arbitrárias, geométricas e estáticas de trabalho-conjugado. A forma mais geral das equações lagrangianas de flambagem para cascas finas é apresentada.

Palavras-chave: Cascas ▪ Teoria Não-Linear ▪ Formulações Incrementais ▪ Equações de Flambagem

---

Invited Lecture Presented at 7th SIBRAT, Florianópolis, Brazil

INTRODUCTION

Within the field of thin shell theory hundreds of specialized versions of shell equations were proposed in the literature, each of them having a limited range of applications. The specialized versions are usually derived assuming different constraints on deformation or stress state in the shell space, restricting the magnitudes of strains, displacements or rotations, discussing only special material behaviour, shell geometry or external loads, using particular sets of independent field variables in the resulting boundary value problem etc., [14÷16].

The rapid development of computer hardware and software based on the finite element method makes it possible to solve more and more complex shell problems with sufficient accuracy. However, the shell finite elements available in the literature are usually based on some particular simplified versions of shell theory, and their applicability is restricted to the limited range of applicability of the shell theory itself. Any change in underlying version of shell theory results in the need of developing a new shell finite element, what makes the shell analysis so complex and time consuming.

The aim of this paper is to present a unified formulation of a wide class of non-linear theories of thin shells. In our development we apply only one apparent assumption: the deformation of the shell as a three-dimensional body is determined entirely by deformation of its reference surface. No restrictions are imposed here on magnitudes of the displacements, rotations, strains and/or changes of curvature of the reference surface. For different material behaviour the reduction from three-dimensional solid mechanics to the two-dimensional shell theory may have different analytic representation, which is treated here as part of constitutive relations of the shell.

Let us note that members of that class of shell theories are various versions of the classical linear and geometrically non-linear theory of thin isotropic elastic shells based on the Kirchhoff-Love type constraints [16]. Another example of member of that class is the bending theory of rubber-like shells developed in [22], where the three-dimensional shell deformation was expressed through deformation of its reference surface applying a relaxed normality hypothesis and incompressibility condition. Still another members of that class are some simple

versions of inelastic shell theory expressed entirely in terms of the reference surface deformation as well, as discussed in [20], for example.

A common feature of that class of shell theories is that their equilibrium conditions have the same form following from the principle of virtual displacements written for the reference surface. The geometry of undeformed reference surface is usually the only one which is known in advance, and an arbitrary deformation of the surface can always be described by components of the displacement vector $\mathbf{u}$ relative to the undeformed surface geometry. Therefore, the resulting boundary value problem of the shell can always be expressed in the Lagrangian description in terms of displacements as the only independent field variables.

The unified formulation of Lagrangian non-linear shell equations presented here is based on generalization of our results given in [19,15] for the geometrically non-linear theory of elastic shells, which were extended in [22] into the large-strain bending theory of rubber-like shells. Our Lagrangian shell equations (8), (9) are two-dimensionally exact for the shell reference surface. They are valid for arbitrary configuration-dependent external surface and boundary forces and moments, as well as for arbitrary work-conjugate set of static and geometric boundary conditions. In order to allow correct numerical implementation, the Lagrangian shell equations are presented in Section 4 in the consistent incremental form applying the general Newton-Kantorovich method [6] to the functional (6) of principle of virtual displacements. In particular, we take into account that, in general, the successive approximations to the unknown equilibrium state may not belong to the equilibrium path. This results in some unballanced forces (14) appearing explicitly at each iteration step. We managed to calculate explicitly Gateaux derivatives of all corresponding fields, and to derive the explicit form of the general Lagrangian incremental shell equations (24)÷(27). As a particular case of the incremental shell equations follows the explicit form of the most general buckling equations (28) for thin shells.

GEOMETRIC RELATIONS

In this report we apply the system of notation used by Pietraszkiewicz [14÷16].

Let the reference surface M of undeformed shell be defined by the position vector $\mathbf{r}(\theta^\alpha)$, where θ^α, $\alpha = 1, 2$, are surface curvilinear coordinates. On M we have the natural base vectors $\mathbf{a}_\alpha = \partial\mathbf{r}/\partial\theta^\alpha \equiv \mathbf{r}_{,\alpha}$, the (covariant components

of the surface) metric tensor $a_{\alpha\beta} = \mathbf{a}_\alpha \cdot \mathbf{a}_\beta$ with determinant $a = |a_{\alpha\beta}|$, the unit normal vector $\mathbf{n} = a^{-1/2}\mathbf{a}_1 \times \mathbf{a}_2$, the curvature tensor $b_{\alpha\beta} = -\mathbf{a}_\alpha \cdot \mathbf{n}_{,\beta}$ and the permutation tensor $\varepsilon_{\alpha\beta} = (\mathbf{a}_\alpha \times \mathbf{a}_\beta)\cdot\mathbf{n}$. The contravariant base vectors $\mathbf{a}^\alpha$ are defined through $\mathbf{a}_\alpha \cdot \mathbf{a}_\beta = \delta^\alpha_\beta$, and $a^{\alpha\beta} = \mathbf{a}^\beta \cdot \mathbf{a}^\beta$ are used to raise indices on M.

The boundary contour C of M consists of the finite set of piecewise smooth curves $\mathbf{r}(s) = \mathbf{r}[\theta^\alpha(s)]$, where s is the arc length along C. With each regular point $M \in C$ we associate the unit tangent vector $\mathbf{t} = d\mathbf{r}/ds \equiv \mathbf{r}' = t^\alpha \mathbf{a}_\alpha$ and the outward unit normal vector $\boldsymbol{\nu} = \mathbf{r}_{,\nu} = \mathbf{t} \times \mathbf{n} = \nu^\alpha \mathbf{a}_\alpha$, $\nu^\alpha = \varepsilon^{\alpha\beta} t_\beta$, where $(\,)_{,\nu}$ denotes the outward normal derivative at C.

Let $\bar{M}$ and $\bar{C}$ be deformed configurations of M and C defined by the position vectors $\bar{\mathbf{r}}(\theta^\alpha) = \mathbf{r}(\theta^\alpha) + \mathbf{u}(\theta^\alpha)$ and $\mathbf{r}[\theta(s)] = \mathbf{r}(s) + \mathbf{u}(s)$, respectively, where $\mathbf{u} = u_\alpha \mathbf{a}^\alpha + w\mathbf{n}$ is the displacement vector while θ^α and s are convected coordinates. With $\bar{M}$ and $\bar{C}$ we can associate analogously defined quantities, only now marked by an overbar: $\bar{\mathbf{a}}_\alpha$, $\bar{a}_{\alpha\beta}$, $\bar{a}$, $\bar{\mathbf{n}}$, $\bar{b}_{\alpha\beta}$, $\bar{\varepsilon}_{\alpha\beta}$, $\bar{\mathbf{a}}^\beta$, $\bar{a}^{\alpha\beta}$, $\bar{\mathbf{t}}$, $\bar{\boldsymbol{\nu}}$ etc. All the quantities can be expressed through the geometry of M or C and the displacement field $\mathbf{u}$ by relations presented in more detail in [15,16]. In particular, on $\bar{M}$ we have

$$\bar{\mathbf{a}}_\alpha = \bar{\mathbf{r}}_{,\alpha} = \mathbf{a}_\alpha + \mathbf{u}_{,\alpha}\,, \quad \bar{\mathbf{n}} = \frac{1}{2} j^{-1} \varepsilon^{\alpha\beta} \bar{\mathbf{a}}_\alpha \times \bar{\mathbf{a}}_\beta\,,$$

$$\bar{a}_{\alpha\beta} = a_{\alpha\beta} + 2\gamma_{\alpha\beta}, \quad \bar{b}_{\alpha\beta} = b_{\alpha\beta} - \kappa_{\alpha\beta},$$

$$\gamma_{\alpha\beta} = \frac{1}{2}(\bar{\mathbf{r}}_{,\alpha}\cdot\bar{\mathbf{r}}_{,\beta} - a_{\alpha\beta}), \quad \kappa_{\alpha\beta} = \bar{\mathbf{r}}_{,\alpha}\cdot\bar{\mathbf{n}}_{,\beta} + b_{\alpha\beta}, \tag{1}$$

$$j^2 = \frac{\bar{a}}{a} = \frac{1}{2}\,\varepsilon^{\alpha\lambda}\varepsilon^{\beta\kappa}\bar{a}_{\alpha\beta}\bar{a}_{\lambda\kappa}\,,$$

$$\bar{\mathbf{a}}^\alpha = \bar{a}^{\alpha\beta}\bar{\mathbf{a}}_\beta, \qquad \bar{a}^{\alpha\beta} = j^{-2}[(1 + 2\gamma^\kappa_\kappa)\, a^{\alpha\beta} - 2\gamma^{\alpha\beta}]\,,$$

where $\gamma_{\alpha\beta}$ and $\kappa_{\alpha\beta}$ are the Lagrangian symmetric surface strain measures.

Along the deformed shell boundary contour $\bar{C}$ we have [16,8]

$$\bar{\mathbf{r}}' = \mathbf{t} + \mathbf{u}' = \bar{a}_t \bar{\mathbf{t}}\,, \quad \bar{\mathbf{n}} = j^{-1}\bar{\mathbf{r}}_{,\nu} \times \bar{\mathbf{r}}'\,,$$
$$\bar{\mathbf{r}}_{,\nu} = \boldsymbol{\nu} + \mathbf{u}_{,\nu} = \bar{a}_t^{-1}(j\bar{\boldsymbol{\nu}} + 2\gamma_{\nu t}\bar{\mathbf{t}})\,,$$

$$\bar{a}_t = |\bar{\mathbf{r}}'| \,, \qquad 2\gamma_{\nu t} = \bar{\mathbf{r}}_{,\nu} \cdot \bar{\mathbf{r}}' \,, \tag{2}$$
$$j^2 = \frac{\bar{a}}{a} = |\mathbf{r}_{,\nu}|^2 |\bar{\mathbf{r}}'|^2 - (\bar{\mathbf{r}}_{,\nu} \cdot \bar{\mathbf{r}}')^2 \,,$$
$$\bar{\mathbf{a}}^\beta = j^{-1}(\bar{a}_t \nu^\beta - 2\gamma_{\nu t} \bar{a}_t^{-1} t^\beta)\bar{\boldsymbol{\nu}} + \bar{a}_t^{-1} t^\beta \bar{\mathbf{t}} \,.$$

All the vectors in (1) and (2) are understood to be expressed through components with respect to the known bases $\mathbf{a}_\alpha$, $\mathbf{n}$ or $\boldsymbol{\nu}$, $\mathbf{t}$, $\mathbf{n}$ of M or C, respectively.

DISPLACEMENT SHELL EQUATIONS

Within the class of non-linear theories of thin shells discussed here the deformation of the shell as a three-dimensional body is assumed to be determined entirely by deformation of its reference surface. Therefore, the equilibrium conditions of the shell should follow from the Lagrangian principle of virtual displacements for the reference surface [15,8,17]

$$G[\mathbf{u}; \delta\mathbf{u}] = \int_M \int (N^{\alpha\beta} \delta\gamma_{\alpha\beta} + M^{\alpha\beta} \delta\kappa_{\alpha\beta}) dA -$$
$$- \int_M \int (\mathbf{p} \cdot \delta\mathbf{u} + \mathbf{h} \cdot \delta\bar{\mathbf{n}}) dA - \int_{C_f} (\mathbf{T} \cdot \delta\mathbf{u} + \mathbf{H} \cdot \delta\bar{\mathbf{n}}) ds = 0 \,, \tag{3}$$

which is valid for all kinematically admissible virtual displacements $\delta\mathbf{u}$. In (3) $N^{\alpha\beta}$ and $M^{\alpha\beta}$ are the internal 2nd Piola-Kirchhoff type stress and couple resultants, $\mathbf{p}(\mathbf{u})$ and $\mathbf{h}(\mathbf{u})$ are the external surface force and moment vectors, per unit area of M, $\mathbf{T}(\mathbf{u})$ and $\mathbf{H}(\mathbf{u})$ are the external boundary force and moment vectors, per unit length of C, while δ is the symbol of variation.

Within M variations of $\gamma_{\alpha\beta}$, $\kappa_{\alpha\beta}$ and $\bar{\mathbf{n}}$ are expressed through $\mathbf{u}$ and $\delta\mathbf{u}$ by

$$\delta\gamma_{\alpha\beta} = \frac{1}{2}(\delta\mathbf{u}_{,\alpha} \cdot \bar{\mathbf{a}}_\beta + \bar{\mathbf{a}}_\alpha \cdot \delta\mathbf{u}_{,\beta}) \,,$$
$$\delta\kappa_{\alpha\beta} = \frac{1}{2}(\bar{\mathbf{n}}_{,\alpha} \cdot \delta\mathbf{u}_{,\beta} + \bar{\mathbf{n}}_{,\beta} \cdot \delta\mathbf{u}_{,\alpha} + \bar{\mathbf{a}}_\alpha \cdot \delta\bar{\mathbf{n}}_{,\beta} + \bar{\mathbf{a}}_\beta \cdot \delta\bar{\mathbf{n}}_{,\alpha}) \,, \tag{4}$$
$$\delta\bar{\mathbf{n}} = -\bar{\mathbf{a}}^\beta (\bar{\mathbf{n}} \cdot \delta\mathbf{u}_{,\beta}) \,.$$

At the boundary contour $\bar{C}$ the vector $\bar{\mathbf{n}} = \bar{\mathbf{n}}(s)$ should satisfy the constraints $\bar{\mathbf{r}}' \cdot \bar{\mathbf{n}} = 0$ and $\bar{\mathbf{n}} \cdot \bar{\mathbf{n}} = 1$. Therefore, $\bar{\mathbf{n}}$ on $\bar{C}$ should be expressible

through the geometry of C, three translations $\mathbf{u}(s)$ and one scalar function $\varphi(s) = \varphi[\mathbf{u}_{,\nu}(s),\ \mathbf{u}'(s)]$ describing the rotational deformation of the shell lateral boundary surface.

The general structure of the function φ, and corresponding four work-conjugate static and geometric boundary conditions compatible with the principle of virtual displacement (3), were discussed by Makowski and Pietraszkiewicz [8]. In particular, three physically reasonable special cases of φ were noted in [8]: 1) $n_\nu = \bar{\mathbf{n}}\cdot\boldsymbol{\nu} = j^{-1}(\mathbf{u}'\times\boldsymbol{\nu}-\mathbf{n})\cdot\mathbf{u}_{,\nu}$ introduced in [19], 2) $v_\nu = \bar{a}_t^{-2}(\bar{\mathbf{n}}-\mathbf{n})\cdot(\bar{\mathbf{r}}'\times\bar{\mathbf{n}})$ introduced in [13], and 3) ω_t, the angle of total rotation of the boundary, defined in [14] through displacements by $2\cos\omega_t = \bar{\boldsymbol{\nu}}\cdot\boldsymbol{\nu}+\bar{\mathbf{t}}\cdot\mathbf{t}+\bar{\mathbf{n}}\cdot\mathbf{n}-1$. In what follows all transformations leading to displacement shell equations are performed applying n_ν as the fourth parameter of boundary deformation. Corresponding results for v_ν and ω_t taken as the fourth parameters of boundary deformation are given in [8,18], respectively.

Thus, in terms of $\mathbf{u}$ and n_ν the variation of $\bar{\mathbf{n}}$ of $\bar{C}$ takes the form [15]

$$\delta\bar{\mathbf{n}} = a_\nu^{-1}[(\bar{\boldsymbol{\nu}}\times\bar{\mathbf{n}})\bar{\mathbf{n}}\cdot\delta\mathbf{u}' + (\bar{\mathbf{r}}'\times\bar{\mathbf{n}})\delta n_\nu]\ , \qquad a_\nu = (\bar{\mathbf{r}}'\times\bar{\mathbf{n}})\cdot\boldsymbol{\nu}\ , \tag{5}$$

where $\delta n_\nu = \delta n_\nu[\mathbf{u}_{,\nu}, \mathbf{u}'; \delta\mathbf{u}_{,\nu}, \delta\mathbf{u}']$ is non-linear in $\mathbf{u}_{,\nu}$, $\mathbf{u}'$ but is linear in $\delta\mathbf{u}_{,\nu}$, $\delta\mathbf{u}'$.

Introducing (4) and (5) into (3), applying the Stokes' theorem to the surface integrals, then applying integration by parts to the line integrals we can transform (3) into [15]

$$\begin{aligned} G[\mathbf{u};\delta\mathbf{u}] = &-\int_M\int\{\mathbf{T}^\beta|_\beta + \mathbf{p} + [(\mathbf{h}\cdot\bar{\mathbf{a}}^\beta)\bar{\mathbf{n}}]_{|\beta}\}\cdot\delta\mathbf{u}dA + \\ &+\int_{C_f}\{[\mathbf{T}^\beta\nu_\beta + \mathbf{F}' - \mathbf{T} - \mathbf{F}^{*\prime} + (\mathbf{h}\cdot\bar{\mathbf{a}}^\beta\nu_\beta)\bar{\mathbf{n}}]\cdot\delta\mathbf{u} + (M - M^*)\delta n_\nu\}ds + \\ &+\sum_n(\mathbf{F}_n - \mathbf{F}_n^*)\cdot\delta\mathbf{u}_n = 0\ , \end{aligned} \tag{6}$$

where

$$\begin{aligned} \mathbf{T}^\beta &= N^{\alpha\beta}\bar{\mathbf{a}}_\alpha + M^{\alpha\beta}\bar{\mathbf{n}}_{,\alpha} + \{[M^{\kappa\rho}\bar{\mathbf{a}}_\kappa)_{|\rho}\cdot\bar{\mathbf{a}}^\beta\}\ \bar{\mathbf{n}}\ , \\ \mathbf{F} &= -a_\nu^{-1}[(\bar{\mathbf{n}}\times\bar{\mathbf{a}}_\alpha)\cdot\boldsymbol{\nu}]M^{\alpha\beta}\nu_\beta\bar{\mathbf{n}}\ , \qquad \mathbf{F}^* = -a_\nu^{-1}[(\bar{\mathbf{n}}\times\mathbf{H})\cdot\boldsymbol{\nu}]\bar{\mathbf{n}}\ , \\ M &= a_\nu^{-1}(\bar{\mathbf{n}}\times\bar{\mathbf{a}}_\alpha)\cdot\bar{\mathbf{r}}'M^{\alpha\beta}\nu_\beta\ , \qquad M^* = a_\nu^{-1}(\bar{\mathbf{n}}\times\mathbf{H})\cdot\bar{\mathbf{r}}'\ , \\ \mathbf{F}_n &= \mathbf{F}(s_n+0) - \mathbf{F}(s_n-0)\ , \qquad \mathbf{u}_n = \mathbf{u}(s_n)\ . \end{aligned} \tag{7}$$

Since (6) should be satisfied identically for all kinematically admissible $\delta\mathbf{u}$, from (6) follow the Lagrangian equilibrium equations and static boundary and corner conditions

$$\begin{aligned}
&\mathbf{T}^{\alpha}|_{\beta} + \mathbf{p} + [(\mathbf{h}\cdot\bar{\mathbf{a}}^{\beta})\bar{\mathbf{n}}]|_{\beta} = \mathbf{0} \qquad \text{in } M\ , \\
&\mathbf{T}^{\beta}\nu_{\beta} + \mathbf{F}' = \mathbf{T} + \mathbf{F}^{*\prime} - (\mathbf{h}\cdot\mathbf{a}^{\beta}\nu_{\beta})\bar{\mathbf{n}}\ , \qquad M = M^{*} \qquad \text{on } C_f\ , \\
&\mathbf{F}_n = \mathbf{F}_n^{*} \qquad \text{at each corner } M \in C_f\ .
\end{aligned} \tag{8}$$

Corresponding work-conjugate geometric boundary conditions are

$$\mathbf{u}(s) = \mathbf{u}^{*}(s)\ , \qquad n_{\nu}(s) = n_{\nu}^{*}(s) \qquad \text{on } C_u\ . \tag{9}$$

All the vectors appearing in (8), (9) are understood to be expressed through components with respect to known bases $\mathbf{a}_{\alpha}$, $\mathbf{n}$ or $\boldsymbol{\nu}$, $\mathbf{t}$, $\mathbf{n}$ of undeformed M or C, respectively.

In the case of an elastic material the constitutive equations for $N^{\alpha\beta}$, $M^{\alpha\beta}$ compatible with (3) are

$$N^{\alpha\beta} = \frac{\partial\Sigma}{\partial\gamma_{\alpha\beta}}\ , \qquad M^{\alpha\beta} = \frac{\partial\Sigma}{\partial\kappa_{\alpha\beta}}\ , \tag{10}$$

where $\Sigma = \Sigma(\gamma_{\alpha\beta}, \kappa_{\alpha\beta})$ is a two-dimensional strain energy function defined over M. In the particular case of isotropic elastic material undergoing small strains (but unrestricted rotations) the strain energy Σ is, to the first approximation, a quadratic function of the surface strain measures, [5,14,16]. In the particular case of large-strain bending theory of shells made of isotropic elastic incompressible rubber-like materials the structure of Σ, to the first approximation, is given in [22]. Therefore, for each particular elastic material the constitutive equations can explicitly be expressed in the form $N^{\alpha\beta} = N^{\alpha\beta}[\gamma_{\alpha\beta}(\mathbf{u}), \kappa_{\alpha\beta}(\mathbf{u})]$, $M^{\alpha\beta} = M^{\alpha\beta}[\gamma_{\alpha\beta}(\mathbf{u}), \kappa_{\alpha\beta}(\mathbf{u})]$ for any $\mathbf{u}$. As a result, the boundary value problem (8), (9) of the Lagrangian non-linear theory of thin elastic shells is expressed entirely in terms of displacements $\mathbf{u}$ as the only independent field variables.

It should be pointed out that the underlying principle of virtual displacements (3) is an incremental principle, which itself does not reguire $N^{\alpha\beta}$ and $M^{\alpha\beta}$ to be derivable from the strain energy function. Therefore, our resulting

shell relations (8), (9) are valid also for inelastic shells. However, in the case of inelastic material behaviour $N^{\alpha\beta}$ and $M^{\alpha\beta}$ at successive equilibrium configurations $\mathbf{u}$ should be calculated in an incremental-iterative way applying appropriate two-dimensional incremental form of constitutive equations for $N^{\alpha\beta}$ and $M^{\alpha\beta}$.

INCREMENTAL SHELL EQUATIONS

The highly non-linear boundary value problem (8), (9) can effectively be solved only by incremental-iterative procedures applying computerized numerical methods, for which the shell equations (8), (9) should be presented in a consistent incremental form.

In general, the external loads $\mathbf{p}$, $\mathbf{h}$, $\mathbf{T}$ and $\mathbf{H}$ may be specified arbitrarily, or through several independent dimensionless parameters $(\lambda_1, \lambda_2, \ldots, \lambda_p) \in \Lambda \subset R^p$. In the latter case any information concerning the principal features of the solution manifold can be obtained analysing the set of solution submanifolds corresponding to a smoothly varying single parameter. Therefore, in the following considerations we restrict ourselves to the case when the external loads are specified by a single parameter $\lambda \in \Lambda \subset R$.

For smoothly varying λ the regular solutions of (8), (9) form an equilibrium path $\mathbf{u}(\lambda)$ for which $G[\mathbf{u}(\lambda); \delta\mathbf{u}] = 0$ for all kinematically admissible virtual displacements $\delta\mathbf{u}$. For tracing $\mathbf{u}(\lambda)$ it is convenient to apply the Newton-Kantorovich method [6].

Let $\mathbf{u}_m = \mathbf{u}(\lambda_m)$ be an equilibrium state associated with some $\lambda = \lambda_m$, and let $\mathbf{u}_m^{(i)}$ be a known i-th approximation to $\mathbf{u}_m$, which in general may not belong to the equilibrium path $\mathbf{u}(\lambda)$. In order to calculate the correction $\Delta\mathbf{u}_m^{(i+1)}$ such that $\mathbf{u}_m^{(i+1)} = \mathbf{u}_m^{(i)} + \Delta\mathbf{u}_m^{(i+1)}$ is the next approximation to $\mathbf{u}_m$ we linearize $G[\mathbf{u}; \delta\mathbf{u}]$ at $\mathbf{u}_m^{(i)}$ in the direction $\Delta\mathbf{u}_m^{(i+1)}$, what leads to the functional equation [6]

$$\mathbf{G}[\mathbf{u}_m^{(i)}; \delta\mathbf{u}] + \Delta G[\mathbf{u}_m^{(i)}; \delta\mathbf{u}, \Delta\mathbf{u}_m^{(i+1)}] = 0 \,, \tag{11}$$

where ΔG is the Gateaux derivative of (3) taken at $\mathbf{u}_m^{(i)}$ in the kinematically admissible direction $\Delta\mathbf{u}_m^{(i+1)}$. When $\mathbf{u}_m^{(i)}$ does not belong to the equilibrium path the first term of (11) allows to calculate the unballanced force vector. The

second term of (11) is linear in the unknown $\Delta\mathbf{u}_m^{(i+1)}$ and allows to calculate the tangent stiffness matrix at $\mathbf{u}_m^{(i)}$ of the problem.

In order to simplify notation, in the following part of this Section we set $\mathbf{u}_m^{(i)} \equiv \mathbf{u}_m^{(i)}$, $\Delta\mathbf{u}_m^{(i+1)} \equiv \Delta\mathbf{u}$, while the values at $\mathbf{u}$ of corresponding external loadings we denote shortly by $\mathbf{p}$, $\mathbf{h}$, $\mathbf{T}$ and $\mathbf{H}$.

Let us consider a curve $\mathbf{u}(\eta)$ through the i-th approximation $\mathbf{u}$ to $\mathbf{u}_m$, which in the neighbourhood of $\mathbf{u}$ takes the form $\mathbf{u}(\eta) = \mathbf{u} + \eta\Delta\mathbf{u}$. The directional Gateaux derivative of the functional G, taken at the i-th approximation $\mathbf{u}$ to $\mathbf{u}_m$ in the direction $\Delta\mathbf{u}$, is given by

$$\Delta G[\mathbf{u}; \delta\mathbf{u}, \Delta\mathbf{u}] = \frac{d}{d\eta}\, G[\mathbf{u}(\eta); \delta\mathbf{u}]_{|\eta=0}\,, \tag{12}$$

where $G[\mathbf{u}(\eta); \delta\mathbf{u}]$ is defined analogously as the functional $G[\mathbf{u}; \delta\mathbf{u}]$, only now $\mathbf{u}(\eta)$ appears in place of $\mathbf{u}$.

Along the curve $\mathbf{u}(\eta)$ the external loads are denoted by $\mathbf{p}(\eta)$, $\mathbf{h}(\eta)$, $\mathbf{T}(\eta)$ and $\mathbf{H}(\eta)$, while the internal stress and couple resultants by $N^{\alpha\beta}(\eta)$ and $M^{\alpha\beta}(\eta)$, respectively. The corresponding Gateaux derivatives of those fields are defined according to

$$\begin{aligned} &\Delta\mathbf{p} = \frac{d}{d\eta}\, \mathbf{p}(\eta)_{|\eta=0}\,, \qquad \Delta\mathbf{T} = \frac{d}{d\eta}\, \mathbf{T}(\eta)_{|\eta=0}\,, \\ &N^{\alpha\beta} = \frac{d}{d\eta}\, N^{\alpha\beta}(\eta)_{|\eta=0}\,, \qquad etc. \end{aligned} \tag{13}$$

Let us apply the linearization (11) to the already transformed functional (6). Since our $\mathbf{u} \equiv \mathbf{u}_m^{(o)}$ may not belong to the equilibrium path, let us introduce the unballanced residual surface and boundary forces and couples

$$\begin{aligned} &\mathbf{p}_R = \mathbf{T}^{\beta}|_{\beta} + \mathbf{p} + [(\mathbf{h}\cdot\bar{\mathbf{a}}^{\beta})\bar{\mathbf{n}}]|_{\beta}\,, \\ &\mathbf{P}_R = \mathbf{T}^{\beta}\nu_{\beta} + \mathbf{F}' - \mathbf{T} - \mathbf{F}^{*\prime} + (\mathbf{h}\cdot\bar{\mathbf{a}}^{\beta}\nu_{\beta})\bar{\mathbf{n}}\,, \\ &M_R = M - M^*,\ \mathbf{F}_{nR} = \mathbf{F}_n - \mathbf{F}_n^*\,. \end{aligned} \tag{14}$$

The quantities (14) allow to evaluate the first term in (11) in the form

$$G[\mathbf{u};\delta\mathbf{u}] = \int_M \int -\mathbf{p}_R\cdot\delta\mathbf{u}dA + \int_{C_f} (\mathbf{P}_R\cdot\delta\mathbf{u} + M_R\delta n_\nu)\, ds + \sum_n \mathbf{F}_{nR}\cdot\delta\mathbf{u}_n \,. \quad (15)$$

In order to calculate the second term of (11), let us remind that along the curve $\mathbf{u}(\eta)$ the shell geometry is defined by $\bar{\mathbf{a}}_\alpha(\eta)$, $\bar{\mathbf{a}}^\beta(\eta)$ and $\bar{\mathbf{n}}(\eta)$. Therefore, taking Gateaux derivatives of the identities $\bar{\mathbf{a}}^\beta(\eta)\cdot\bar{\mathbf{a}}_\alpha(\eta) = \delta^\alpha_\beta$, $\bar{\mathbf{a}}^\beta(\eta)\cdot\bar{\mathbf{n}}(\eta) = 0$ we have in M

$$\begin{aligned} &\Delta\bar{\mathbf{a}}_\alpha = \Delta\mathbf{u}_{,\alpha}\,, \qquad \Delta\bar{\mathbf{n}} = -\bar{\mathbf{a}}^\kappa(\bar{\mathbf{n}}\cdot\Delta\mathbf{u}_{,\kappa})\,, \\ &\Delta\bar{\mathbf{a}}^\beta = -(\bar{\mathbf{a}}^\beta\cdot\Delta\mathbf{u}_{,\kappa})\,\bar{\mathbf{a}}^\kappa + \bar{a}^{\beta\kappa}(\bar{\mathbf{n}}\cdot\Delta\mathbf{u}_{,\kappa})\,\bar{\mathbf{n}}\,. \end{aligned} \quad (16)$$

$$\begin{aligned} &\Delta(\delta\bar{\mathbf{n}}) = \mathbf{B}^\beta\cdot\delta\mathbf{u}_{,\beta}\,, \\ &\mathbf{B}^\beta = [(\bar{\mathbf{a}}^\beta\cdot\Delta\mathbf{u}_{,\kappa})\,\bar{\mathbf{a}}^\kappa - \bar{a}^{\beta\kappa}(\bar{\mathbf{n}}\cdot\Delta\mathbf{u}_{,\kappa})\bar{\mathbf{n}}]\otimes\bar{\mathbf{n}} + (\bar{\mathbf{n}}\cdot\Delta\mathbf{u}_{,\kappa})\,\bar{\mathbf{a}}^\beta\otimes\bar{\mathbf{a}}^\kappa\,. \end{aligned} \quad (17)$$

Similarly, let us introduce $\bar{\mathbf{n}}(\eta)$ and $\delta\bar{\mathbf{n}}(\eta)$ on $\bar{C}$, defined by respective formulae $(2)_1$ and (5), where now $\mathbf{u}(\eta)$ stands for $\mathbf{u}$. This allows to calculate Gateaux derivatives of $\bar{\mathbf{n}}$ and $\delta\bar{\mathbf{n}}$ on $\bar{C}$ in the form

$$\begin{aligned} &\Delta\bar{\mathbf{n}} = a_\nu^{-1}[(\boldsymbol{\nu}\times\bar{\mathbf{n}})\,\bar{\mathbf{n}}\cdot\Delta\mathbf{u}' + (\bar{\mathbf{r}}'\times\bar{\mathbf{n}})\Delta n_\nu]\,, \\ &\Delta(\delta\bar{\mathbf{n}}) = \mathbf{A}\cdot\delta\mathbf{u}' + \mathbf{B}\delta n_\nu + a_\nu^{-1}(\bar{\mathbf{r}}'\times\bar{\mathbf{n}})\,\Delta(\delta n_\nu)\,, \end{aligned} \quad (18)$$

$$\begin{aligned} &\mathbf{A} = -a_\nu^{-2}[\boldsymbol{\nu}\cdot(\Delta\mathbf{u}'\times\bar{\mathbf{n}} + \bar{\mathbf{r}}'\times\Delta\bar{\mathbf{n}})](\boldsymbol{\nu}\times\bar{\mathbf{n}})\otimes\bar{\mathbf{n}} + a_\nu^{-1}[\boldsymbol{\nu}\times(\Delta\bar{\mathbf{n}}\otimes\bar{\mathbf{n}} + \bar{\mathbf{n}}\otimes\Delta\bar{\mathbf{n}}]\,, \\ &\mathbf{B} = -a_\nu^{-2}[\boldsymbol{\nu}\cdot(\Delta\mathbf{u}'\times\bar{\mathbf{n}} + \bar{\mathbf{r}}'\times\Delta\bar{\mathbf{n}})](\bar{\mathbf{r}}'\times\bar{\mathbf{n}}) + a_\nu^{-1}(\bar{\mathbf{r}}'\times\Delta\bar{\mathbf{n}} + \Delta\mathbf{u}'\times\bar{\mathbf{n}})\,. \end{aligned} \quad (19)$$

With the help of (16)÷(19), (12), (13), (6), (7) and some transformations, the second term of (11) can be presented in the form

$$\Delta G[\mathbf{u};\delta\mathbf{u},\Delta\mathbf{u}] = -\int_M\int \{[(\Delta\mathbf{T}^\beta + \mathbf{S}^\beta)_{|\beta} + \Delta\mathbf{p} + [(\Delta\mathbf{h}\cdot\bar{\mathbf{a}}^\beta)\,\bar{\mathbf{n}} -$$
$$-\mathbf{h}\cdot\mathbf{B}^\beta]_{|\beta}\}\cdot\delta\mathbf{u}dA + \tag{20}$$
$$+\int_{C_f}\Big(\Big\{(\Delta\mathbf{T}^\beta + \mathbf{S}^\beta)\,\nu_\beta + (\Delta\mathbf{F}+\mathbf{C})' - \Delta\mathbf{T} - (\Delta\mathbf{F}^* + \mathbf{C}^*)' + [(\Delta\mathbf{h}\cdot\bar{\mathbf{a}}^\beta)\,\bar{\mathbf{n}} -$$
$$-\mathbf{h}\cdot\mathbf{B}^\beta]\nu_\beta\Big\}\cdot\delta\mathbf{u} + (\Delta M + K - \Delta M^* - K^*)\,\delta n_\nu + M_R\Delta(\delta n_\nu)\Big)ds +$$
$$+\sum_n(\Delta\mathbf{F}_n + \mathbf{C}_n - \Delta\mathbf{F}_n^* - \mathbf{C}_n^*)\cdot\delta\mathbf{u}_n\,,$$

where

$$\Delta\mathbf{T}^\beta = \Delta N^{\alpha\beta}\bar{\mathbf{a}}_\alpha + \Delta M^{\alpha\beta}\bar{\mathbf{n}}_{,\alpha} + [(\Delta M^{\kappa\rho}\bar{\mathbf{a}}_\kappa)_{|\rho}\cdot\bar{\mathbf{a}}^\beta]\bar{\mathbf{n}}\,,$$
$$\mathbf{S}^\beta = N^{\alpha\beta}\Delta\mathbf{u}_{,\alpha} + M^{\alpha\beta}\Delta\bar{\mathbf{n}}_{,\alpha} + [(M^{\kappa\rho}\Delta\mathbf{u}_{,\kappa})_{|\rho}\cdot\bar{\mathbf{a}}^\beta]\,\bar{\mathbf{n}} - (M^{\kappa\rho}\bar{\mathbf{a}}_\kappa)_{|\rho}\cdot\mathbf{B}^\beta\,, \tag{21}$$

$$\Delta\mathbf{F} = -a_\nu^{-1}[(\bar{\mathbf{n}}\times\bar{\mathbf{a}}_\alpha)\cdot\boldsymbol{\nu}]\Delta M^{\alpha\beta}\nu_\beta\bar{\mathbf{n}}\,,$$
$$\mathbf{C} = -a_\nu^{-1}[(\boldsymbol{\nu}\times\bar{\mathbf{n}})\cdot\Delta\mathbf{u}_{,\alpha}]M^{\alpha\beta}\nu_\beta\bar{\mathbf{n}} - M^{\alpha\beta}\bar{\mathbf{a}}_\alpha\nu_\beta\cdot\mathbf{A}\,, \tag{22}$$
$$\Delta M = a_\nu^{-1}(\bar{\mathbf{n}}\times\bar{\mathbf{a}}_\alpha)\cdot\bar{\mathbf{r}}'\Delta M^{\alpha\beta}\nu_\beta\,,$$
$$K = a_\nu^{-1}[(\bar{\mathbf{r}}'\times\bar{\mathbf{n}})\cdot\Delta\mathbf{u}_{,\alpha}]\,M^{\alpha\beta}\nu_\beta + M^{\alpha\beta}\bar{\mathbf{a}}_\alpha\nu_\beta\cdot\mathbf{B}\,,$$

$$\Delta\mathbf{F}^* = -a_\nu^{-1}[(\bar{\mathbf{n}}\times\Delta\mathbf{H})\cdot\boldsymbol{\nu}]\bar{\mathbf{n}}\,,\qquad \mathbf{C}^* = -\mathbf{H}\cdot\mathbf{A}\,, \tag{23}$$
$$\Delta M^* = a_\nu^{-1}(\bar{\mathbf{n}}\times\Delta\mathbf{H})\cdot\bar{\mathbf{r}}'\,,\qquad K^* = \mathbf{H}\cdot\mathbf{B}\,,$$

The fields $\Delta\mathbf{T}^{\beta}$, $\Delta\mathbf{F}$, ΔM, $\Delta\mathbf{F}_n$ are linear in $\Delta\mathbf{u}$ and represent the material part of changes of $\mathbf{u}$, while the fields $\mathbf{S}^{\beta}$, $\mathbf{C}$, $\mathbf{K}$, $\mathbf{C}_n$ are also linear in $\Delta\mathbf{u}$ but represent the geometric part of changes of $\mathbf{u}$ at the incremental step.

Since (11) with (15) and (20) should vanish for any kinematically admissible $\delta\mathbf{u}$, from (11) we obtain the following incremental equilibrium equations as well as the incremental static boundary and corner conditions for the Lagrangian non-linear theory of thin shells

$$(\Delta\mathbf{T}^{\beta}+\mathbf{S}^{\beta})_{|\beta}+\Delta\mathbf{p}+[(\Delta\mathbf{h}\cdot\bar{\mathbf{a}}^{\beta})\bar{\mathbf{n}}-\mathbf{h}\cdot\mathbf{B}^{\beta}]_{|\beta}+\mathbf{p}_R=\mathbf{0} \qquad \text{in } M\,, \tag{24}$$

$$\left.\begin{aligned}&(\Delta\mathbf{T}^{\beta}+\mathbf{S}^{\beta})\,\nu_{\beta}+(\Delta\mathbf{F}+\mathbf{C})'=\Delta\mathbf{T}+(\Delta\mathbf{F}^{*}+\mathbf{C}^{*})'-\\&-[(\Delta\mathbf{h}\cdot\bar{\mathbf{a}}^{\beta})\,\bar{\mathbf{n}}-\mathbf{h}\cdot\mathbf{B}^{\beta}]\nu_{\beta}-\mathbf{P}_R\\&\Delta M+K=\Delta M^{*}+K^{*}\,,\qquad M_R=0\end{aligned}\right\}\ \text{on } C_f\,, \tag{25}$$

$$\Delta\mathbf{F}_n+\mathbf{C}_n=\Delta\mathbf{F}_n^{*}+\mathbf{C}_n^{*}-\mathbf{F}_{nR} \qquad \text{at each corner } M_n\in C_f\,.$$

The corresponding work-conjugate geometric boundary conditions to be satisfied at each incremental step are

$$\Delta\mathbf{u}=\mathbf{0}\,,\qquad \Delta n_{\nu}=0 \qquad \text{on } C_u \tag{26}$$

All the vectors in (24)÷(26) are given through components in the respective undeformed bases $\mathbf{a}_{\alpha}$, $\mathbf{n}$, and $\boldsymbol{\nu}$, $\mathbf{t}$, $\mathbf{n}$.

The incremental shell equations (24)÷(26) constitute the linearized boundary value problem for the increment $\Delta\mathbf{u}\equiv\Delta\mathbf{u}^{(i+1)}$ which allows from known $\mathbf{u}_m^{(i)}$ to calculate the next approximation $\mathbf{u}_m^{(i+1)}$ to the equilibrium state $\mathbf{u}_m$.

In the case of an elastic material $\Delta N^{\alpha\beta}$ and $\Delta M^{\alpha\beta}$ follow directly from the constitutive equations (10)

$$\begin{aligned}\Delta N^{\alpha\beta}&=C_1^{\alpha\beta\lambda\mu}\Delta\gamma_{\lambda\mu}+C_2^{\alpha\beta\lambda\mu}\Delta\kappa_{\lambda\mu}\,,\\ \Delta M^{\alpha\beta}&=C_3^{\alpha\beta\lambda\mu}\Delta\gamma_{\lambda\mu}+C_4^{\alpha\beta\lambda\mu}\Delta\kappa_{\lambda\mu}\,,\end{aligned} \tag{27}$$

where $C_k^{\alpha\beta\lambda\mu}$, $k=1,\ldots,4$ are the tangent elasticities at $\mathbf{u}$, defined as second partial derivatives of Σ with respect to $\gamma_{\alpha\beta}$, $\kappa_{\alpha\beta}$ (see (85) of [22]), while

$\Delta\gamma_{\alpha\beta}$, $\Delta\kappa_{\alpha\beta}$ are Gateaux derivatives at $\mathbf{u}$ of the surface strain measures (see (82) of [22]). Therefore, for each particular form of Σ, [5,16,22], the tangent elasticities can be explicitly calculated as known functions of $\mathbf{u}$. In the case of inelastic material behaviour the tangent elasticities at each $\mathbf{u}$ should be calculated by some independent incremental-iterative procedure.

The set of incremental shell equations (24)÷(27) with (14), (16), (17), (19) and (21)÷(23) derived here generalizes considerably the previous incremental formulations [7,15,1] which were valid for small strains, linear elastic behaviour and restricted class of external loads or boundary conditions.

LAGRANGIAN BUCKLING SHELL EQUATIONS

Buckling shell equations are usually derived through linearization of the boundary value problem about an equilibrium state of the shell [23].

Let $\mathbf{u}$ be an equilibrium state whose stability properties are analysed. Since at $\mathbf{u}$ we have $G[\mathbf{u};\delta\mathbf{u}] = 0$, according to (3), linearization of G at $\mathbf{u}$ in a kinematically admissible direction $\Delta\mathbf{u}$ (note that now $\Delta\mathbf{u}$ has different meaning from $\Delta\mathbf{u} \equiv \Delta\mathbf{u}_m^{(i+1)}$ used in the previous Section) leads according to (11) to the functional equation $\Delta G[\mathbf{u};\delta\mathbf{u},\Delta\mathbf{u}] = 0$. Here ΔG can be explicitly calculated from (6), and the calculation procedure is exactly the same as the one performed in the previous Section, where ΔG has been calculated at an approximation $\mathbf{u}_m^{(i)}$ to an equilibrium $\mathbf{u}_m$ in a kinematically admissible direction $\Delta\mathbf{u}_m^{(i+1)}$. Therefore, it is apparent that now ΔG at $\mathbf{u}$ in the direction $\Delta\mathbf{u}$ takes formally exactly the form (20) with $M_R \equiv 0$. From vanishing of ΔG for any $\delta\mathbf{u}$ we immediately arrive at the following explicit form of Lagrangian buckling equations for thin shells

$$(\Delta\mathbf{T}^\beta + \mathbf{S}^\beta)_{|\beta} + \Delta\mathbf{p} + [(\Delta\mathbf{h}\cdot\bar{\mathbf{a}}^\beta)\bar{\mathbf{n}} - \mathbf{h}\cdot\mathbf{B}^\beta]_{|\beta} = 0 \qquad \text{in } M\ ,$$

$$\left.\begin{aligned} &(\Delta\mathbf{T}^\beta + \mathbf{S}^\beta)\,\nu_\beta + (\Delta\mathbf{F} + \mathbf{C})' = \Delta\mathbf{T} + (\Delta\mathbf{F}^* + \mathbf{C}^*)' - \\ &- [(\Delta\mathbf{h}\cdot\bar{\mathbf{a}}^\beta)\,\bar{\mathbf{n}} - \mathbf{h}\cdot\mathbf{B}^\beta]\nu_\beta \\ &\Delta M + K = \Delta M^* + K^* \end{aligned}\right\} \text{ on } C_f\ , \qquad (28)$$

$$\Delta\mathbf{F}_n + \mathbf{C}_n = \Delta\mathbf{F}_n^* + \mathbf{C}_n^* \qquad \text{at each corner } M_n \in C_f\ ,$$

$$\Delta\mathbf{u} = \mathbf{0}\ , \qquad \Delta n_\nu = 0 \qquad \text{on } C_u\ ,$$

where all the quantities are defined through $\mathbf{u}$ and $\Delta\mathbf{u}$ by exactly the same formulae as analogously denoted respective quantities of the previous Section have been defined through $\mathbf{u}_m^{(i)} \equiv \mathbf{u}$ and $\Delta\mathbf{u}_m^{(i+1)} \equiv \Delta\mathbf{u}$. All the vectors in (28) are understood again to be expressed through components with respect to known bases $\mathbf{a}_\alpha, \mathbf{n}$ and $\boldsymbol{\nu}, \mathbf{t}, \mathbf{n}$ of M and C, respectively.

The explicit Lagrangian buckling shell equations (28) extend to the large-strain range of deformation and arbitrary loading the stability equations derived within small-strain theory of elastic shells by Stumpf [23] in operator form and by Nolte [9] in explicit form.

REMARKS ON COMPUTER IMPLEMENTATION

The unified formulation of the non-linear displacement 3-field theory of shells presented here is necessarily quite complex because of its generality and versatility. Note that $\kappa_{\alpha\beta}$ appearing in the underlying principle of virtual displacements (3) is expressible according to $(1)_3$ in terms of $\mathbf{u}_{,\alpha}$ and $\mathbf{u}_{,\alpha\beta}$. As a result, in any consistent finite element approximation of the resulting displacement boundary value problem C^1 interelement continuity is required. Additionally, in order to allow numerical analysis for various material laws, the element geometry and kinematics should be decoupled from the constitutive equations.

These requirements were fulfilled by Harte [4] in the case of thin shells made of linearly-elastic material undergoing small strains and moderate rotations and extended by Schieck [21] to the case of shells made of rubber-like incompressible elastic material undergoing large strains and unrestricted rotations. In those papers a triangular high-precision doubly-curved shell finite element with 54 degrees of freedom proposed already by Cowper [3] is selected. In the element of [21] biquintic polynomials are applied as shape functions for all three displacement components. As 18 degrees of freedom at each node the quantities u_α, w; $u_{\alpha,\beta}, w_{,\beta}$; $u_{\alpha,\beta\gamma}, w_{,\beta\gamma}$ are used, and the Gauss integration is performed in 21 points. The geometry of the element is calculated exactly from the given shell geometry. The shape functions are then condensed in such a way that C^1 interelement continuity of all displacement components is assured. The element is capable to represent only approximately the constant strain modes and the strain-free rigid-body modes. Test show, however, that the approximation error

quickly approaches zero with the mesh refinement. The strain-displacement relations and material laws are disconnected from the finite element kinematics. Therefore, they can easily be changed, if necessary.

The C^1 shell element described above was used with the MESY 3 computer code of structural analysis, and several test examples were run on CDC Cyber 205 vector computer applying special algorithms and programming techniques. In particular, the number of DOF of the element was combined with the number of integration points, what led to the vector length $54 \times 21 = 1134$ and allowed to increase the computation speed by the factor 23 over non-vectorized algorithms. The concise description of the vectorized algorithms developed is given by Nolte and Schieck [10,11] while the modified vectorized subroutine for calculation of the element tangent stiffness matrix and the residual force vector is described in Schieck [21].

With the help of the C^1 triangular shell finite element described above, several numerical results for highly non-linear one- and two-dimensional problems of elastic shells were presented in [21,22]. The application of the element to problems of elasto-plastic shells undergoing large strains is under development. The use of other material laws, and application of other C^1 shell finite elements, within the proposed unified displacement formulation of the non-linear theory of thin shells will hopefully be the subject of research in the future.

The C^1 continuity requirement, and associated complexity of the finite elements, is considered to be a disadvantage of the displacement formulation of thin shell theory as compared with a more complex 6-field theory of shear-deformable shells [14]. In the latter one both displacements and rotations are the independent field variables, and the finite element approximation expressed in terms of those variables requires only C^0 interelement continuity [2]. However, while the 3-field shell theory has been presented here in supposedly ultimate formulation, the 6-field shell theory is still under development and several important questions of the theory itself and its FE approximation are still under discussion. C^0 shell finite elements bring themselves some problems (locking effects, spurious zero-energy modes etc.) which are still waiting for commonly accepted satisfactory solutions. The complexity of 3-field C^1 finite elements may become less important already in the near future when powerful parallel processors of the next generation are installed into computers of PC

class, and then much better approximation quality of C^1 finite elements may become a decicive advantage. One can also expect that 6-field shell models will be absorbed in the future by unified computer codes of 3D analysis of structures, while the special structure of boundary conditions required by the 3-field shell theory does not allow it to be degenerated from the structure of 3D theory. Therefore, one might anticipate that this theory would remain as the only "shell" theory also in the future structural analysis. These are some arguments why the derivation of 2D constitutive laws for various material behaviour, and development of computer codes based on C^1 shell finite elements, seems to be of some importance also for future analysis of shell structures.

CONCLUSIONS

In this report a unified formulation of a wide class of non-linear theories of thin shells has been presented. The analysis has been based on only one assumption: the deformation of the shell as a three-dimensional body is determined entirely by deformation of its reference surface. Basic shell equations, in the global (8), (9) and consistent incremental (24)÷(26) forms, have been explicitly derived in the Lagrangian description in terms of displacements of the reference surface as the only independent field variables. The most general explicit form of Lagrangian buckling shell equations (28) have also been derived. Particular attention has been paid to consistency of work-conjugate boundary conditions, and to precise evaluation of unballanced forces when successive approximations to an equilibrium state do not follow the equilibrium path.

Our formulation of shell equations is valid for an arbitrary geometry of the shell reference surface, for unrestricted displacements, rotations, strains and/or changes of curvatures of the reference surface, for arbitrary configuration-dependent external surface and boundary loadings, and for arbitrary set of four work-conjugate static and geometric boundary conditions. Therefore, our formulation contains many specialized versions of non-linear shell equations available in the literature.

We have explicitly applied here the constitutive equations of elastic shells (10), (27), since for such material bahaviour effective computer FEM programs were developed, and several one- and two-dimensional non-linear problems of shells within small-strain [4,9,12] and large-strain [21,22] range of deformation were

analysed. However, our formulation of the non-linear shell theory is applicable to some problems of inelastic shells as well, provided corresponding incremental constitutive equations for the surface stress measures are available.

REFERENCES

[1] Y.Başar and Y.Ding. Finite-rotation elements for the non-linear analysis of thin shell structures, Int.J.Solids and Stuctures, vol.26, No.1, 83-97, 1990.

[2] J.Chróścielewski, J.Makowski and H.Stumpf. Genuinely resultant shell finite elements accounting for geometric and material non-linearity, Int. J. Num. Met. Engng, vol.35, No 1, 63-94, 1992.

[3] G.R.Cowper. A high-precision finite element for shells of arbitrary shape, Aeronautical Report, Nat. Res. Council of Canada, 1972.

[4] R.Harte. Doppelt gekrümmte finite Dreiekelemente für die lineare und geometrisch nichtlineare Berechnung allgemeiner Flachentragwerke, Tech.-Wiss. Mitt. Nr 82-10, Inst. f. Konstr. Ingb., Ruhr-Universität, Bochum 1982.

[5] W.T.Koiter. A consistent first approximation in the general theory of thin elastic shells, in: Theory of Thin Shells, ed.by W.T.Koiter, 12-33; North-Holland, Amsterdam 1960.

[6] M.A. Krasnosel'skii, G.M. Vainikko, P.P. Zabreiko, Ya.B. Rutitskii and V.Ya. Stetsenko. Approximate Solution of Operator Equations, Moscow 1969 (in Russian). English translation: Wolters-Noordhoff Pub.,Groningen 1972.

[7] J.Makowski and W.Pietraszkiewicz. Incremental formulation of the non- - linear theory of thin shells in the total Lagrangian description, ZAMM, vol.64, No 4, T65-T67, 1983.

[8] J.Makowski and W.Pietraszkiewicz. Work-conjugate boundary conditions in the non-linear theory of thin shells, ASME Journal of Applied Mechanics, vol.56, No 2, 395-402, 1989.

[9] L.-P.Nolte. Beitrag zur Herleitung und vergleichende Untersuchung geometrisch nichtlinear Schalentheorien unter Berücksichtigung groβer Rotation, Ruhr-Universität, Mitt.Inst.f.Mech., Nr 39, Bochum 1983.

[10] L.-P.Nolte and B.Schieck. Beitrag zur Vektorisierung höherwertiger Finiter Elemente, in: Proc. 1985 Conference on Supercomputers and Applications, ed. by H.Ehlich et al., Ruhr-Universität, Bochum 1985.

[11] L.-P.Nolte and B.Schieck. Vectorized high precision finite elements with application to non-linear problems, in: Parallel Computing 85, ed. by M.Feilmeier et al., 305-310, Elsevier Sci.Publ., 1986.

[12] L.-P.Nolte, J.Makowski and H.Stumpf. On the derivation and comparative analysis of large rotation shell theories, Ingenieur-Archiv, vol.56, No 2, 45-160, 1986.

[13] V.V.Novozhilov and V.A.Shamina. On kinematic boundary conditions in non- -linear elasticity problems, Mechanics of Solids (transl. Izvestiia AN SSSR, MTT), No 5, 63-74, 1975.

[14] W.Pietraszkiewicz. Finite Rotations and Lagrangean Description in the Non-Linear Theory of Shells, Polish Sci.Publ., Warszawa-Poznań 1979.

[15] W.Pietraszkiewicz, Lagrangian description and incremental formulation in the non-linear theory of thin shells, Int.J.Non-Linear Mechanics, vol.19, No, 115-140, 1984.

[16] W.Pietraszkiewicz. Geometrically non-linear theories of thin elastic shells, Advances in Mechanics, vol.12, No 1, 51-130, 1989.

[17] W.Pietraszkiewicz. Explicit Lagrangian incremental and buckling equations for the non-linear theory of thin shells, Int.J.Non-Linear Mechanics (in print).

[18] W.Pietraszkiewicz. Work-conjugate boundary conditions associated with the total rotation angle of the shell boundary, ASME Journal of Applied Mechanics (in print).

[19] W.Pietraszkiewicz and M.L.Szwabowicz. Entirely Lagrangian non-linear theory of thin shells, Archives of Mechanics, vol.33, No 2, 273-288, 1981.

[20] A.Sawczuk. On plastic analysis of shells, in: Theory of Shells, ed. by W.T.Koiter and G.K.Mikhailov, 27-63; North-Holland Publ.Co., Amsterdam 1980.

[21] B.Schieck. Grosse elastische Dehnungen in Schalen aus hyperelastischen inkompressiblen Materialen, Mitt. Inst. f. Mech.,Nr 69, Ruhr-Universität, Bochum 1989.

[22] B.Schieck, W.Pietraszkiewicz and H.Stumpf. Theory and numerical analysis of shells made of hyperelastic incompressible material, Int.J.Solids and Structures, vol.29, No 6, 689-709, 1992.

[23] H.Stumpf. General concept of the analysis of thin elastic shells, ZAMM, vol.66, No 8, 337-350, 1986.

RBCM – J. of the Braz.Soc.Mech.Sc.
Vol.XIV – nº 4 – 1992

ISSN 0100-7386
Impresso no Brasil

Prêmio JOSÉ REIS de divulgação científica

De 1 de dezembro/92 a 29 de janeiro/93
estarão abertas as inscrições para o
Prêmio José Reis de Divulgação Científica 1992.

Categoria Jornalismo Científico
Destinada a jornalistas que cobrem a área de C&T.

Categoria Divulgação Científica
Destinada a cientistas que também realizam trabalho de promoção da Ciência para o público leigo.

Categoria Instituição
Destinada a veículos de comunicação ou entidades que realizam trabalho de divulgação científica.

Ficha de inscrição e regulamento

CNPq
Secretaria-Executiva do Prêmio José Reis
SEPN, Quadra 507, Bloco B, 3º andar
CEP 70740-901 - Brasília, DF.
Telefone (061) 274-1155, ramal 222

MINISTÉRIO DA CIÊNCIA E TECNOLOGIA
CNPq

RBCM – J. of the Braz.Soc.Mech.Sc. ISSN 0100-7386
Vol.XIV - nº 4 - pp. 347 - 368 - 1992 Impresso no Brasil

ARBITRARY LAGRANGIAN-EULERIAN FINITE ELEMENTS FOR FLUID-SHELL INTERACTION PROBLEMS

ELEMENTOS FINITOS COM FORMULAÇÕES LAGRANGIANAS-EULERIANAS ARBITRÁRIAS PARA PROBLEMAS DE INTERAÇÃO FLUIDO-CASCAS

Wing Kam Liu
Northwestern University
Evanston, Illinois 60208
USA

Rasim Aziz Uras
Reactor Engineering Division
Argonne National Laboratory
Argonne, Illinois 60439, USA

ABSTRACT

This paper presents a survey of the arbitrary Lagrangian-Eulerian (ALE) Finite Element Formulation with various mesh updating techniques. Moreover, an efficient element for solving problems involving shells is also mentioned. Some applications of the ALE formulation and the shell element are given with a final emphasis on the shell-fluid interaction.

Keywords: Finite Element ▪ Arbitrary Lagrangian-Eulerian Formulations ▪ Mesh Updating ▪ Shell-Fluid Interaction

RESUMO

Este artigo apresenta um levantamento das Formulações de Elementos Finitos Lagrangianas – Eulerianas Arbitrárias, com várias técnicas de atualização de malha. Adicionalmente, um elemento eficiente na resolução de problemas de cascas é também mencionado. Algumas aplicações da formulação Lagrangiana-Euleriana Arbitrária e do elemento de casca são apresentadas com uma ênfase final na interação fluido-casca.

Palavras-chave: Elementos Finitos ▪ Formulações Lagrangianas-Eulerianas Arbitrárias ▪ Atualização de Malhas ▪ Interação Fluido-Casca

---

Invited Lecture Presented at 7th SIBRAT, Florianópolis, Brazil

INTRODUCTION

Athough the finite element method (FEM) is one of the most powerful and sophisticated numerical techniques available, most of its early developments were applied to structural analysis and it was not until the late 1960's that finite element techniques were applied to potential flow problems. Recently, considerable finite element research is being devoted to viscous flows, transport processes, fluid-structure interaction, compressible inviscid flows, and free surface flows, among others. This paper is devoted to the development of arbirary Lagrangian-Eulerian (ALE) techniques for viscous flows with free surface.

The kinematic description (i.e. the relationship between the moving fluid and the finite element grid) is extremely important in multidimensional fluid dynamics problems. Two classical descriptions are used in continuum mechanics. The first is Lagrangian, in which the mesh points coincide with the material particles. In this description, no convective effects appear and this simplifies considerably the numerical calculations; moreover, a precise definition of moving boundaries and interfaces is obtained. However, the Lagrangian description does not handle satisfactorily the material distortions that lead to element entanglement.

On the other hand, the second description is the Eulerian viewpoint, which allows strong distortions without problems because the mesh is fixed with respect to the laboratory frame and the fluid moves through it. However, this latter approach presents two important drawbacks: (i) convective effects, which introduce numerical difficulties, arise due to the relative movement between the grid and the particles; and (ii) sophisticated mathematical mappings between the stationary and moving boundaries are required.

Because of the shortcomings of purely Lagrangian and Eulerian descriptions, arbitrary Lagrangian-Eulerian (ALE) techniques were developed, first in finite differences by Noh [19] and Hirt et al.[6], among others, and then in finite elements by Donea et al.[5], Belytschko et al.[1], Hughes et al.[10], and Donea [3]. This new approach is based on the arbitrary movement of the reference frame, which is continuously rezoned in order to allow a precise description of the moving interfaces and to maintain the element shape. Convective terms

are still present in the ALE equations, but the ability to prescribe the mesch movement may allow them to be reduced.

The organization of this paper is as follows: The fundamentals of the arbitrary Lagrangin-Eulerian (ALE) formulation are presented, mesh updating techniques are indicated and the Finite Element Method in ALE is introduced [7]. Two applications of ALE on large-amplitude sloshing are presented from [7,8]. An efficient and reliable shell element formulation is adopted from Ref[13]. An example problem studied in [14] is restated to show the effectiveness of this element in shell buckling analysis. Following the study of the influence of the tank wall flexibility by Ma et al.[17], conclusions are stated.

KINEMATICS IN THE ALE DESCRIPTION

Review of the ALE Description

Two classic viewpoints are considered to describe the motion of a continuous medium. The first is Langrangian, in which the material region and the coordiantes of any point are denoted by R_x and $\mathbf{X}$, respectively. In the second, known as Eulerian, the spatial region is symbolized by R_x, and the spatial coordinates by $\mathbf{x}$. In the ALE description, the computational frame is a reference independent of the particle movement and which may be moving with an arbirary velocity in the laboratory system; the continuum view from this reference is denoted as R_χ, and the coordinates of any point are denoted as χ (Figure 1).

Consider a physical property, $f(\mathbf{x},t)$, expressed in a spatial representation

$$f(\mathbf{x},t) = f^*(\chi,t) = f^{**}(\mathbf{X},t)\ , \tag{1}$$

where * and ** denote "with respect to χ and $\mathbf{X}$", respectively,

If the physical property is the spatial coordinate $\mathbf{x}$, then

$$x_i = x_i^*(\chi,t) = x_i^{**}(\mathbf{X},t) \tag{2}$$

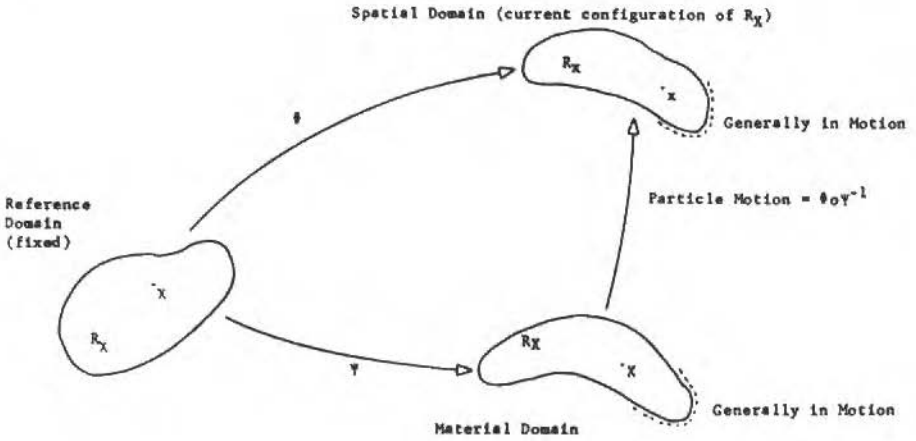

Figure 1. Diagram of domains for the arbitrary Lagrangian-Eulerian description.

and

$$\frac{\partial x_i^{**}}{\partial t}(\mathbf{X},t)|_X = \frac{\partial x_i^{*}}{\partial t}(\chi,t)|_\chi + w_j \frac{\partial x_i^{*}}{\partial \chi_j}(\chi,t) \ . \tag{3}$$

The material velocity v, the mesh velocity $\hat{v}$, and the convective velocity c are defined as

$$v_i = \frac{\partial x_i^{**}}{\partial t}\ (\mathbf{X},t)|_X \tag{4}$$

and

$$\hat{v}_i = \frac{\partial x_i^{*}}{\partial t}\ (\chi,t)|_\chi \ , \tag{5}$$

$$c_i = w_j \frac{\partial x_i^{*}}{\partial \chi_j} \tag{6}$$

The relationship between the material time derivative and the referential time

derivative can be expressed as

$$\frac{\partial f^{**}}{\partial t}(\mathbf{X},t)|_{\chi} = \frac{\partial f^{*}}{\partial t}(\chi,t)|_{\chi} + c_i \frac{\partial f}{\partial x_i}(x,t) . \tag{7}$$

Lagrangian Versus Referential Updates

In the Lagrangian description, the updating of any physical property is simple and is done through a Taylor series expansion in time

$$f^{**}(\mathbf{X},t+dt) = f^{**}(\mathbf{X},t) + dt \frac{\partial f^{**}}{\partial t}(\mathbf{X},t)|_{\chi} + \cdots \tag{8}$$

A similar approach can be used in a referetial description

$$f^{*}(\chi,t+dt) = f^{*}(\chi,t) + dt \frac{\partial f^{*}}{\partial t}(\chi,t)|_{\chi} + \cdots \tag{9}$$

However, in a referential description, a simple updating technique, such as Eq.(9), cannot be used for material point-related variables, such as state variables in path-dependent materials. For homogeneous materials with no memory, such as generalized Newtonian fluids, Eq.(9) cab be implemented with no further complications. Examples of ALE techniques applied to path-dependent materials may be found in [12,13].

INITIAL/BOUNDARY VALUE PROBLEM

Field Equations in the ALE Method

Conservation of Mass (Equation of Continuity)

The principle of mass conservation is derived in referential form. Consider an arbitrary volume V_χ fixed in the referential domain, R_χ, and surface ∂V_χ; the medium has a density $\hat{\rho}(\chi,t)$. The total mass in V_χ is

$$M = \int_{V_\chi} \hat{\rho} d\Omega_\chi = \int_{V_\chi} \rho d\Omega_\chi = \int_{V_\chi} \rho^0 d\Omega_\chi , \tag{10}$$

where

$$\hat{\rho}(\chi,t) = \hat{J}\rho(x,t) , \tag{11}$$

$$\rho^0(\mathbf{X}, t_0) = J\rho(x,t) \ , \tag{12}$$

$$\hat{J} = \det\left[\frac{\partial x_i}{\partial \chi_j}\right] \ , \tag{13}$$

$$J = \det\left[\frac{\partial x_i}{\partial \mathbf{X}_j}\right] \ . \tag{14}$$

The principle of mass conservation states that the *local* rate of increase of the total mass in the volume must be equal, if no mass is created or destroyed inside V_χ, to the rate of inflow of mass through the bounding surface ∂V_χ.

Conservation of Momentum (Equilibrium Equation)

Using the same definitions as in the conservation of mass, the principle of conservation of momentum states that the *total* rate of change of the total momentum of the medium occupying at time t the referential volume V_χ,

$$\frac{\partial}{\partial t}\Big|_\chi \int_{V_\chi} \hat{\rho}(\chi,t)\ v(\chi,t)\ d\Omega\chi \ , \tag{15}$$

is equal to the net force exerted on it.

The final form of the field equations to be used in the finite element method in conjunction with ALE are given as

$$\frac{\partial \hat{\rho}}{\partial t}\Big|_\chi + \frac{\partial \hat{\rho} w_i}{\partial \chi_i} = 0 \qquad \text{in } R_\chi \ , \tag{16}$$

$$\hat{\rho}\ \frac{\partial v_i}{\partial t}\Big|_\chi + \hat{\rho} w_j\ \frac{\partial v_i}{\partial \chi_j} = \frac{\partial \hat{T}_{ji}}{\partial \chi_j} + \hat{\rho} g_i \qquad \text{in } R_\chi \ , \tag{17}$$

ρ is the fluid density, g is the acceleration of gravity, and σ and $\widehat{T}$ are the Cauchy and first Piola-Kirchhoff stress tensors, respectively.

AUTOMATIC REZONING

In the ALE description the moving boundaries can be tracked with the accuracy characteristic of the Lagrangian methods and the mesh can conserve its regularity to avoid element entanglement [4,11,16,20]. The rezoning techniques are based on heuristic developments.

The reference frame is fixed, but its movement with respect to the laboratory or the continuum is arbitrary. The particle velocity viewed from the reference, w, and the mesh velocity, $\hat{v}$, are interrelated by

$$v_i = \hat{v}_i + w_j \frac{\partial x_i^*}{\partial \chi_j} \tag{18}$$

Depending on which velocity ($\hat{v}$, w, or mixed) is prescribed, three different cases may be studied.

Mesh Motion Prescribed a Priori

The case where $\hat{v}$ is given corresponds to an analysis where the domain boundaries are known at every instant. The rigid-body viscous fluid problem studied in [8] falls into this type of ALE problem.

Lagrange-Euler Matrix Method

Let w be

$$w_i = \left.\frac{\partial \chi_i}{\partial t}\right|_X = (\delta_{ij} - \alpha_{ij})\, v_j \ , \tag{19}$$

where δ_{ij} is the Kroneker delta and $[\alpha_{ij}]$ is the Lagrange-Euler parameter matrix such that $\alpha_{ij} = 0$ if $i \neq j$ and α_{ij} is real (underlined indexes meaning no sum on them). The Lagrange-Euler matrix needs to be given once and for

all at each grid point. It is very difficult to maintain regular shaped elements inside the fluid domain by just prescribing the α's.

ALE technique based on the Lagrange-Euler parameters is very useful in problems such as the propagation of long waves ('tsunamis') and, in general, in very free surface flow where the free surface may be written as $x_{3s}(x_1, x_2, t)$ with an Eulerian description used in the x_1- and x_2-directions.

Mixed Formulation

One of the goals of the ALE method is the accurate mapping of the moving boundaries which are usually material surfaces. The other goal of the ALE technique is to avoid element entanglement.

FINITE ELEMENT FORMULATION

The Petrov-Galerkin formulation is used for the equilibrium and mesh updating equations, while the Galerkin method is applied to the continuity equation. Furthermore, a pressure-velocity $(P - v)$ formulation is implemented for numerical efficiency and accuracy. Constant pressure elements are used; thus, both weight and trial pressure functions are constant inside the element and discontinuous across interelement boundaries. The pressure weighting function is denoted as δP, and the integral equation associated with the continuity equation is

$$\sum_e \int_{R_x^e} \delta P \, \frac{1}{B} \, \frac{\partial P}{\partial t}\Big|_x \, dR_x + \sum_e \int_{R_x^e} \delta P \, \frac{\partial v_i}{\partial x_i} \, dR_x = 0 \,, \tag{20}$$

where the spatial domain, R_x, is discretized into element subdomains, R_x^e, and $\sum_e$ symbolizes the sum over all elements.

For the equilibrium equation the streamline-upwind/Petrov-Galerkin formulation requires discontinuous weighting functions of the form

$$\delta v = \delta \omega + \partial \mathbf{p} \tag{21}$$

where $\delta\omega$ is continuous in R_x and $\delta\mathbf{p}$ is the discontinuous streamline upwind perturbation; $\delta_{\mathbf{p}}$ is assumed smooth in the element interior. The variational equation can be written as

$$\sum_e \int_{R_x^e} \delta v_i \rho \left.\frac{\partial v_i}{\partial t}\right|_\chi dR_x + \sum_e \int_{R_x^e} \delta v_i \rho c_j \frac{\partial v_i}{\partial x_j} dR_x$$
$$- \int_{R_x} \frac{\partial(\delta\omega_i)}{\partial X_i} P dR_x + \int_{r_x} \frac{\mu}{2}\left[\frac{\partial(\delta\omega_i)}{\partial X_j} + \frac{\partial(\delta\omega_j)}{\partial X_i}\right]\left[\frac{\partial v_i}{\partial X_j} + \frac{\partial v_j}{\partial X_i}\right] dR_x$$
$$- \sum_e \int_{R_x^e} \partial p_i \frac{\partial \sigma_{ij}}{\partial X_j} dR_x - \sum_e \int_{R_x^3} \delta v_i \rho g_i \, dR_x - \int_{\partial R_x^h} \delta\omega_i h_i \, dS = 0. \quad (22)$$

The mesh updating formulas are obtained using again the streamline-upwind/Petrov-Galerkin Method, where the weighting functions, $\delta\mathbf{x}$, are considered to be composed of both the continuous interpolation functions and the perturbation functions.

$$\int_{R_\chi} \delta x_i \left.\frac{\partial x_i}{\partial t}\right|_\chi dR_\chi + \int_{R_\chi} (\delta_{jk} - \alpha_{jk}) v_k \delta x_i \frac{\partial x_i}{\partial \chi_j} dR_\chi - \int_{R_\chi} \partial x_i v_i \, dR_\chi = 0 . \quad (23)$$

$$\int_{R_x} \delta x_i \left.\frac{\partial x_i}{\partial t}\right|_\chi dR_\chi - \int_{R_\chi} \delta x_i \sum_{\substack{j=1 \\ j\neq i}}^{NSD} \frac{v_j - \hat{v}_j}{\hat{j}^{ii}} \hat{j}^{ji} dR_\chi - \int_{R_\chi} \delta x_i \left(v_i - \frac{\hat{j}}{\hat{j}^{ii}} w_i\right) dR_\chi = 0. \quad (24)$$

MATRIX EQUATIONS AND PREDICTOR-MULTICORRECTOR ALGORITHM

The spatial discretization of the integral Eqs. (21), (22), (23) and (24) leads to the following system of partical differential equations:

$$\mathbf{M}^{\mathbf{P}}\dot{\mathbf{P}} + \eta^P(\mathbf{P}) + \mathbf{G}^{\mathbf{t}} v = 0 , \quad (25)$$
$$\mathbf{M}\mathbf{a} + \eta(v) + \mathbf{K}_\mu v - \mathbf{G}\mathbf{P} = \mathbf{f}^{\mathbf{ext}} , \quad (26)$$
$$\widehat{\mathbf{M}}\hat{v} + \hat{\eta}(x) - \widehat{\mathbf{M}} v = 0 , \quad (27)$$

Numerical Results

Figure 4 shows the discretization of the fluid domain used for the computations. It consists of 2758 constant pressure-bilinear velocity elements (25 layers) which imply 3052 nodes. Notice the concentration of elements around the blocks needed to caputre recirculation. Two areas are defined in the domain, see Figure 4; an Eulerian description is implemented in the bottom one (i.e., the mesh is fixed), while the mixed ALE formulation [7] is used in the upper zone. The latter formulation allows a continuous remeshing such that element shapes are maintained.

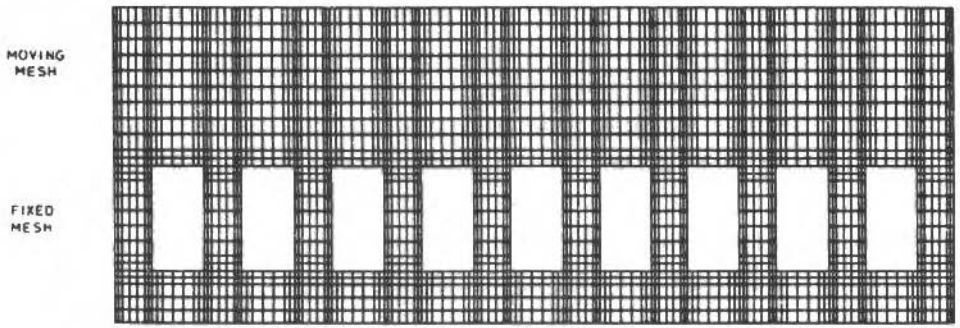

Figure 4. Mesh discretization.

The time step chosen is such that 200 time steps are needed in every cycle; that is, Δt is obtained dividing 2π by $200 \times \omega$. However, for $Re = 500000$, 300 time steps must be used in the tenth cycle due to large convection.

Concerning the boundary conditions, zero velocities are prescribed around the blocks, while perfect sliding boundaries are assumed for the bottom and sides of the tank. The material surface conditions described in the previous section are imposed on the free surface.

The case corresponding to pure water, i.e., $Re = 500000$, is studied first. Instantaneous configurations of the domain with velocity vectors and streamlines are plotted in Figure 5 for the tenth cycle. At $\omega t = n\pi$ (n integer), i.e.,at maximum amplitude and minimum velocity,the recirculation around the

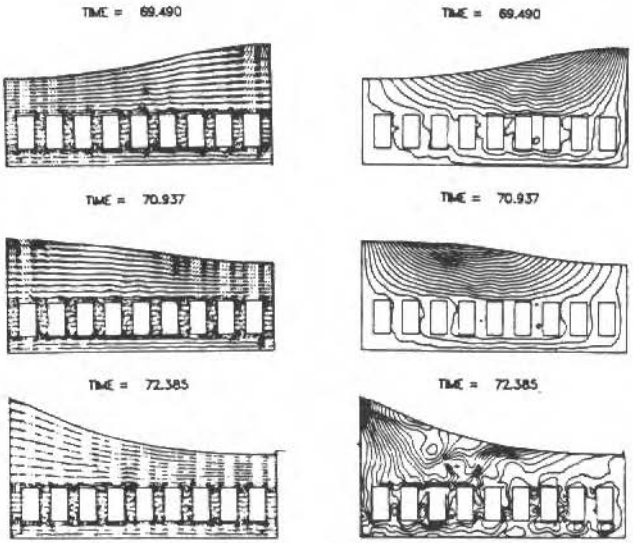

Figure 5. Instantaneous configurations of the domain velocities, and streamlines for tenth cycle.

blocks is obvious. At minimum amplitude and maximum velocity, most of the flow is concentrated in the upper half of the tank; nevertheless, the flow perturbation due to the presence of blocks is clear. The non-linear evalutation of the free surface is reflected by its vertical motion at the center of the tank, in spite of the vertical material velocity at that point being equal to zero. The presence of blocks induces a reduction in the wave height and a magnification of the horizontal particle oscillation at the central portion of the tank.

The influence of viscous effects is observed in Figure 6 for three Reynolds numbers. The free vibration part after the tenth cycle shows a 6% damping.

RESULTANT STRESS DEGENERATED SHELL ELEMENT

The general nonlinear shell formulation of Hughes and Liu [9] is expanded to develop degenerated shell elements with stabilization through an improved representation of a fiber coordinate system.

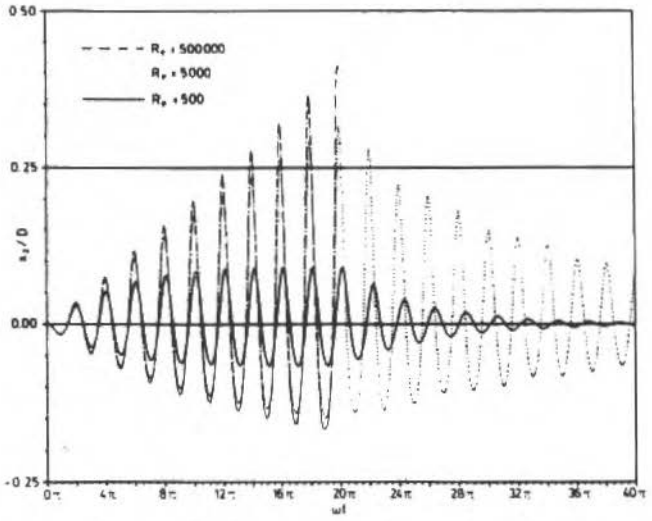

Figure 6. Time history of the wave height at the left wall with submerged blocks.

This variational approach developed by Liu et al.[15] is applied to the buckling analysis of shells in Ref.[14].

Prior to the nonlinear calculation, linear buckling analyses of the cylindrical shell with two different boundary conditions are performed: one with clamped ends and the other free; however, all rotations are fixed. In both cases, the buckling loads for different modes are very close to each other. A comparison shows no significant effect of the edge constraints. In other words, the initial stress field is not influenced by the end conditions.

In the nonlinear analysis, the prebuckling deformation is accounted for by an incremental displacement formulation.

As shown in the load-displacement curve (Figure 7), a postbuckling branch (BD) for the buckling mode ($\cos 14\theta$) is traced out by a succession of equilibrium states of the cylindrical shell. Along the postbuckling curve, the deformation is characterized by a special trend: the radial displacements increase drastically while the end displacements decrease. On the postbuckling curve (BD), each point represents an equilibrium state of the cylindrical shell whose internal

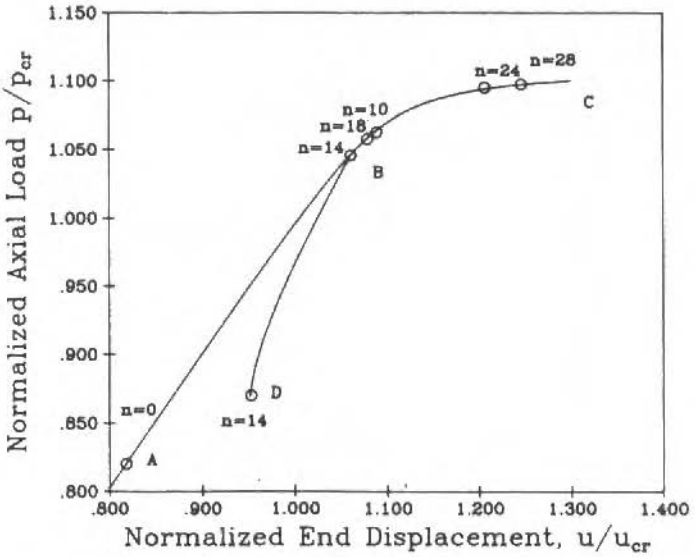

Figure 7. Normalized load-displacement curve.

strain energy can be considered as the sum of two components, membrane compression and bending. At point B the internal energy is dominated by membrane compression, while at point D the internal energy is dominated by bending. The path from B to D represents a simultaneous process transforming the membrane compression energy to bending energy. Since the deflection associated with bending deformation is substantially larger than the deflection associated with membrane compression, the reduction of end displacements of the cylindrical shell is accompanied by a large accumulation of radial displacements. Figure 8 depicts a summary of diamond modes.

SEISMIC RESPONSE OF 3-D FLEXIBLE TANK

In order to demonstrate the importante of the tank wall flexibility in the seismic design the hydrodynamic response of a $3-D$ flexible tank is studied.

The finite element model and the dimensions of the tank are shown in Figure 9. This model consist of 180 fluid, 56 shell and 63 contact elements. A 10 s duration acceleration history with a maximum of 0.5 g is applied at the base. Two cases for the sloshing wave height and the fluid dynamic pressure at

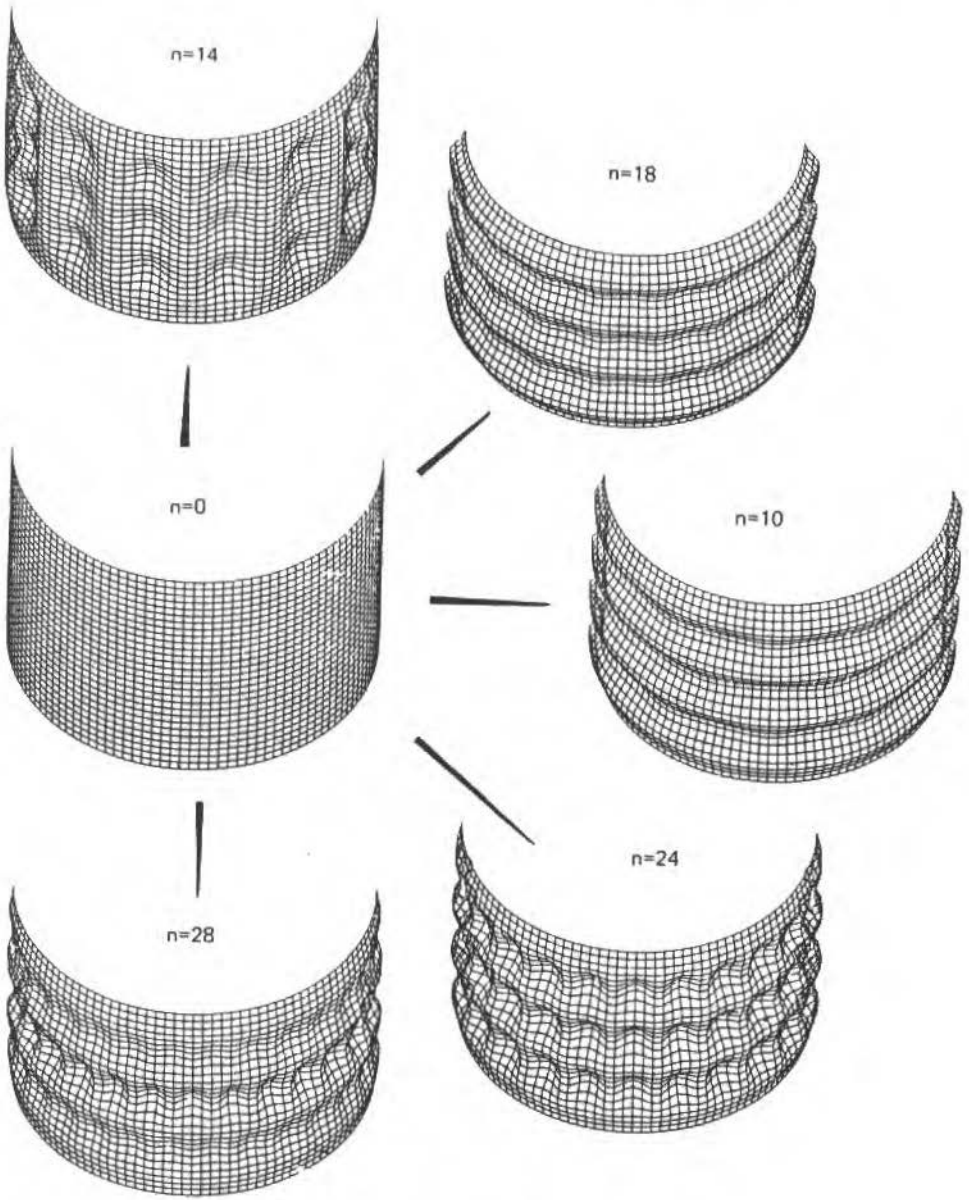

Figure 8. Summary of diamond buckles.

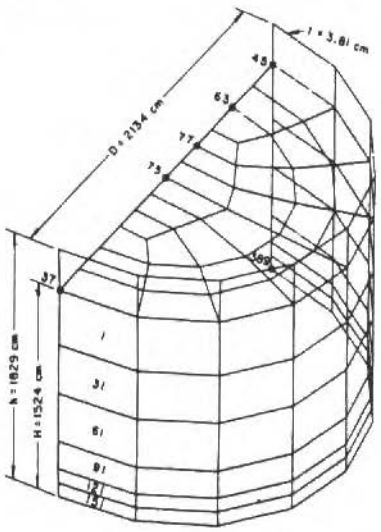

Figure 9. Finite element model of a 3-D fluid-tank system.

the tank top are presented here. One assumes rigid walls, the other one with a tank fundamental frequency of 2.5 Hz. The results are depicted in Figures 10 and 11 for the pressure and the wave height, respectively. The observations can be summarized as follows:

(1) The fluid dynamic pressures in a flexible tank are substantially greater than those induced in a similarly excited rigid tank. For the flexible tank, the fluid dynamic pressures become very sensitive to the frequency variation, as the frequency of the tank system approaches to the maximum amplification region of response spectrum of the base acceleration. Hence, it is very important to properly include the fluid inertia in assessing the dynamic characteristic of the fluid-tank systems.

(2) The coupling effect between the tank flexibility and sloshing response may be important, even if the frequency between the tank system and sloshing motion is well separated.

(3) Higher modes of sloshing motion are important to the post-earthquake sloshing analysis. The phenomena are not fully understood yet, more studies are required.

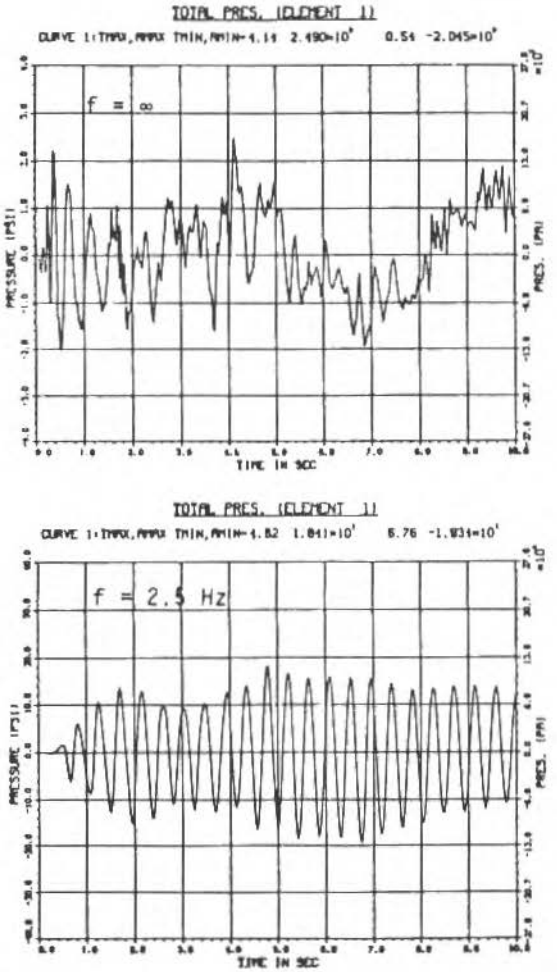

Figure 10. Fluid dynamic pressure at the top of the tank (a) rigid tank, (b) tank fundamental frequency $f = 2.5$ Hz.

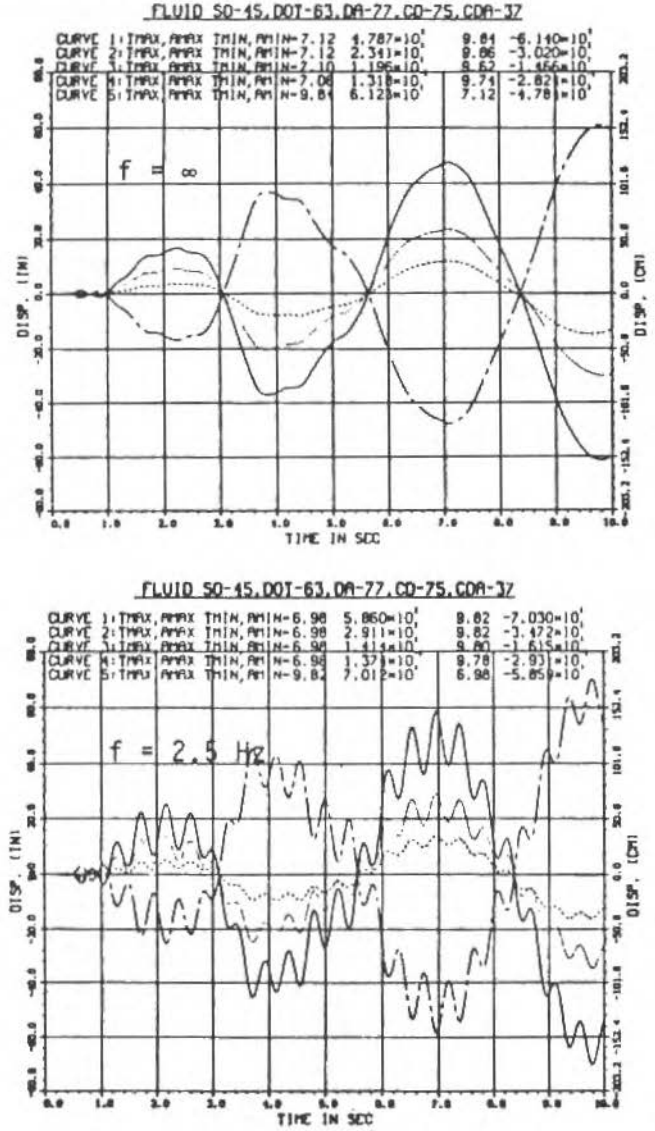

Figure 11. Fluid wave height (a) rigid tank, (b) tank fundamental frequency $f = 2.5$ Hz.

CONCLUSIONS

The development and some applications of the arbitrary Lagrangian-Eulerian techniques to solve free surface viscous flow problems are presented. Various mesh updating methods are indicated including the streamline-upwind Petrov-Galerkin formulation. The applications presented here show that ALE approach allows an efficient and accurate description of large free surface motions. The formulation of a reliable resultant stress degenerated shell element together with stabilization procedures facilitates a large increase in computational efficiency. This is tested on the diamond buckling of shells.

The coupled fluid-structure-free surface formulation is used to study the seismically induced sloshing phenomenon. The numerical analysis of a three-dimensional flexible fluid-tank system provides a better understanding of sloshing response.

ACKNOWLEDGMENT

The support of W.K. Liu by the National Science Foundation is gratefully acknowledged. R.A. Uras would like to thank Dr. Y.W. Chang of the Reactor Engineering Division at Argonne National Laboratory for his support.

REFERENCES

[1] BELYTSCHKO, T.; KENNEDY, J.M.; and SCHOEBERLE, D.F. Quasi-Eulerian Finite Element Formulation for Fluid Structure Interaction, ASME J. Pressure Vessel Technol., Vol. 102, 62–69, 1980.

[2] BELYTSCHKO, T. and LIU, W.K. Computer Methods for Transient Fluid-Structure Analysis of Nuclear Reactors, Nuclear Safety, Vol. 26, 14–31, 1985.

[3] DONEA, J. Arbitrary Lagrangian-Eulerian Finite Element Methods, in: T. Belytschko and T.J.R. Hughes, ed., Computational Methods for Transient Analysis, North-Holland, Amsterdam, 473–516, 1983.

[4] DONEA, J. A Taylor-Galerkin Method for Convective Transport Problems, Intl. J. Numer. Meths. Engrg., Vol. 20, 101–119, 1984.

[5] DONEA, J.; FASOLI-STELLA, P. and GIULIANI, S. Lagrangian and Eulerian Finite Element Techniques for Transient Fluid Structure Interaction Problems, in: Transactions of the 4th Intl. Conf. on Structural Mechanics in Reactor Technology, Paper B1/2, 1977.

[6] HIRT, C.W.; AMSDEN, A.A. and COOK, J.L. An Arbitrary Lagragian Eulerian Computing Method for All Flow Speeds, J. Comp. Phys., Vol. 14, 227–253, 1974.

[7] HUERTA, A. and LIU, W.K. Viscous Flow Structure Interaction, J. Pressure Vessel Technol., Vol. 110, 15–21, 1988.

[8] HUERTA, A. and LIU, W.K. Viscous Flow with Large Free Surface Motion, Comp. Meths. Appl. Mech. Engrg., Vol. 69, 277–324, 1988.

[9] HUGHES, T.J.R. and LIU, W.K. Nonlinear Finite Element Analysis of Shells: Part I, Three-Dimensional Shells. Comp. Methods Appl. Mech. Engrg., Vol. 26, 331-362, 1981.

[10] HUGHES, T.J.R.; LIU, W.K. and ZIMMERMAN, T.K. Lagrangian-Eulerian Finite Element Formulation for Incompressible Viscous Flows, Comp. Meths. Appl. Mech. Engrg., Vol. 29, 329–349, 1981.

[11] HUGHES, T.J.R. and TEZDUYAR. Finite Element Methods for First-Order Hyperbolic Systems with Particular Emphasis on the Compressible Euler Equations, Comp. Meths. Appl. Mech. Engrg., Vol. 45, 217–284, 1984.

[12] LIU, W.K. and CHANG, H.G. Efficient Computational Procedures for Long-Time Duration Fluid-Structure Interaction Problems, ASME J. Pressure Vessel Technol., Vol. 106, 317–322, 1984.

[13] LIU, W.K. and GVILDYS, J. Fluid Structure Interactions of Tanks with an Eccentric Core Barrel, Comp. Meths. Appl. Mech. Engrg., Vol. 58, 51–57, 1986.

[14] LIU, W.K. and LAM, D. Numerical Analysis of Diamond Buckles, Finite Elements in Analysis and Des., Vol. 4, 291-302, 1989.

[15] LIU, W.K.; LAW, E.; LAM, D. and BELYTSCHKO, T. Resultant Stress Degenerated Shell Element, Comp. Methods Appl. Mech. Engrg., Vol. 55, 259–300, 1986.

[16] LÖHNER, R.; MORGAN, K. and ZIENKIEWICZ, O.C. The Solution of Nonlinear Hyperbolic Equations Systems by the Finite Element Method, Intl. J. Numer. Meths. Fluids, Vol. 4, 1043–1063, 1984.

[17] MA, D. GVILDYS, J.; CHANG, Y.W. and LIU, W.K. Seismic Behavior of Liquid Filled Shells, Nucl. Engrg. & Design, Vol. 70, 437–455, 1982.

[18] MUTO, K.; KASAI, Y.; NAKAHARA, M. and ISHIDA, Y. Experimental Tests on Sloshing Response of a Water Pool with Submerged Blocks, Proceedings of the 1985 Pressure Vessel and Piping Conference, Vol. 98-7, ed., S.J. Brown, ASME, 209–214, 1985.

[19] NOH, W.F. CEL: A Time-Dependent Two-Space-Dimensional Coupled Eulerian-Lagrangian Code, in: B. Alder, S. Fernbach and M. Rotenberg, eds., Methods in Computational Physics, Vol. 3, Academic Press, New York, 1964.

[20] RICHTMYER, R.D. and MORTON, K.W. Difference Methods for Initial-Value Problems, Interscience, New York, 2nd. ed., 1967.

RBCM – J. of the Braz.Soc.Mech.Sc. ISSN 0100-7386
Vol.XIV – nº 4 – pp. 369 – 386 – 1992 Impresso no Brasil

FLEXIBLE-SHELL THEORY AND ANALYSIS OF TUBES AND BELLOWS

TEORIA DE CASCAS FLEXÍVEIS E ANÁLISE DE TUBOS E FOLES

E.L.Axelrad
Universität der BW München
Inst. für Mechanik

ABSTRACT

Significant displacements and rotations by small strains are made possible in thin-walled structures by a special design, one assuring a stressed state of the kind inherent for flexibility. The relevant specialization of the general theory simplifies it to the flexible shell theory. This theory helps to gain an insight into the design properties of flexible shells and to treat them numerically. Applied to curved tubes and bellows it covers the influences of the imperfect geometry, edge stiffening (flanges etc.), as well as nonlinearity.

Keywords: Thin Walled Structures ▪ Flexibility ▪ Fexible Shell Theory ▪ Curved Tubes and Bellows

RESUMO

Considerando-se o estado de tensões apropriado a estruturas de paredes finas, são obtidos em pequenas deformações os relevantes deslocamentos e rotações necessários a avaliação da flexibilidade de cascas. A especialização dos resultados a partir da teoria geral rezuz-se a teoria de cascas flexíveis. Esta permite o entendimento das características de projeto das cascas flexíveis e o seu tratamento numérico. Aplicada a tubos curvos e foles esta teoria inclui os efeitos de imperfeições na geometria, da rigidez nas extremidades (flanges, etc.) bem como da não linearidade no comportamento geral de cascas flexíveis.

Palavras-chave: Estruturas de Paredes Finas ▪ Flexibilidade ▪ Teoria de Cascas Finas ▪ Tubos Curvos e Foles

---

Invited Lecture Presented at 7th SIBRAT, Florianópolis, Brazil

INTRODUCTION

The main types of flexible shells employed by industry are presented in Fig.1. By all the obvious diversity, these shells are similar in two essential respects: the kind of loading and the kind of the stress state. The load is applied to the movable edge of the shell and/or consists of a normal pressure. The stress state has the *semi-momentless* character.

The kind of stress state immanent for flexibility becomes clear in the simplest case shown in Fig.2. It is a cantilever plate bent by edge moments M. By thickness h and the extensional strain ε_2 , the plate has elastic curvature $1/R$ determined by the relation $h/(2R) = \varepsilon_2$. The edge of the plate has thereby an angle of rotation $\alpha = L/R = 2L\varepsilon_2/h$ and its displacement is $w = R - R\cos\alpha$. For a steel plate with $\varepsilon_2 = 0.002$ and $h/L = 0.002$ this means $\alpha = 2.0$ radian and $w = 0.708L$. The plate is indeed flexible. This is rendered by the *bending* of the thin wall, not its membrane extension, being dominant. This case is extreme - the membrane strain occurs merely inside a narrow edge zone.

In general, the deformation of a flexible shell cannot be restricted to wall bending and twisting. Avoiding the membrane strain as far as possible remains an optimization aim.

A few words on the position of the theory of flexible shells (short FS) in the entire theory of shells. Since the first publications on shells (*Aron*, 1874 and *Love*, 1888), shells designed to be *stiff*, to work with as *small displacements* as possible (in buildings, ships etc.), have been the predominant concern in the literature. An ideal *stiff shell* must have as little wall bending as possible: the "inextensional bending" is "... nearly always excluded in well-designed shell structures" (*W.T.Koiter* [2], p.38). In a *stiff* shell the wall bending may occur merely in narrow zones near the edges or as a buckling deformation. The two kinds of deformation are ideally served by the two classical branches of the shell theory (presented, e.g., in [1]): the membrane theory and the *Donnell – Mushtary* theory (extended to large displacements by *Koiter*, [2]). The two specialised branches, together with the *Reissner* theory [3] of axisymmetrical shells, have served virtually all of the applications concerning the stiff shells.

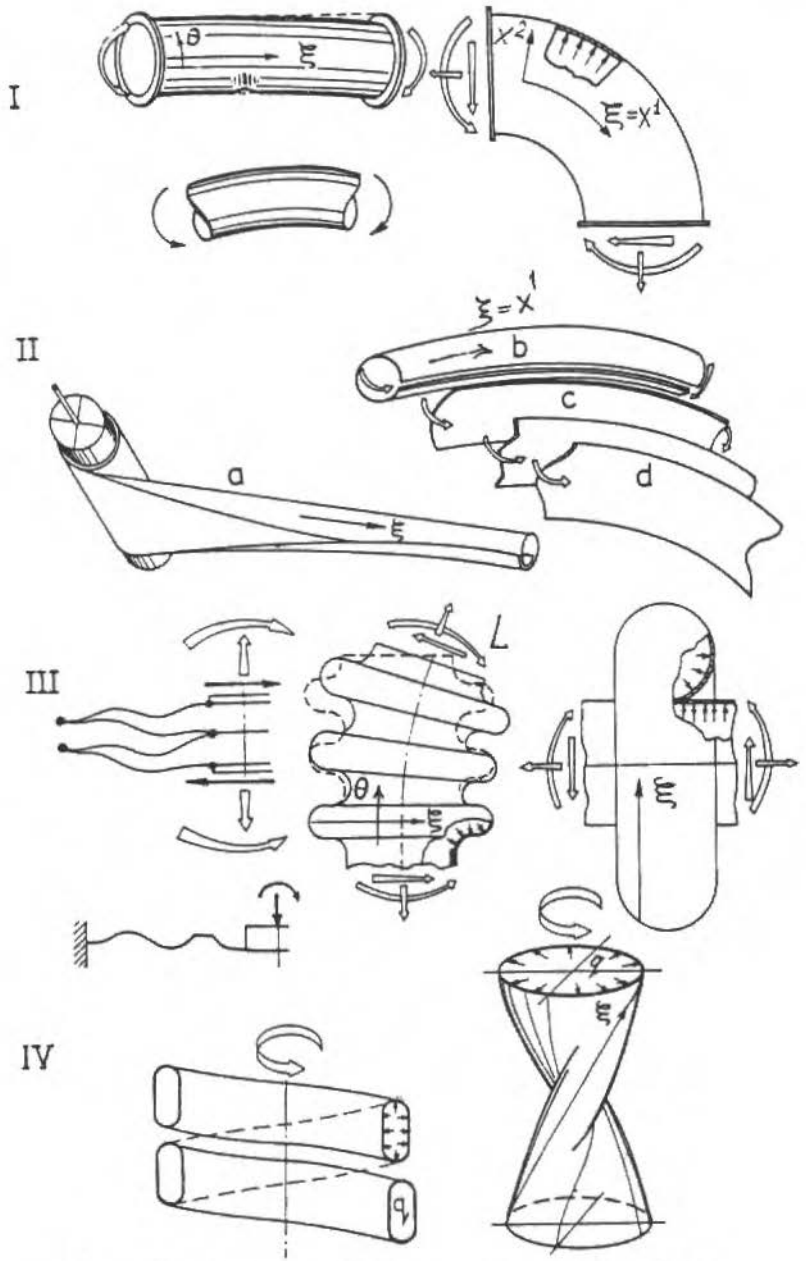

Figure 1. Types of flexible shells encountered in industry.

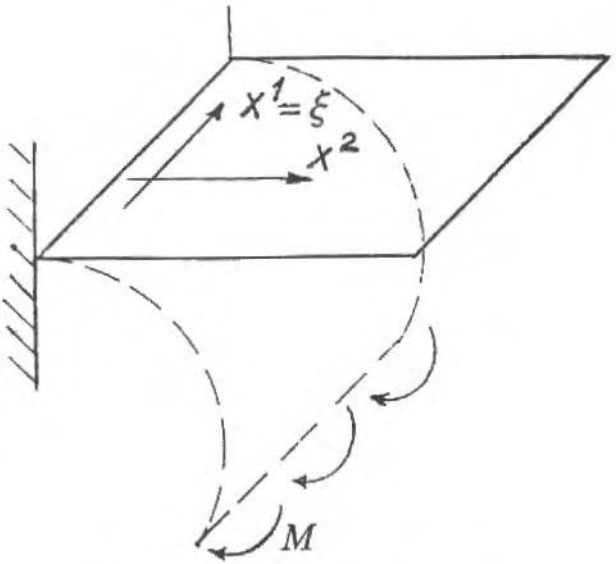

Figure 2. Flat plate in bending.

One-dimensional, problems of FS, have been covered by the *Reissner* axisymmetrical theory. This includes the *Karman* (1911) famous solution for curved tubes. Two-dimensional FS problems were no exception. They were treated with the aid of a *specialized* branch of the shell theory - the FS theory. It has been proposed, first for the analysis of the nonlinear bending of finite tubes, by *Axelrad* [4]. A review of development of the FS theory and further references can be found in [1], [5] and [6].

The significance and role of the general shell theory, including its recent nonlinear developements, has been, actually, to provide the basis for the specialized branches of the theory, responsible for applications.

The following is written by engineer for engineers. It gives an outline of the hypotheses, equations, edge conditions of the FS theory (*Sect.*2) and the uses of this theory for tubes and bellows (*Sect.*3,4). A fuller presentation of the FS theory and its applications, specifically, in the treatment of tubes and bellows, can be found according to the text references.

BASIC FEATURES OF STRAIN AND STRESS IN FS

The inherent features of the FS deformation, that is of *large displacements* by *small strain*, constitute the basic hypotheses of the FS theory. Taken into account in the general shell theory the hypotheses simplify it without any additional inaccuracy. The hypotheses can be stated [7] either as a set of physical assumptions or as a single mathematical restriction on the variation of strain and local shape along the shell middle surface.

Consider these two mutually complementary versions of the hypotheses.

Physical hypotheses

The schemes of Fig.1 illustrate, in fact, suggest, the following two features immanent for the flexibility. Their formulation produces a full set of FS hypotheses. Concerning the strain and, respectively, the equilibrium but not the matherial properties of shells, the hypotheses are relevant also for large and even nonelastic strain.

i) The relative extension ε_2 along one of the surface coordinates ($x^2 = \theta$ in Fig.1) can be neglected in the analysis of strain.

ii) The wall-bending moment M_1 (Fig.3) per unit length of the cross section running along the x^2 - lines can be neglected in all relations of equilibrium.

Consistent with these hypotheses the *Hookean* shell-theory *elasticity relations* must, as has been shown in [8], be specifically simplified. Namely, for isotropic homogeneous shells these relations become:

$$\left.\begin{aligned} \varepsilon_1 Eh = N_1 - \nu N_2 \cong N_1,\ \frac{M_2}{D} = \kappa_2 + \nu\kappa_1 \cong \kappa_2,\ D = \frac{Eh^3}{12(1-\nu^2)} \\ Gh\gamma = S,\ H = 2\tau\frac{Gh^3}{12} \end{aligned}\right\} \quad (1)$$

The stress resultants N_1, N_2, $S_1 = S + H_2/R_2$ and the normal-section curvature $1/R_2$ are shown in *Fig.*3. The strain parameters $\varepsilon_1, \gamma, \kappa_1$ and κ_2 are defined, e.g., in [1], Ch.1.

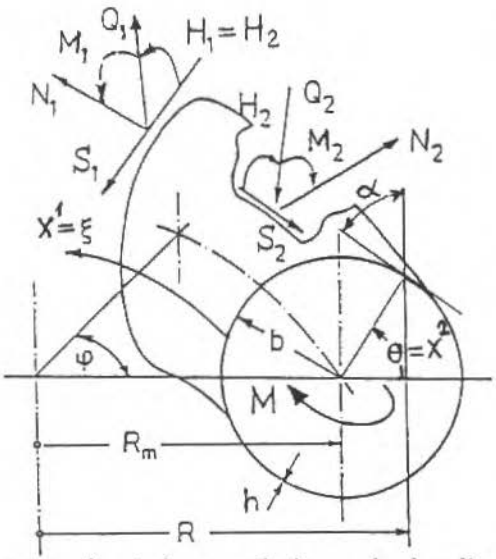

Figure 3. Stress resultants in curved pipe under bending loading.

iii) *Additional simplifications*, possible for *isotropic* FS are: a) disregarding the shear strain resultant γ (angle of shear between the coordinate lines) in the analysis of strain, and b) neglecting the torsional moment H in the relations of equilibrium.

Disregarding γ and H terms is not justified, in particular, for materials with relatively small shear stiffeness ($G/E \ll 1$) and for problems with large intensively variable N_1 forces, as for the tube with the "stiff" flanges, discussed in *Sect.*3.

Mathematical FS hypothesis

It has been shown in [1] and more generally in [6], [7], that the above physical hypotheses are equivalent to a single mathematical statement. The simplifications (i), and (ii) are, namely, *consistently due* for any stress state, which varies with respect to the surface coordinate x^1 much less intensively, than with respect to x^*. Specifically, this means for all the stress and strain resultants (denoted summarily by F) the condition (a and b determine the lengths adx^1 and bdx^2 of the elements of the respective coordinate lines $\xi = x^1, \theta = x^2$):

$$\left|\frac{\partial^2 F}{a^2 \partial \xi^2}\right| \quad \sim \quad \varepsilon \left|\frac{\partial^2 F}{b^2 \partial \theta^2}\right|, \qquad \varepsilon \ll 1 \tag{2}$$

All other equations of the FS theory, as well as its boundary conditions, follow with the hypotheses (i), (ii) or (2) plus the elasticity relations (1) from the classical shell theory. The assumptions (i) and (ii) introduce an error of the order of $\nu\varepsilon$, the error of (iii) is of the order of $(E/G)\varepsilon$. Has ε, defined in (2), the order of magnitude of the error of the general thin-shell theory (h/R_2) or less, so has the FS theory the same accuracy as the general one.

Actually, the FS theory can be based on all three hypotheses (i), (ii) and (iii). With the assumptions (i) and (ii), but not (iii), the shell theory reduces to the "extended" semi-momentless theory, somewhat more general than the theory of FS (cf.[1]).

Discussion

The FS theory contrasts on one principle to the general shell theory and to its other specialized branches. The membrane theory and the *Donnell*-type theories describe strain states which vary slowly or, respectively, strongly with *both* coordinates. The FS theory describes strain states which vary slowly with *one* of the surface coordinates, ξ in (2), and vary strongly with the other, θ in (2). It does *not* regard the stress and deformation in the directions of the two coordinates in an equal way. The coordinate $\xi = x^1$ is intended for a direction specific for the entire class of FS , the $\theta = x^2$ - for the other specific direction. This is conspicious enough in all the hypotheses (i)-(iii) and (2) and in the examples of *Fig.*1. The difference of the FS stress and strain along the coordinate x^1 to that along x^2 does, of course, determine the difference of conditions on the respective shell edges. The conditions on an edge $x^2 = const$ are all those (four) imposed in the general shell theory. On an edge $x^1 = const$ the FS theory imposes, in accordance with (i)-(ii), only two conditions, those of the membrane stress and strain.

Conditions on a shell edge $x^1 = const$ are of two kinds.

a) Those concerning the extension ε_2 of the x^2 line and the wall-bending moment M_1 determine the edge effect deformation which dies out inside a short distance from the edge.(This distance has for a tube (*Fig.*3) the assessment of $3.5\sqrt{hb}$, well-known for cylinder shells).

b) Conditions determining the *main deformation* which varies with x^1 slowly . The main deformation concerns the entire shell *outside* the *edge-effect* zone and determines the strength and deformability of a FS almost entirely. It fulfills the condition (2) and is adequately described by the FS theory. The relevant two edge constraints or forces are of the "membrane", tangential to the middle surface, sort.

For a FS there is usually *no need* to consider the edge effect at the edge $x^1 = const$. Moreover, the relevant edge constraints and moments, are seldom known reliably. If need be, the edge effect can be determined comparatively simply and superimposed on the main deformation. It will not be discussed further in what follows.

Numerical solutions are made essentially easier by the FS theory. For one, by substantial simplification of both the field equations and the boundary conditions. Still more crucial is the facilitation of the numerics, which results from the exclusion of the edge-effect part of the solution. - The FS stress state varies with respect to x^1 as much as R_2/h times less intensively than the edge effect ($1/R_2$ is the normal-section curvature), of which the general-theory description of a problem has to be freed numerically.

Thus, the clearly delimited class of problems, those in the analysis of large deformations by small strain, has a consequently specialized simple theory. Whether a problem can be adequately treated with the aid of the FS theory is usually perceivable without calculations. A solution already obtained can be checked by applying the criterium (2).

A more complete treatment of the FS theory can be found in [1] and [6], its discussion from certain general viewpoints in [7]. Consider the possibilities of the FS theory on hand of two applications.

TUBES

The problem

A thin-walled tube is flexible in the cases shown in $Fig.1-I$. The flexibility is a consequence of wall bending. As can be perceived in $Fig.3$, the longitudinal, tangential to the x^1-line, stresses have in a curved tube resultant forces acting to or from the curvature center of that line. These forces deform the cross sections. This, transverse, deformation, in turn, influences the longitudinal stresses. - The x^1-lines are displaced in their curvature planes so, that their elongation is diminished. The described effect (the Karman effect) becomes substantial when: a)the curvature of the tube (initial or caused by elastical deformation) is not too small, b) the tube wall is sufficiently thin and c) the tube between the end constraints or ribs is long enough to allow a substantial wall bending.

Consider now, summarily, the FS-theory description of the flexure of curved tubes. The following is restricted to linear analysis. Large deformations and buckling are discussed in [1] and [7]. (The history of the tube analysis can be found in [6], [9]. It is rather instructive with sidesteps and downright retrogressions.)

Let the tube have initial curvature $1/R_m$ ($Fig.3$), in the limit case $1/R_m = 0$ (cylinder shell). The cross section is initially circular. The load is applied on the edges which are constrained by flanges. The chosen surface coordinates have the lengths determined by

$$ad\xi = \frac{R}{R_m} bd\xi, \qquad bd\theta, \qquad R = R_m + b\cos\theta \tag{3}$$

At the tube ends $\xi = const$ two (limiting) cases of flanges and the case of transition to an adjoining tube have beeen considered.

(a) *Thin flange*, while preventing deformation of the tube edge in its plane, does not restrict its warping. Any external longitudinal forces are thus directly transmitted to the edge . With the edge forces distributed as $b\cos\theta$

and statically equivalent to a moment M shown in *Fig.*3 the described conditions on the tube edge are

$$\kappa_2 = 0, \qquad N_1 = \frac{M}{\pi b^2 h}\cos\theta \tag{4}$$

(b) *Stiff flange* prevents both the deformation of the tube edge in its plane and its warping out of this plane. The relevant boundary conditions of the semi-momentless theory based on (i) and (ii) (but retaining H and γ - not using the hypothesis (iii)) are according to [1], (3.108), (3.105), (1.86):

$$\kappa_2 = 0, \quad \tau - \frac{1}{2}\left(\frac{(r^2\gamma)_{,2}}{r^2}\right)_{,2} = 0, \qquad (\,)_{,2} = \frac{\partial(\,)}{\partial x^2} = \frac{\partial(\,)}{\partial\theta} \tag{5}$$

(c) On a line $\xi = const$ dividing a tube from the other part of a pipeline (e.g., of different curvature $1/R_m$) must be satisfied four conditions of continuity: κ_2, τ, N_1 and S must be equal on the two sides of the dividing line. (The remaining four continuity conditions are excluded in the FS theory, they determine the mentioned "edge effect".)

Solution

The FS *equilibrium equations* of an element of a curved tube follow from the general theory (e.g.,[1], (1.59)) with the assumption (ii) in the form (notation of $Fig.3$, $c = \cos\alpha$ *and* $s = \sin\alpha determine the shape of the cross-section$, $(\,)_{,1} = \partial(\,)/\partial(x^1)$):

$$\left.\begin{aligned} &\frac{N_{1,1}}{a} + \frac{(R^2S)_{,2}}{R^2 b} + \frac{1}{cR}\frac{(c^2H)_{,2}}{b} + \frac{c}{R}Q_1 + q_1 = 0 \\ &\frac{S_{,1}}{a} + \frac{(RN_2)_{,2}}{Rb} + \frac{1}{R_2 a}H_{,1} + \frac{s}{R}N_1 + \frac{Q_2}{R_2} + q_2 = 0 \end{aligned}\right\} \tag{6}$$

Where N_2, Q_1 and Q_2 are expressed in terms of H and M_2:

$$\left.\begin{aligned} \frac{N_2}{R_2} &= \frac{Q_{1,1}}{a} + \frac{(RQ_2)_{,2}}{Rb} - \frac{c}{R}N_1 + q \\ Q_1 &= \frac{(R^2H)_{,2}}{R^2b} \qquad Q_2 = \frac{(RM_2)_{,2}}{Rb} + \frac{H_{,1}}{a} \end{aligned}\right\} \tag{7}$$

The corresponding compatibility equations are obtained from those of the general theory (e.g.,(1.36) of [1]) with the hypothesis (i). There is no need to write them out here. They follow from (6) and (7) by replacing the stress resultants with the strains according to the static-geometric duality:

$$[\, N_1 \quad S \quad M_2 \quad H \,] \rightarrow [\, \kappa_2 \quad -\tau \quad -\varepsilon_1 \quad \gamma/2 \,]. \tag{8}$$

Two equations (6) with the expressions (7) together with the analogous two equations of compatibility and the equations (1) comprize a system of four partial differential equations:

$$\mathbf{X}_{,1} = \mathbf{A}\mathbf{X} + \mathbf{B}, \qquad \mathbf{X} = \{N_1 \quad \kappa_2 \quad S \quad \tau\}. \tag{9}$$

This system determines the column matrix $\mathbf{X}$ of four resultants which fully represent the stress in the cross-section $\xi = const$ and its deformation (including warping). In the case of zero distributed load $\mathbf{B} = \mathbf{0}$

The deformation of the tube, symmetric with respect to the plane $\theta = 0$, can be represented by the series:

$$[N_1 \quad \kappa_2] = \Sigma[g_j \quad f_j]\cos j\theta\,, \qquad [S \quad \tau] = \Sigma[p_j \quad r_j]\sin j\theta. \tag{10}$$

The g_0 and p_1 represent the resultant forces in a cross section. In the case under discussion (*Fig.*3)they are equal to zero and $g_1 = M/(\pi b^2 h)$ for $h = const$. Conditions of closedness of the cross-sections, i.e., of the θ-lines, give $f_0, f_1, r_1 = 0$. Inserting (10) into (9) gives a system of $4N - 4$ differential equations for the remaining $g_j(\xi)$, $f_j(\xi)$, $p_j(\xi)$, $r_j(\xi)$. The system can be integrated numerically, this is drastically facilitated by the exclusion of the edge effect. The *Euler*-form general solution $C_i \exp d_i\xi$ requires calculation of

the eigenvalues d_i, possible with the aid of standard procedures (cf.reference in [1], p.222). The FS-theory eigenvalues are near to those of the general theory, which represent the *main deformation*. (It must be clear, that dropping at a tube end those terms $C_i \exp d_i\xi$ with $Re(d_i) > 0$, as done in the literature, can lead to substantial error. - Some of the main-deformation terms $C_i \exp d_i$ do *not* "decay with the distance from the end" intensively enough.)

Much simpler than both mentioned is the double Fourier-series solution [1]. It combines (10) with the ξ-series of the form

$$[f_n \quad g_n] = \Sigma [f_{nj} \quad g_{nj}] \cos j\xi \tag{11}$$

This reduces (9) to a system of algebraic equations for the $f_{nj}, \ldots$.

Results

The design requires the basic relations of a problem to be stated *explicitly* and be hand-calculable. Such *simplest solution* has been obtained (cf. [1]) for a wide class of pipe bends. It encompasses most tubes intended for high pressure - all tubes with the thickness and curvature satisfying the condition:

$$\mu = \frac{b}{R_m h^\circ} < 8, \quad h^\circ = \sqrt{\frac{D_m}{E h_m b^2}} \tag{12}$$

Where D_m and h_m are the values of D and h (h may vary with θ) on the line $R = R_m$. For tubes with D defined in (1): $h^\circ = 0.303 h_m/b$.

When the condition (12) is fulfilled, it is sufficient to retain in the series (10) merely the terms with $n < 3$. The system (9) then can be reduced to one differential equation. Its Euler solution contains only four constants C_i which are determined by the conditions on the tube ends explicitely. This gives for the flexure angle, caused by the moments M ($Fig.3$) and the normal pressure q (external pressure - negative) the formulas:

$$\varphi^* - \varphi = FM \frac{\varphi R_m}{E\pi b^3 h}, \quad F = F_0 - F_0 k + k, \tag{13}$$

$$F_0 = \frac{144 + 10\mu^2 + \frac{48qb^3}{D}}{144 + \mu^2 + \frac{48qb^3}{D}} . \tag{14}$$

a) *For "thin flanges"*

$$k = \frac{\sinh l + \sin l}{l\cosh l + l\cos l}, \qquad l = \left(36 + \frac{\mu^2}{4}\right)^{1/4} \sqrt{h^\circ}\, \frac{\varphi R_m}{b}. \tag{15}$$

b) *For "stiff flanges"*

$$k = 2\,\frac{\cosh l - \cos l}{l\sinh l + l\sin l} . \tag{16}$$

The stress state and flexibility of the tubes are exemplified in *Figs.4 and 5.* The solid-line graphs represent the solution of eqs. (9), broken lines - formulas (13)-(16). The pertinent discussion of the specific role of the hypotheses (i)-(iii) and of applicability range of the simplest solution (13)-(16) can be found in [1], pp.234-241 (cf.also [12]), together with the (substantial) simplification of equations (9) by setting $R = R_m$.

A cautionary remark is called for, concerning the *warping of the tube edges.* - A section of the relevant publications is still anaware of the effect of the edge warping. It is this effect, what causes the striking difference, seen in *Figs.*4 and 5, between the cases (a) - free warping of the edges - and (b) - zero warping. In the case (a) for the example of *Fig.*4 the maximum stress is $12.5/1.76 = 7.1$ times higher than in the case (b). The angle of flexure is $16.6/2.89 = 5.7$ times more. The experiments show (*Fig.*5) the flexibility of real tubes to lie *between* those of the limit cases (a) and (b). But the experiments are obviously nearer to the case (a). (Moreover, a flange stiff enough to eliminate the warping, to model the case (b), is difficult to realize, even in experiments.) The oversight of the edge warping leads to errors of up to 200 % and more.

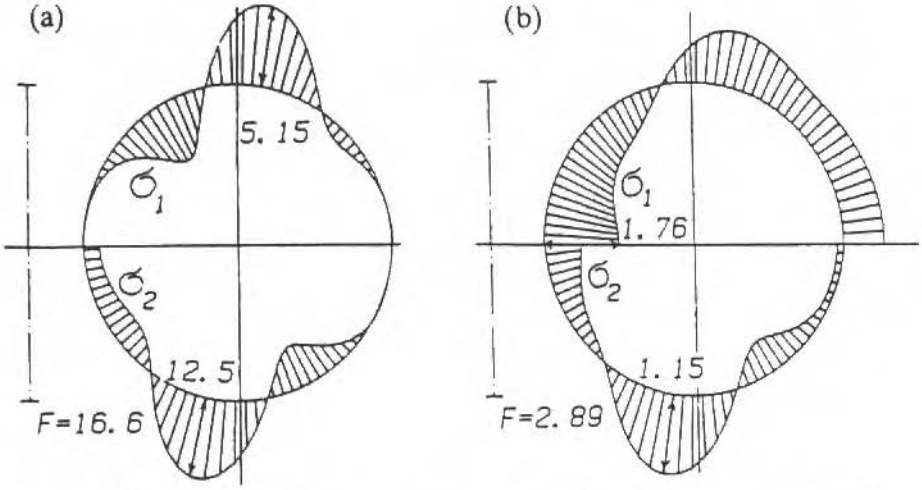

Figure 4. Flexibility factor and stresses in the midlength cross-section of tubes with $h/b = 0.02$, $b/R_m = 1/3$, $\mu = 55.07$, $\varphi = 90^0$. (a) Thin flanges. (b) Stiff flanges. Notation: $\sigma_1 = N_1/(h\sigma_B)$, $\sigma_2 = M_2 6/(h^2\sigma_B)$, $\sigma_B = M/(\pi b^2 h)$.

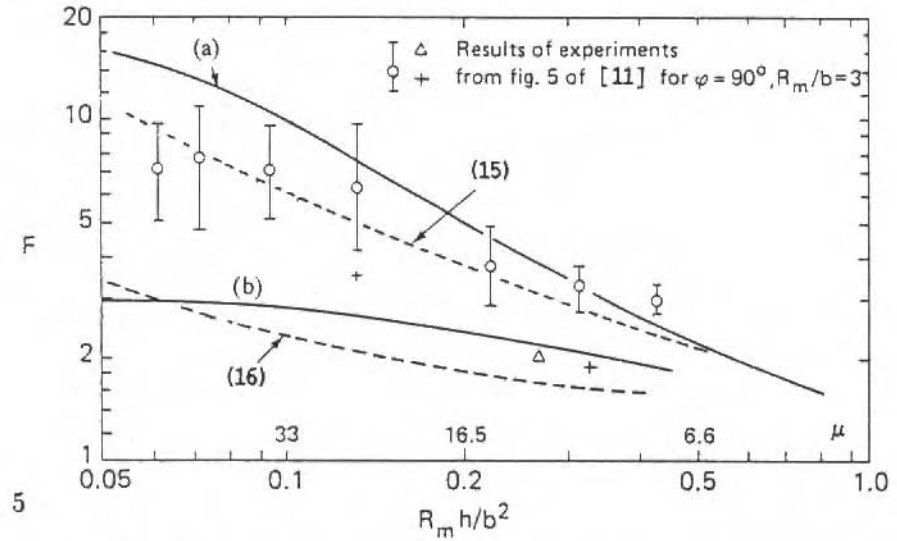

Figure 5. Flexibility factors of pipe bends under different warpping boundary conditions at the edges.

BELLOWS

The problem

Bellows is the most flexible of shells of revolution (*Fig.*1). The *nominal shape* of a bellows, is set forth by detail drawings as composed of straight lines and circle arcs (*Fig.*6), with $h = const$. The *real* shape and thickness depend on the manufacturing technology (cf.profiles and a ground edge presented in [1], *Figs.*63 – 65). The hydraulic shaping of a cylinder tube with $R = R_0$, $h = h_0$ into a bellows with $R = R(\theta)$ produces $h = h(\theta) = h_0\sqrt{R_0/R}$. This relation has been derived analytically [13] and confirmed by measurements.

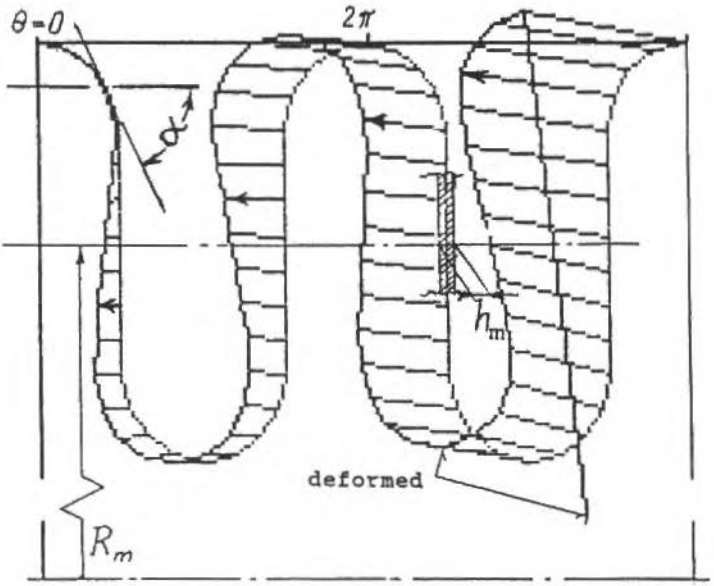

Figure 6. Bellows convolutions in both undeformed and after large elastic deformation configurations.

The axisymmetric nonlinear solution for bellows with arbitrary profile and $h = h(\theta)$ has been obtained in 1966 [13]. (This problem setting has been rediscovered in 1984 - Proc. Int. Conf. Pressure Vessel Technol., San Francisco, v.1, New York).

A substantial simplification of the analysis leans on the possibility to disregard the edge effect on the ends of bellows. - This deformation extends not further from an edge than one convolution and its influence *decreases* the stress [1]. Without the edge effect the axial extension and pure flexure deform all convolutions of a bellows identically. These problems become periodical with respect to $x_2 = \theta$ ($Fig.1 - III$).

For the bending by lateral forces at the ends of a bellows the periodicity has a more general form. - The cross-sectional bending moment (L in $Fig.1 - III$) varies along the bellows $L = L(\theta)$. It is, however, as a rule, possible [1] to apply to this case the description obtained for $L = const$. The accuracy is not thereby impaired when the bellows consists of three or more convolutions. In any case, the deformation can be regarded as periodical in θ with the period encompassing the entire bellows. Is the coordinate θ chosen so, that it varies from θ_0 to $\theta_0 + 2\pi$, inside one period of deformation, so can the stress state be represented by the Fourier series (10), (11).

Solution

The basic problems of large displacements and rotations of bellows, both the axisymmetrical deformation and the flexure, can be effectively treated with the aid of the following FS equations ([1], p.110):

$$\left(F_{,2}\,\frac{r}{t}\right)_{,2} + \mu\sin(\alpha+W) - \mu\sin\alpha = 0, \quad (W_{,2}\,rt^3)_{,2} - \mu F\cos(\alpha+W) = Q. \quad (17)$$

In the axisymmetric case, when F and W depend only on θ, these equations reduce to *Reissner* equations simplified by the FS assumption (2).

The variables F and W represent all stress and strain resultants substantial in the FS theory; in particular

$$N_1 = F_{,2}Ehh^\circ, \quad \kappa_2 = W_{,2}. \quad (18)$$

It is denoted in (17): $r = R/R_m$, $t = h/h_m$. The angle α, the middle radius R_m and middle wall-thickness h_m are denoted in $Fig.6$. The term Q represents in (17) the loading, both applied on the edges and distributed over the surface.

The equations (17) are obtained from the integrals of the FS equilibrium and compatibility equations. They are additionally simplified by dropping terms which are for bellows of the order of $b/(nR_m) = \sqrt{\varepsilon}$, with ε defined in (2) and $2\pi b$ - the extended length of one wave of corrugation. Further, n denotes here the number of the most substantial *Fourier*-series term in (10). Practically n can be assessed by $\sqrt{\mu}$.

The coefficients f_{nj}, g_{nj} of the solution (10), (11) are determined by incremental iterative procedure. The increments of the Fourier coefficients are calculated by solving a system of linear algebraic equations, separate for each $j = 0, 1, 2, \ldots$. This system is obtained from (17) with (10), (11) using the matrix operations with Fourier series ([1], p.130-) and the numerical spectral method, due to V.Axelrad [14]. The iterative procedure assures simplicity of the algorithmus and a chosen accuracy of satisfying the equations (17). It is realizable in a short time with a portable computer.

Results

Two of convolutions of a bellows are shown in *Fig.*6 in both the undeformed state and after large elastic deformation of pure flexure. It is the meridianal section in the plane of flexure, on the compressed side of the bellows. The dimensions are (mm): $R_m = 25$, $R(0) = 30$, $h = h_m = 0.4$, the length of the bellows consisting of 20 corrugation waves is $20 \cdot 8.8 = 176$, the extended length of one convolution $2\pi b$ determines b . The deformation has been computed in the manner indicated in *Sect.*4.2. By small, elastic, extensional strain, here $\varepsilon_2 = \kappa_2 h/2 = 0.0058$, the angular and linear displacements are really considerable: the angle of flexure of each convolution - 3.6 degr., the entire angle of rotation of an end of the bellows with respect to the other end amounts to 72 degr..

The applications of bellows often encompass their use with strains above the elasticity limit. The FS theory can, as mentioned in Sect.2, be extended to the *elastic – plastic* range. Specifically, such a generalization is possible for the solution summarized in Sect.4.2. The basis would be provided by equations analogous to leading to (17).

REFERENCES

[1] AXELRAD, E.L. Flexible Shells. North-Holland, Amsterdam, 1987.

[2] KOITER, W.T. On the Nonlinear Equations of Thin Elastic Shells. Proc. Kon. Ned. Akad. Wetenschappen, B69 (1966) 1/2.

[3] REISSNER, E. On Axisymmetrical Deformations of Thin Shells of Revolution. Proc. Symp. Appl. Math. 3,(1950) 27-52.

[4] AXELRAD, E.L. Refinement of Critical Load Analysis for Tube Flexure by Way of Considering Precritical Deformation. Izv. AN SSSR, OTN, Mekhanika i Mash., n.4 (1965) 133-137 [in Russian].

[5] AXELRAD, E.L. Flexible Shells. Theoret. and Applied Mechanics; Proc. of the 15th Internat. Congr., Toronto (1980). F.P.J.Rimrott and B.Tabarrok, Eds., North-Holland, Amsterdam (1981).

[6] AXELRAD, E.L. Elastic Tubes – Assumptions, Equations, Edge Conditions. Thin-Walled Structures. 3 (1985) 193-215.

[7] AXELRAD, E.L. and EMMERLING, F.A. Intrinsic Shell Theory Relevant for Realizable Large Displacements. Internat. J. Non-Linear Mechanics. 22 (1987)139-150.

[8] AXELRAD, E.L. and EMMERLING, F.A. On Variational Principles and Consistency of Elasticity Relations of Thin Shells. Internat. J. Non-Linear Mechanics. 25 (1990) 27-44.

[9] AXELRAD, E.L. and EMMERLING, F.A. Elastic Tubes. Appl. Mechanics Reviews. 37 (1984) no.7, 891-897.

[10] WHATHAM, J.F. Pipe Bend Analysis by Thin-Shell Theory. Journ. of Appl.Mech, 108 (1986) 173-180.

[11] THOMSON, G and SPENCE, J. The Influence of Flanged end Constraints on Smooth Curved Tubes Under in-plane Bending. Int. Journ. Pressure Vessels and Piping. 13 (1983) 65-83.

[12] HÜBNER, W. Biegung von Torusschalen unter Berücksichtigung der Schubdeformation. ZAMM, 70 (1990) 285-283.

[13] AXELRAD, E.L. Periodic Solutions of Axisymmetrical Problems in Shell Theory. Mechanics of Solids (Transl. of Izv. AN SSSR), 1966, n.2.

[14] AXELRAD, V. A Space-Domain Preconditional Spectral Method for Non-Linear Boundary Value Problems. Intern. Journ. of Numer. Modelling: Electronic Networks, Devices and Fields, V.5 (1992) 67-81.

RBCM – J. of the Braz.Soc.Mech.Sc. ISSN 0100-7386
Vol.XIV – nº 4 – pp. 387 – 402 – 1992 Impresso no Brasil

SNAP-BACK AND TANGENT BIFURCATION PHENOMENA IN ONE-DIMENSIONAL SOFTENING STRUCTURES IN TENSION

OCORRÊNCIA DE BIFURCAÇÃO TANGENTE E RETRAÇÃO EM UMA BARRA TENSIONADA CAPAZ DE APRESENTAR AMOLECIMENTO

J.A.C. Martins
Instituto Superior Técnico
Departamento de Engenharia Civil e CMEST
Av. Rovisco Pais, 1096 Lisboa Codex
Portugal

Rubens Sampaio – ABCM Member
Pontifícia Universidade Católica do Rio de Janeiro
Departamento de Engenharia Mecânica
Rua Marquês de São Vicente, 225 – Gávea
22453 Rio de Janeiro – Brasil

ABSTRACT

In this report we revisit the analysis of [1] and [2] on the behavior of softening bars in tension. We show that when the length of the softening portion of a bar is smaller than some critical value the "incomplete" load-displacement equilibrium trajectory found in [1] can actually be smoothly continued until failure at zero applied load. The point where the load-displacement trajectory was left incomplete in [1] is a point with a vertical tangent and the continuation of that trajectory corresponds to a snap-back: both the load and the displacement decrease thereater because the rate at which the softening portion of the bar elongates is smaller than the rate of shortening of the elastically unloading portion of the bar. We also show that in a continuous bar with a finite region of minimal strength and with smooth stress-strain loading curves ($d\sigma/d\varepsilon = 0$ at the point of maximum stress) the correspoding load-displacement equilibrium trajectories have a tangent bifurcation at the point where the applied load attains its maximum value: at that point all post-bifurcation trajectories have the same (horizontal) tangent as the pre-bifurcation trajectory. Each of the infinite post-bifurcation trajectories corresponds to a specific combination of the portions in the region of minimal strengh where strain-softening or elastic unloading occur thereafter.

Keywords: Damage ▪ Softening Bars in Tension ▪ Snap-Back ▪ Tangent Bifurcation

RESUMO

Neste trabalho estudamos o comportamento de barras tensionadas capazes de apresentar amolecimento. Usando idéias desenvolvidas em [2] retormamos o problema apresentado em [1] reformulando-o e completando-o. O estudo inicial é feito considerando duas barras homogêneas em série e depois generalizamos a análise considerando o caso de uma barra onde as propriedades variam ao longo do comprimento. No caso das duas barras aparece um ponto de retorno que corresponde a uma retração da estrutura. Após este ponto tanto o carregamento aplicado quanto a deformação decrescem até o rompimento da estrutura. Para a barra contínua apresentando uma região de resistência mínima de medida não nula e uma curva de tensão-deformação suave encontramos uma situação interessante, aparentemente inédita na literatura de engenharia. No ponto onde a tensão é máxima todas as trajetórias pós-bifurcação têm a mesma tangente horizontal, ao que denominamos de bifurcação tangente.

Palavras-chave: Dano ▪ Amolecimento de Barras Tensionadas ▪ Retração ▪ Bifurcação Tangente

Submetido em Fevereiro/92 Aceito em Julho/92

A SYSTEM WITH TWO BARS IN SERIES

Governing Equations

Following [1] we consider a one dimensional system of two bars in series with undeformed lengths L_i, as shown in Fig. 1. We assume that the materials of both bars satisfy the following constitutive equations (see Fig. 2)

$$\sigma_i = E_i(1 - D_i)\,\varepsilon_i, i = 1,2 \tag{1}$$

$$\dot{D}_i = K_i\langle\dot{\varepsilon}_i\rangle, i = 1,2 \tag{2}$$

Here σ_i, ε_i and $D_i \in [0,1]$ are the stress, the strain and the damage at bar i, respectively. E_i is the elasticity modulus of bar i at zero damage, the constants K_i in the damage evolution laws (2) are positive and $\langle x\rangle = \max\{0,x\}$. All the above quantities are constant within each of the bars, but σ_i, ε_i and $D_i, i = 1,2$, depend on a strictly increasing time-like parameter t. The equilibrium equation is

$$\sigma_1 = \sigma_2 (= \sigma) \tag{3}$$

and the kinematic compatibility condition is

$$L_1\varepsilon_1 + L_2\varepsilon_2 = \delta\ , \tag{4}$$

where δ is the imposed total elongation of the bar at each time t. We further assume that at the initial time the two bars are virgin and undeformed, i.e.,

$$D_1 = D_2 = \varepsilon_1 = \varepsilon_2 = 0 \text{ at } t = 0\ . \tag{5}$$

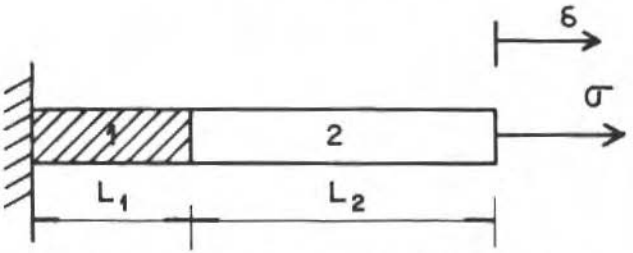

Figure 1. Two bars in series subjected to tension.

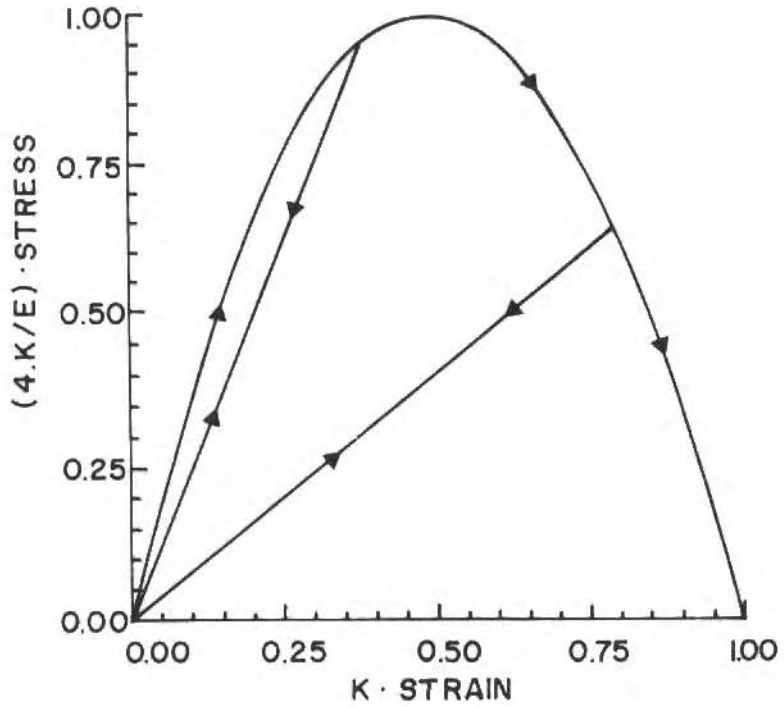

Figure 2. Loading and unloading-reloading $\sigma - \varepsilon$ paths for the constitutive equations (1,2).

Solving the problem

Continuing to follow [1] we combine (1) and (3) to get

$$E_1(1 - D_1)\,\varepsilon_1 = E_2(1 - D_2)\,\varepsilon_2\ . \tag{6}$$

Integrating (2) and taking into account the initial conditions (5) we obtain

$$D_i = K_i\,\varepsilon_i\ , \tag{7}$$

which is valid only while $\dot{\varepsilon}_i > 0, i = 1, 2$. Inserting (7) in (6) we obtain

$$\sigma = \sigma_1 = E_1(1 - K_1\varepsilon_1)\,\varepsilon_1 = E_2(1 - K_2\varepsilon_2)\,\varepsilon_2 = \sigma_2\ , \tag{8}$$

which can be rearranged in the form

$$K_2 E_2 \left(\varepsilon_2 - \frac{1}{2K_2}\right)^2 = K_1 E_1 \left(\varepsilon_1 - \frac{1}{2K_1}\right)^2 + \frac{1}{4}\left(\frac{E_2}{K_2} - \frac{E_1}{K_1}\right) . \quad (9)$$

Without loss of generality, only the cases (a) $E_2/K_2 > E_1/K_1$ and (b) $E_2/K_2 = E_1/K_1$ need to be considered.

(a) The case $E_2/K_2 > E_1/K_1$

In this case (9) represents an hyperbola, as shown in Fig. 3. Only the lower branch of this hyperbola contains the initial state $\varepsilon_1 = \varepsilon_2 = 0$ and leads to quasistatic solutions to the problem, while $\dot{\varepsilon}_1 > 0$ and $\dot{\varepsilon}_2 > 0$. From Fig. 3 we conclude that $\dot{\varepsilon}_2 > 0$ holds only in the interval $0 \leq \varepsilon_1 < \varepsilon_1^* = 1/2K_1$ which corresponds to $0 \leq \varepsilon_2 \varepsilon_2^* = 1/2K_1, \varepsilon_2$ attains a maximum, so that, differentiating (9) and imposing $\dot{\varepsilon}_2 = 0$, we get

$$\varepsilon_2^* = \frac{1}{2K_2}\left[1 - \sqrt{1 - \frac{E_1 K_2}{E_2 K_1}}\right] , \quad (10)$$

and then

$$D_2^* = K_2\, \varepsilon_2^* = \frac{1}{2}\left[1 - \sqrt{1 - \frac{E_1 K_2}{E_2 K_1}}\right]$$

$$E_2^* = (1 - D_2^*)\, E_2 = \frac{E_2}{2}\left(1 + \sqrt{1 - \frac{E_1 K_2}{E_2 K_1}}\right) \quad (11)$$

For $\varepsilon_1 > \varepsilon_1^* = 1/2\ K_1$ we have $\dot{\varepsilon}_2 < 0$, so that bar 2 must unload elastically while bar 1 softens ($\dot{\sigma} = \dot{\sigma}_1 = \dot{\sigma}_2 < 0$ and $\dot{\varepsilon}_1 > 0$). For bar 1 equation (7) continues to apply, while for bar 2 we have now $\dot{D}_2 = 0$ and

$$\sigma_2 = E_2^* \varepsilon_2 = E_2 (1 - D_2^*)\, \varepsilon_2 , \quad (12)$$

with E_2^* and D_2^* constant and given by (11). From (6), (7) and (12) we have now

$$E_2^* \varepsilon_2 = E_1 (1 - K_1\, \varepsilon_1)\, \varepsilon_1 , \quad (13)$$

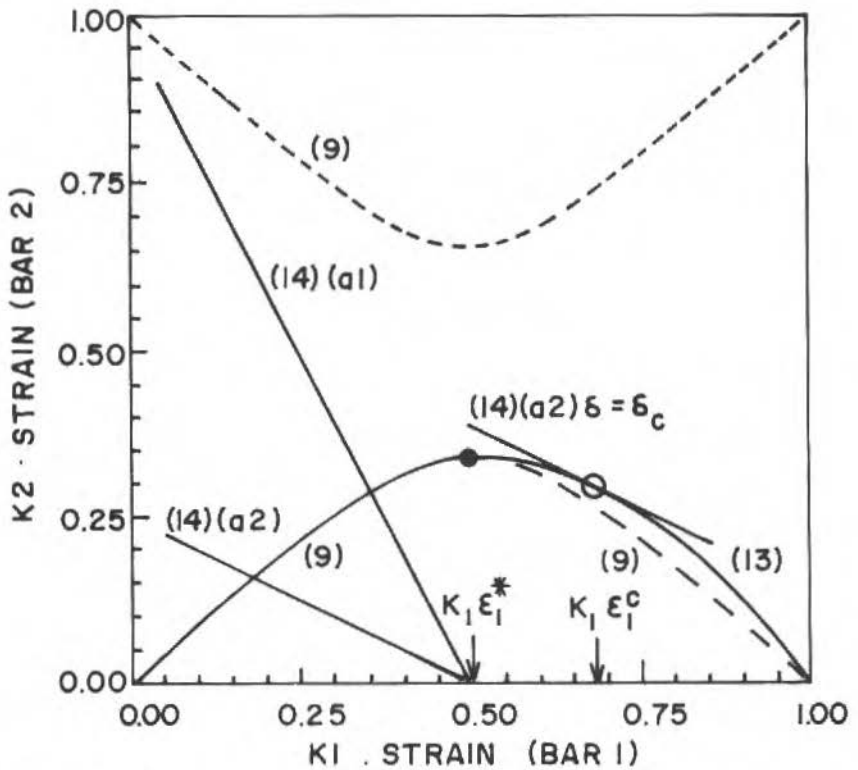

Figure 3. The hyperbola (9) and the parabola (13) for a case (a) ($E_1K_2/E_2K_1 = 0.9$). The straight lines (14) for a case (a1) ($L_1/L_2\ K_1 = 2$, with $\delta = 0.5L_1/K_1$) and for a case (a2) ($L_1K_2/L_2K_1 = 0.5$ with $\delta = 0.5L_1/K_1$ and $\delta = \delta_c = 1.275L_1/K_1$).

which replaces (8,9). This is the equation of a parabola and, comparing it with (9), we may check that for each value $1/2\ K_1 < \varepsilon_1 < 1/K_1$ the value of ε_2 given by (13) is larger than the corresponding value given by (9): the parabola is above the hyperbola (see Fig. 2).

In the present case (a) the problem (1-5) is thus reduced to the determination of the intersections between the curve made of the hyperbola (9) (for $0 \leq \varepsilon_1 \leq 1/2\ K_1$) and the parabola (13) (for $1/2\ K_1 < \varepsilon_1 \leq 1/K_1$) with the straight

lines (4)

$$\varepsilon_2 = -\frac{L_1}{L_2}\,\varepsilon_1 + \frac{\delta}{L_2}\,, \tag{14}$$

for continuously varying values of the total elongation δ. Depending on the angular coefficient $-L_1/L_2$ of these straight lines, two situations may occur:

(a1) For each δ there exists a unique intersection if the slope of the curve (9, 13) is everywhere (algebraically) larger than the slope $(-L_1/L_2)$ of the straight lines (14) (see Fig. 3). From (13) we have that the minimum slope of the curve (9, 13) is

$$\left.\frac{d\varepsilon_2}{d\varepsilon_1}\right|_{\varepsilon_1=\frac{1}{K_1}} = -\frac{E_1}{E_2^*}\,,$$

so that the solution to (9, 13, 14) is unique if

$$\frac{L_1}{L_2} \geq \frac{E_1}{E_2^*}\,. \tag{15}$$

(a2) On the other hand, if

$$\frac{L_1}{L_2} < \frac{E_1}{E_2^*}\,, \tag{16}$$

then for small values of $\delta (0 \leq \delta < \delta_0)$ the intersection is unique, for $\delta_0 \leq \delta < \delta_c$ there exist two points of intersection and, finally, for $\delta = \delta_c$ the straight line (14) is tangent to the parabola (13) (see Fig. 3). It is easy to check that

$$\delta_0 = L_1/K_1$$

and that

$$\varepsilon_1^c = \frac{1}{2K_1}\left(1 + \frac{L_1 E_2^*}{L_2 E_1}\right)\,.$$

In order to interpret the above results we shall now study the load-displacement equilibrium trajectories (σ versus δ).

Differentiating (4) and (8) for $0 \leq \varepsilon_1 \leq \varepsilon_1^* = 1/2\ K_1$ and $0 \leq \varepsilon_2 \leq \varepsilon_2^* < 1/2\ K_2$ we get

$$\frac{d\sigma}{d\delta} = \frac{1}{\dfrac{L_2}{E_2}\dfrac{1}{1-2K_2\varepsilon_2} + \dfrac{L_1}{E_1}\dfrac{1}{1-2K_1\varepsilon_1}} \tag{17}$$

and then $d\sigma/d\delta$ decreases monotonically from $(L_2/E_2+L_1/E_1)^{-1}$ at $\varepsilon_1 = \varepsilon_2 = 0$ to zero at $\varepsilon_1 = \varepsilon_1^*, \varepsilon_2 = \varepsilon_2^*$. On the other hand for $1/2K_1 = \varepsilon_1^* \leq \varepsilon_1 \leq 1/K_1$, we get

$$\frac{d\sigma}{d\delta} = \frac{1}{\dfrac{L_1}{E_1}\dfrac{1}{1-2\,K_1\,\varepsilon_1} + \dfrac{L_2}{E_2^*}}\,, \tag{18}$$

and then, for $\varepsilon_1 = \varepsilon_1^* \doteq 1/2\ K_1$, $d\sigma/d\delta$ is zero. This means that at the point where bar 2 starts to unload elastically and bar 1 initiates softening there exists no discontinuity on the slope of the plot of σ versus δ. Continuing our study, we consider first the case (a1): we have $L_1/E_1 > L_2/E_2^*$ and from (18) it follows that $d\sigma/d\delta$ decreases monotonically from zero at $\varepsilon_1 = 1/2\ K_1$ to $-(L_1/E_1 - L_2/E_2^*)^{-1} < 0$ at $\varepsilon_1 = 1/K_1$. Considering now the case (a2), we have $L_1/E_1 < L_2/E_2^*$ and: (I) when ε_1 increases from $1/2\ K_1$ to ε_1^c then the slope $d\sigma/d\delta$ decreases from zero to $-\infty$; (II) when ε_1 increases from ε_1^c to $1/K_1$ then the slope $d\sigma/d\delta$ decreases from $+\infty$ to $-(L_1/E_1 - L_2/E_2^*)^{-1}$, which is now a positive quantity.

In Fig. 4 we show the equilibrium trajectories (σ versus δ) for both cases (a1) and (a2). These trajectories were evaluated by computing for each ε_1 in the interval $[0, 1/K_1]$ the corresponding pair (δ, σ): σ is given by (8) as a function of ε_1, and δ is given by (4) as a function of ε_1 and ε_2, the latter being evaluated from the hyperbola (9) or the parabola (13). It is clear that in case (a2) the region II ($\varepsilon_1^2 < \varepsilon_1 \leq 1/K_1$) corresponds to a snap-back: both the load σ and the total elongation δ decrease. This happens because, when the length L_1 of the bar in strain-softening is smaller than the critical value L_2E_1/E_2^* (16) and $\varepsilon_1^c < \varepsilon_1 \leq 1/K_1$, the rate at which bar 1 elongates in softening is larger than the rate at which bar 2 shortens elastically:

$$\dot{\varepsilon}_1\ L_1 + \dot{\varepsilon}_2\ L_2 = \left[\frac{L_1}{E_1(1-2\,K_1\,\varepsilon_1)} + \frac{L_2}{E_2^*}\right]\ \dot{\sigma} < 0\ .$$

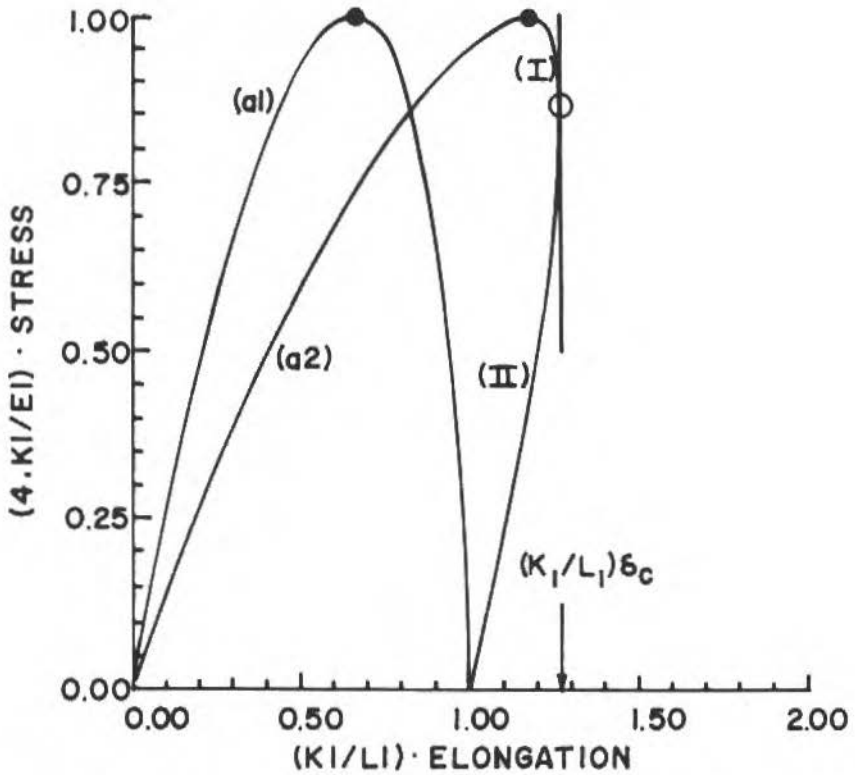

Figure 4. Load-displacement equilibrium trajectories (σ versus δ) for two cases (a): $E_1K_2/E_2K_1 = 0.9$, and $L_1/L_2\ K_1 = 2$, (case (a1)) or $L_1K_2/L_2K_1 = 0.5$ (case (a2)).

Note that from this analysis the only possible conclusion is that, as soon as the elongation δ attains the critical value δ_c, it becomes impossible to increase it further in a quasistatic manner. The staterment of [1] that "there is no solution for values of δ larger than a certain critical value" is correct. However it is at least misleading to classify the point where $\delta = \delta_c$ as the point "where the damaged solution ceases to exist" because the damaged solution continues thereafter with decreasing σ and δ (snap-back).

Before concluding the study of case (a) we wish to point out that the solutions shown above are unique in the sense that any other possible solutions only involve trivial trajectories of elastic unloading or reloading of both bars 1 and 2, which neither dissipate energy nor lead to failure.

(b) The case $E_2/K_2 = E_1/K_1$

As found in [1] the hyperbola (9) degenerates in this case into the two straight-lines (see Fig. 5).

$$\varepsilon_2 = \frac{K_1}{K_2}\,\varepsilon_1 \tag{19}$$

$$\varepsilon_2 = \frac{1}{K_2} - \frac{K_1}{K_2}\,\varepsilon_1 \tag{20}$$

Only the first of these contains the initial state (5) and leads to solutions to the problem, for $\dot{\varepsilon}_1 > 0$ and $\dot{\varepsilon}_2 > 0$. For $\varepsilon_1 = \varepsilon_1^* = 1/2K_1$, $\varepsilon_2 = \varepsilon_2^* - 1/2K_2$ the stresses in both bars attain the maximum value

$$\sigma^* = \sigma_1^* = \sigma_2^* = E_1/4K_1 = E_2/4K_2$$

and thereafter the stresses must decrease. At $\varepsilon_1 = 1/2K_1$, $\varepsilon_2 = 1/2K_2$ we have the possibilities:

(b1) bar 1 strain-softens and bar 2 unloads elastically,

(b2) both bars strain-soften,

and, of course, the trivial unloading of both bars or the situation (b1) with bars 1 and 2 interchanging their roles.

With the arguments used earlier, it follows immediatly that the left derivative $d\sigma/d\delta$ at $\varepsilon_1 = 1/2K_1$, $\varepsilon_2 = 1/2K_2$ is null. In case (b1) the equations that apply on the right of that point are the same as those that apply on the left, so that the right derivative is also null. Case (b2) leads to a situation analogous to the case (a) for $1/2K_1 \leq \varepsilon_1 \leq 1/K_1$ and equation (18) applies again. This shows that the right derivative $d\sigma = d\delta$ at $\varepsilon_1 = 1/2K_1$, $\varepsilon_2 = 1/2K_2$ it is also null.

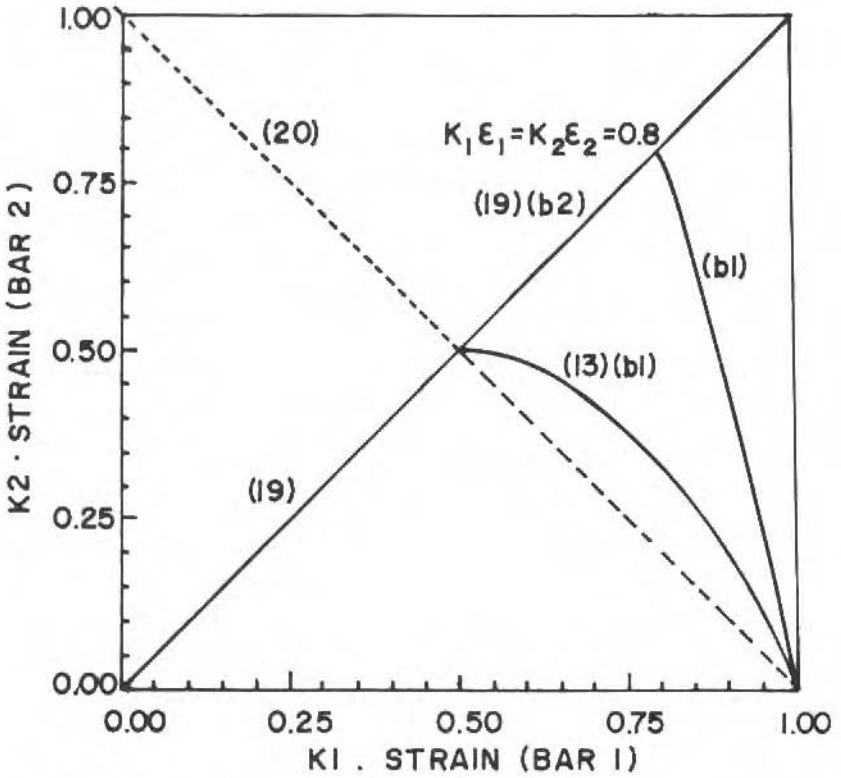

Figure 5. The straight lines (19,20) for case (b). In the post-bifurcation range $1/2K_1 \leq \varepsilon_1 \leq 1/K_1$, case (b1) corresponds to the parabola (13) and case (b2) corresponds to the straight line (19). Also on the same figure the parabola that corresponds to the trajectory of the type (b1) that bifurcates from the trajectory of the type (b2) at a point where $\varepsilon_1 = 0.8K_1$ $\varepsilon_2 = 0.8/K_2$.

We conclude that the bifurcation on the equilibrium trajectories at the point of maximum load is a tangent bifurcation: all the post-bifurcation trajectories have the same (horizontal) slope as the pre-bifurcation trajectory (see Fig. 6).

Without giving the details we finally observe that every point of the post-bifurcation trajectory (b2) is also a bifurcation point from which a trajectory

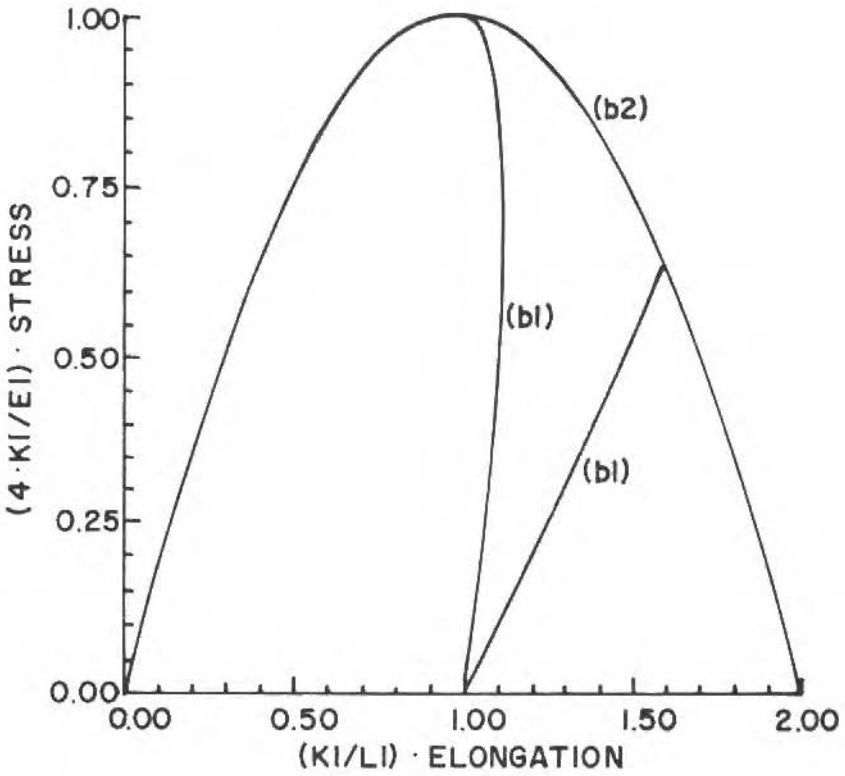

Figure 6. Load-displacement equilibrium trajectories (σ versus δ) for case (b) ($E_1K_2/E_2K_1 = 1$, $L_1K_2/L_2K_1 = 1$). Post-bifurcation trajectories of the type (b1) and (b2). Trajectory of the type (b1) that bifurcates from the trajectory of the type (b2) at a point where $\varepsilon_1 = 0.8/K_1\varepsilon_2 = 0.8/K_2$.

of the type (b1) emanates. These additional bifurcations are not tangent bifurcations for $\sigma^* > \sigma > 0$ (see Figs. 5 and 6).

A CONTINUOUS BAR IN TENSION

Governing Equations

We consider now a bar $\Lambda = \{x : 0 \leq x \leq L\}$ such that the constitutive

equations

$$\sigma(x) = E(x)(1 - D(x))\, \varepsilon(x) \tag{21}$$

$$\dot{D}(x) = K(x)\langle \dot{\varepsilon}(x) \rangle \tag{22}$$

hold at each point of the bar. Here $E(x)$ and $K(x)$ are strictly positive functions of $x \in \Lambda$ and $\sigma(x)$, $\varepsilon(x)$ and $D(x)$ are the unknown stress, strain and damage, repsectively, at each $x \in \Lambda$. The equilibrium equations is

$$\sigma(x) = \sigma \qquad \forall x \in \Lambda \tag{23}$$

and the kinematic compatibility condition is

$$\int_0^L \varepsilon(x)\, dx = \delta\ , \tag{24}$$

where δ is the imposed total elongation of the bar. For simplicity, we omit from the notations the dependence of $\sigma(x)$, $\varepsilon(x)$, $D(x)$, σ and δ on a strictly increasing time-like parameter t. We also assume that at the initial time the bar is virgin and undeformed, i.e.,

$$D(x) = \varepsilon(x) = 0 \qquad \forall x \in \Lambda \ \text{ at } t = 0\ . \tag{25}$$

Solving the Problem

Similarly to (8) we get

$$\sigma = \sigma(x) = E(x)(1 - K(x)\, \varepsilon(x))\, \varepsilon(x) \tag{26}$$

for all $x \in \Lambda$, while

$$\dot{\varepsilon}(x) > 0 \qquad \forall x \in \Lambda\ . \tag{27}$$

It follows that, while (27) holds, we have

$$\varepsilon(x) = \frac{1}{2K(x)} \left[1 - \sqrt{1 - \frac{4K(x)\, \sigma}{E(x)}} \right]\ ,$$

with

$$0 \le \varepsilon(x) < \frac{1}{2K(x)} \quad \text{and} \quad 0 \le \sigma < \frac{E(x)}{4K(x)}\ . \tag{28}$$

While (27) and (28) hold, the positive stress and elongation rates are given by

$$\dot{\sigma} = E(x)\sqrt{1 - \frac{4K(x)\,\sigma}{E(x)}}\;\dot{\varepsilon}(x)\;,$$

$$\dot{\delta} = \dot{\sigma}\int_0^L \frac{dx}{E(x)\sqrt{1 - \frac{4K(x)\,\sigma}{E(x)}}}\;,$$

so that the positive slope of the σ versus δ curve is

$$\frac{d\sigma}{d\delta} = \frac{1}{\int_0^L \frac{dx}{E(x)\sqrt{1-\frac{4K(x)\,\sigma}{E(x)}}}}\;. \tag{29}$$

Let σ^* be the maximum admissible stress at the points of the bar with minimal strength

$$\sigma^* = \min_{x\in\Lambda}\;\frac{E(x)}{4K(x)}\;.$$

We assume that the set

$$\Lambda_1^* = \left\{x \in \Lambda\;:\;\frac{E(x)}{4K(x)} = \sigma^*\right\}$$

has non-zero length and we denote

$$\Lambda_2^* = \Lambda\backslash\Lambda_1^* = \left\{x \in \Lambda\;:\;\frac{E(x)}{4K(x)} => \sigma^*\right\}$$

Now, if t^* is the time at which the increasing stress σ equals σ^*, it is clear that the expressions (28) hold for $0 \le t < t^*$, while for $t = t^*$ we get

$$\varepsilon(x) = \frac{1}{2K(x)}\;,\;\sigma(x) = \sigma^* = \frac{E(x)}{4K(x)} \qquad \forall x \in \Lambda_1^*$$

$$\varepsilon(x) < \frac{1}{2K(x)}\;,\;\sigma(x) = \sigma^* < \frac{E(x)}{4K(x)} \qquad \forall x \in \Lambda_2^*\;.$$

The constitutive behavior in Λ_1^* then implies that $\dot{\sigma}(x) \leq 0$ for all $x \in \Lambda_1^*$ and for all $t \geq t^*$. It follows that

$$\dot{\sigma} = \dot{\sigma}(x) \leq 0 \qquad \forall x \in \Lambda \qquad \forall t \geq t^* \ .$$

which in turn implies that all the points of Λ_2^* initiate elastic unloading at $t = t^*$. If "trivial" elastic unloadings of the whole bar are excluded, then, for some $t > t^*$ and some subset of points x of Λ_1^*, equation (26) is still valid with $\sigma(x) = \sigma < \sigma^*$, $\varepsilon(x) > 1/2K(x)$, $\dot{\sigma}(x) = \dot{\sigma} < 0$, $\dot{\varepsilon}(x) > 0$. For $t \geq t^*$ we shall denote

$$\Lambda_1 = \left\{ x \in \Lambda \ : \ \dot{\varepsilon}(x) = \frac{1}{2K(x)} \left[1 + \sqrt{1 - \frac{4K(x)\,\sigma}{E(x)}} \right] \right\} \subset \Lambda_1^* \ ,$$

$$\Lambda_2 = \left\{ x \in \Lambda \ : \ \frac{1}{2K(x)} \left[1 - \sqrt{1 - \frac{4K(x)\,\sigma}{E(x)}} \right] \leq \varepsilon(x) < \frac{1}{2K(x)} [1 + \sqrt{1 - \frac{4K(x)\,\sigma}{E(x)}} \right] \right\} \supset \Lambda_2^*$$

$$\Lambda_{11} = \left\{ x \in \Lambda_1 \ : \ \dot{\sigma}(x) = -E(x) \sqrt{1 - \frac{4K(x)\,\sigma}{E(x)}}\ \dot{\varepsilon}(x) \right\} \subset \Lambda_1 \ ,$$

$$\Lambda_{12} = \{ x \in \Lambda_1 \ : \ \dot{\sigma}(x) = E_{12}(x)\ \dot{\varepsilon}(x) \} \subset \Lambda_1 \ ,$$

where $\dot{\sigma}$ amd $\dot{\varepsilon}$ denote right stress and strain rates, respectively, and $E_{12}(x)$ is given by

$$E_{12}(x) = \frac{E(x)}{2} \left(1 - \sqrt{1 - \frac{4K(x)\,\sigma}{E(x)}} \right) \ , \tag{30}$$

for $x \in \Lambda_1$, $\sigma^* \geq \sigma > 0$, $t \geq t^*$. Note that Λ_1 is the set of points on the strain-softening portions of the $\sigma(x) - \varepsilon(s)$ constitutive relations, Λ_{12} is the set of points in Λ_1 where elastic unloading unitiates precisely at the time t, Λ_2 is the set $\Lambda \backslash \Lambda_1$ and Λ_{11} is the set $\Lambda_1 \backslash \Lambda_{12}$. Note also that for all $x \in \Lambda_2$ the right stress and strain rates at time $t(\geq t^*)$ are related by

$$\dot{\sigma}(x) = E_2\ \dot{\varepsilon}(x) \ ,$$

where (compare with (11) and (30))

$$E_2(x) = \begin{cases} \dfrac{E(x)}{2}\left(1+\sqrt{1-\dfrac{4K(x)\,\sigma^*}{E(x)}}\right), & \text{if } x \in \Lambda_2 \cap \Lambda_2^* \\ \dfrac{E(x)}{2}\left(1-\sqrt{1-\dfrac{4K(x)\,\sigma^*}{E(x)}}\right), & \text{for some } \sigma \in]\sigma^*,\sigma^*[, \text{if } x \in \Lambda_2 \backslash \Lambda_2^* \end{cases} \tag{31}$$

For $t \geq t^*$ and $\sigma^* \geq \sigma \geq 0$ the elongation δ is thus related to the stress σ by

$$\delta = \int_{\Lambda_1} \frac{1}{2K(x)}\left[1+\sqrt{1-\frac{4K(x)\,\sigma}{E(x)}}\right] dx + \sigma \int_{\Lambda_2} \frac{dx}{E_2(x)},$$

while the corresponding (right) rates are related by

$$\dot{\delta} = \dot{\sigma}\left[-\int_{\Lambda_{11}} \frac{dx}{E(x)\sqrt{1-\frac{4K(x)\,\sigma}{E(x)}} + \int_{\Lambda_{12}} \frac{dx}{E_{12}(x)} + \int_{\Lambda_2} \frac{dx}{E_2(x)}}\right]$$

The (right) slope of the σ versus δ curve at $t \geq t^*$, $\sigma \in]0,\, \sigma^*]$ is thus

$$\frac{d\sigma}{d\delta} = \frac{1}{-\int_{\Lambda_{11}} \frac{dx}{E(x)}\sqrt{1-\frac{4K(x)\,\sigma}{E(x)}} + \int_{\Lambda_{12}} \frac{dx}{E_{12}(x)} + \int_{\Lambda_2} \frac{dx}{E_2(x)}}. \tag{32}$$

Having excluded "trivial" elastic unloadings of the whole bar (length of $\Lambda_{11} > 0$ for all $\sigma \in]0, \sigma^*]$), we may conclude from (29) and (32) that, independently of the size and the distribution of Λ_{11} and Λ_{12} along Λ_1^*, the right slope of the σ versus δ curve at $\sigma = \sigma^*$ is always equal to the null left slope of that curve at the same point. This means that the equilibrium point at the maximal load ($\sigma = \sigma^*$) is a point of tangent bifurcation from which an infinite number of equilibrium trajectories emanates. These trajectories differ from each other on the size and the distribution of softening and unloading portions along the finite-length region of minimal strength (Λ_1^*). In addition, all the points in these post-bifurcation trajectories are also bifurcation points at which different

sizes and distributions of Λ_{11} and Λ_{12} in Λ_1 also originate an infinite number of distinct solutions. These additional bifurcations are not in general tangent bifurcations. For a discussion on the stability of these bifurcated trajectories in related problems see [2]. Finally we observe that expression (32) also shows that a snap-back may also occur in a continuous bar: when the softening portion Λ_{11} of a bar and the stress σ are sufficiently small the slope $d\sigma/d\delta$ may become positive.

ACKNOWLEDGMENT

This work was suported by JNICT (Portugal) and CNPq (Brasil).

REFERENCES

[1] René Billardon, Jorge G.S. Patiño, "One Dimensional Softening and Stability Due to Continum Damage", COBEM 87, IX Congresso Brasileiro de Engenharia Mecânica, Florianópolis, SC, Dezembro 1987, pp. 491–493.

[2] Gianpietro del Piero, Rubens Sampaio, "Localization in Damage and Plasticity Predicted by a Principle of Minimum Dissipation Rate" (in preparation).

RBCM – J. of the Braz.Soc.Mech.Sc. ISSN 0100-7386
Vol.XIV – nº 4 – 1992 Impresso no Brasil

DINAME 93 — V Symposium on Dynamic Problems of Mechanics

March 01-05, 1993 – Santa Catarina — Brasil

Sponsor: ABCM – Associação Brasileira de Ciências Mecânicas

Organization: Comittee of Dynamics, ABCM

DINAME is a symposium held bi-yearly since 1986. It is already a well established forum for significant participation of very known international researchers in dynamics. In the last four meetings, the number of participants has grown from about eighty to over a hundred and twenty, with about twenty per cent being from abroad. The meetings are always held in a quiet and pleasant hotel, on a friendly regime of immersion, with intense interchange of knowledge and information amongst participants. Further, all the tecnical sessions occur in just one room, so that every single work is addressed to all participants. In parallel with the symposium, a series of short courses are offered by brazilian and foreign specialists to practicing engineers.

The V DINAME will be held in the Plaza Caldas da Imperatriz. This is a first class hotel with complete infra-structure for sports, leisure and meetings. It is located in a mountainous region surrounded by a luxurious green unspoilled area. The hotel is only about fourty minutes by car or bus from Florianópolis, the capital of Santa Catarina state, where about fourty two white fine sand beaches stand. Arrangements can be made for those wishing to stay in Florianópolis after the symposium.

Over seventy papers from brasilian researchers and other eighteen from relevant foreigners have been accepted. They come from various countries, such as Coreia, France, England, USA, Switzerland, Germany and Czechoslovakia.

The following short courses will be offered to participant engineers: *Robot Vision and Autonomous Vehicles* (Prof. Dr. V. Graefe/Munchen); *Método de Elemento Finitos em Aplicações na Indústria* (Prof. C.A. Almeida/PUC-Rio); *Random Vibrations of Structures* (Prof. I. Elishakof/Florida); *Análise Modal Experimental* (Profs. P.R. Kurka and C. Arruda/Campinas); *Complementary Topics on Model Analysis* (Prof. D.J. Ewins/London); *Monitoramento de Maq. Rotativas I* (B& K do Brasil); *Monitoramento de Maq. Rotativas II* (Prof. Arthur Ripper/UFRJ-Rio). To the participants, hands on session on modal identification will be provided by MTS Sistemas do Brasil Ltda.

For further information please contact:
Prof. José J. de Espindola
Lab. de Vibrações e Acústica, Departº de Engenharia Mecânica
Universidade Federal de Santa Catarina, C.P. 476
88049 – Florianópolis, SC – Brasil

RBCM – J. of the Braz.Soc.Mech.Sc. ISSN 0100-7386
Vol.XIV – nº 4 – 1992 Impresso no Brasil

Agradecimentos

O Conselho Editorial da Revista Brasileira de Ciências Mecânicas, agradece a contribuição de todos os revisores que se empenharam para a boa apresentação dos trabalhos publicados durante os anos de 1987 a 1992.

A. BUSCHINECCI (UFSC)
Abimael F.D. LOULA (LNCC)
Afonso TELLES (COPPE/UFRJ)
Alacys MORGENSTERN JR. (IAE)
Alcir de Faro ORLANDO (PUC-Rio)
Alvaro G. Badan PALHARES (UNICAMP)
Alvaro Toubes PRATA (UFSC)
Angela O. NIECKELE (PUC-Rio)
Antonio Celso F. ARRUDA (UNICAMP)
Antonio F.C. SILVA (UFSC)
Antonio F.P. FORTES (UnB)
Antonio MACDOWELL Figueiredo (COPPE/UFRJ)
Antonio S. VARGAS (PUC-Rio)
Arno BLASS (UFSC)
Arno KRENZIGIR (UFRGS)
Arthur BRAGA Filho (PUC-Rio)
Arthur RIPPER (COPPE/UFRJ)
Atila P. FREIRE (COPP/UFRJ)
Benedito M. PURQUERIO (EESC/USP)
Berend SNOEIJER (UFSC)
Boleslaw SKARSKI (UNICAMP)
Carlos A. ALMEIDA (PUC-Rio)
Carlos A.C. ALTEMANI (UNICAMP)
Carlos Alberto C. SELKE (UFSC)
Carlos E.A. MANESCHY (PUC-Rio)
Carlos V.M. BRAGA (PUC-Rio)
Cesar C. SANTANA (UNICAMP)
Cid Santos GESTEIRA (UFBA)
Clovis R. MALISKA (UFSC)
Clovis S. BARCELLOS (UFSC)
Edmundo KOELLE (USP)
Edson BAZZO (UFSC)
Edson L. ZAPAROLLI (ITA)
Eduardo Cleto PIRES (USP)

Erico E.A. de ARAGÃO
Ettore BRESCIANI FILHO (UNICAMP)
Fathi Aref Ibrahim DARWISH (PUC-Rio)
Fernando IGUTI (UNICAMP)
Fernando L. BASTIAN (COOPE/UFRJ)
Fernando VENÂNCIO FILHO (COPPE/UFRJ)
Francisco E.M. SABOYA (PUC-Rio)
Francisco P.L. LEPORE (UFU)
Genesio J. MENON (UFU)
Giorgio E.O. GIACAGLIA (USP)
Guilherme MOREIRA (COPESP)
Hans Ingo WEBER (UNICAMP)
HALEI F. Vasconcelos (UFPA)
Hazim A. Al-Qureshi (ITA)
Helio NANNI (INST. MAUA DE TECNOLOGIA)
Henner Alberto GOMIDE (UFU)
Heraldo S.C. MATTOS (PUC-Rio)
I-Shih LIU (COPPE/UFRJ)
Jaime T.P. CASTRO (PUC-Rio)
Jan Leon SZIESKO (COPPE/UFRJ)
Jersey T. SIELAWA (INPE)
JESUS A. Costa (PUC-Rio)
João B. APARECIDO (UNESP)
João Carlos MENEZES (ITA/CTA)
João F. ESCOBEDO (UNESP)
João F.G. de OLIVEIRA (EESC/USP)
João Luiz F. AZEVEDO (ITA)
João Luiz P. ROEHL (PUC-Rio)
João Nisan C. GUERREIRO (LNCC)
Jorge D. RIERA (UFRGS)
José Alberto R. PARISE (PUC-Rio)
J.C. DUTRA (UFSC)
José C.F. TELLES (COPPE/UFRJ)
José C. GEROMEL (UNICAMP)
José Daniel B. MELO (UFU)
José Herskovits NORMAN (COPPE/UFRJ)
José João de ESPINDOLA (UFSC)
José Luiz F. FREIRE (PUC-Rio)
José M.S. JABARDO (USP)
José R.F. ARRUDA (UNICAMP)
Jules SLAMA (COPPE/UFRJ)
Julio MILITZER (UNIV. NOVA SCOTIA)

Agradecimentos

K. GHAVAMI (PUC-Rio)
Kamal A.R. ISMAIL (UNICAMP)
Leonardo GOLDSTEIN (UNICAMP)
Leopoldo P. FRANCA (LNCC)
Lirio SHAEFFER (UFRGS)
Liu KAY (UFPB)
Lourival BOEHS (UFSC)
Luiz Carlos MARTINS (COPPE/UFRJ)
Luiz Carlos WROBEL (COPPE/UFRJ)
Luiz C.V. FERNANDES (COOP/UFRJ)
LUIZ ELOY Vaz (PUC-Rio)
Luiz Fernando A. AZEVEDO (PUC-Rio)
Luiz Fernando MILANEZ (UNICAMP)
LUIZ HENRIQUE de Almeida (COPPE/UFRJ)
Marcelo LEMOS (ITA/CTA)
Mauri FORTES (UFMG)
Mauricio Prates de CAMPOS FILHO (UNICAMP)
Miguel HIRATA (COPPE/UFRJ)
Moyses ZINDELUK (COPPE/UFRJ)
Nelson Back (UFSC)
NESTOR A.ZOUAIN Pereira (COPPE/UFRJ)
Ney Augusto DUMONT (PUC-Rio)
Nisio C.L. BRUM (COPPE/UFRJ)
Nivaldo L. CUPINI (UNICAMP)
Olegario PEREZ (ITA)
Osvair Vidal TREVISAN (UNICAMP)
Patricio LAURA (UNIV. DER SUR, BAIA BLANCA)
Paulo A.O. SOVIERO (ITA)
Paulo Cesar PHILIPPI (UFSC)
Paulo Jorge PAES LEME (PUC-Rio)
PAULO MURILLO S. Araujo (PUC-Rio)
Paulo R.G. KURKA (UNICAMP)
Paulo RIZZI (ITA)
Paulo R. SOUZA MENDES (PUC-Rio)
Pedro CARAJILESCOV (PUC-Rio)
Perrin S. NETO (UFU)
Raul ROSAS E SILVA (PUC-Rio)
Renato COTTA (COPPE/UFRJ)
Raul FEIJOO (LNCC)
Roberto A. TENENBAUM (COPPE/UFRJ)
Roberto LAMBERTS (UFSC)
Rogério M. SALDANHA DA GAMA (LNCC)

Rogério P. KLÜPEL (UFPb)
Rogério T.S. FERREIRA (UFSC)
Ronaldo D. VIEIRA (PUC-Rio)
Ronaldo KRAUSS (RHODIA S.A.)
Rosalvo T. RUFFINO (EESC/USP)
Rubens SAMPAIO (PUC-Rio)
Samuel CELERE (EESC/USP)
Sergio COLLE (UFSC)
Sergio L.V. COELHO (COPPE/UFRJ)
Sergio M.G. GUERRA (UNICAMP)
Sergio M. SABOYA (ITA)
Sergio Neves MONTEIRO (COPPE/UFRJ)
Sergio V. BAJAY (UNICAMP)
Sergio Tonini BUTTON (UNICAMP)
Silvia A. NEBRA PEREZ (UNICAMP)
Solly SEGENREICH (PUC-Rio)
Valder STEFFEN JR. (UFU)
Waldemir Gutierrez RODRIGUES (IPEN)
Walter L. WEINGAERTNER (UFSC)
Washington BRAGA FILHO (PUC-Rio)
Webe João MANSUR (COPPE/UFRJ)

Revista Brasileira de Ciências Mecânicas.
Vol. 1. Nº 1 (1979)-
Rio de Janeiro: Associação Brasileira de Ciências Mecânicas.
Trimestral
Inclui referências bibliográficas.
1. Mecânica
ISSN-0100-7386

OBJETIVO E ESCOPO

A Revista Brasileira de Ciências Mecânicas visa a publicação de trabalhos voltados ao projeto, pesquisa e desenvolvimento nas grandes áreas das Ciências Mecânicas. É importante apresentar os resultados e as conclusões dos trabalhos submetidos de forma que sejam do interesse de engenheiros, pesquisadores e docentes.

O escopo da Revista é amplo e abrange as áreas essenciais das Ciências Mecânicas, incluindo interfaces com a Engenharia Civil, Elétrica, Metalúrgica, Naval, Nuclear, Química e de Sistemas. Aplicacões da Física e da Matemática à Mecânica também serão consideradas.

Em geral, os Editores incentivam trabalhos que abranjam o desenvolvimento e a pesquisa de métodos tradicionais bem como a introdução de novas idéias que possam potencialmente ser aproveitadas na pesquisa e na indústria.

AIMS AND SCOPE

The Journal of the Brazilian Society of Mechanical Sciences is concerned primarily with the publication of papers dealing with design, research and development relating to the general areas of Mechanical Sciences. It is important that the results and the conclusions of the submitted papers be presented in a manner which is appreciated by practicing engineers, researchers, and educators.

The scope of the Journal is broad and encompasses essential areas of Mechanical Engineering Sciences, with interfaces with Civil, Eletrical, Metallurgical, Naval, Nuclear, Chemical and System Engineering as well as with the areas of Physics and Applied Mathematics.

In general, the Editors are looking for papers covering both development and research of traditional methods and the introduction of novel ideas which have potential application in science and in the manufacturing industry.

Notes and Instructions To Contributors

1. The Editors are open to receive contributions from all parts of the world; manuscripts for publication should be sent to the Editor-in-Chief or to the appropriate Associate Editor.
2. (i) Papers offered for publication must contain unpublished material and will be refereed and assessed with reference to the aims of the Journal as stated above. (ii) Reviews should constitute an outstanding critical appraisal of published materials and will be published by suggestion of the Editors. (iii) Letters and communications to the Editor should not exceed 400 words in length and may be: Criticism of articles recently published in the Journal; Preliminary announcements of original work of importance warranting immediate publication; Comments on current engineering matters of considerable actuality.
3. Only papers not previously published will be accepted. Authors must agree not to publish elsewhere a paper submitted to and accepted by the Journal. Exception can be made in some cases of papers published in annals or proceedings of conferences. The decision on acceptance of a paper will be taken by the Editors considering the reviews of two outstanding scientists and its originality, and contribution to science and/or technology.
4. All contributions are to be in English or Portuguese. Spanish will also be considered.
5. Manuscripts should begin with the title of the article, including the english title, and the author's name and address. In the case of co-autors, both addresses should be clearly indicated. It follows the abstract; if the paper's language is different from english, an extended summary in this language should be included. Up to five words for the paper are to be given. Next, if possible, should come the nomenclature list.
6. Manuscripts should be typed with double spacing and with ample margins. Material to be published should be submitted in triplicate. Pages should be numbered consecutively.
7. Figures and line drawing should be originals and include all relevant details; only excelent photocopies should be sent. Photographs should be sufficiently enlarged to permit clear reproduction in half-tone. If words or numbers are to appear on a photograph they should be sufficiently large to permit the necessary reduction in size. Figure captions should be typed on a separate sheet and placed at the end of the manuscript.

REVISTA BRASILEIRA DE CIÊNCIAS MECÂNICAS
JOURNAL OF THE BRAZILIAN SOCIETY OF MECHANICAL SCIENCES

Vol. XIV - Nº 4 *1992*

ÍNDICE / CONTENTS